

UNIVERSITY OF NAPLES
"FEDERICO II"

FACULTY OF MATHEMATICS, PHYSICS AND NATURAL SCIENCES
PH.D. IN CHEMISTRY - XVIII CYCLE
2002-2006

New Molecular Scaffolds for the
Construction of Complex
Biomolecules

Candidate : Dr. Mireille Engelen

Tutor : Prof. V. Pavone

Supervisor : Prof. L. Paolillo

Coordinator: Prof. R. Lanzetta

Contents

List of abbreviations	i
Summary	iv
Chapter 1 Porphyrins as scaffold	1
Introduction	
1.1 Porphyrins	3
1.1.1 Properties of the porphyrin macrocycle	
1.1.2 Tetraphenylporphyrins	
1.1.3 Metalloporphyrins	
1.1.4 UV-VIS spectrum of porphyrin	
1.1.5 Photo- and redox chemistry	
1.2 Synthesis of porphyrins	10
1.2.1 General synthesis	
1.2.2 Insertion of metal ions	
1.3 Applications of porphyrins	20
1.3.1 Porphyrins as scaffold	
1.3.2 MRI and photodynamic therapy	
1.3.3 Interaction with DNA	
1.3.4 Molecular recognition	
1.3.5 Super-molecular assembly of porphyrins	
1.3.6 Porphyrins as templates in <i>de novo</i> design	
1.4 Design of new porphyrin scaffolds	27
1.4.1 Tetraphenylporphyrin bearing functional groups	
1.4.2 Choice of –NH ₂ as functional group	
1.5 References	30
Chapter 2 Thrombin	33
2.1 Biological function of thrombin	33
2.1.1 The coagulation cascade	
2.1.2 Reaction of thrombin with fibrinogen	
2.1.3 Regulation of the coagulation cascade	
2.2 Structure of thrombin	38
2.2.1 α , β , γ thrombin	
2.2.2 Crystal structure of human α -thrombin	
2.2.3 Specific binding of fibrinogen	
2.2.4 Thrombin and fibrin	

2.3	Natural inhibitors	49
2.3.1	Inhibitors of thrombin in the coagulation cascade	
2.3.2	Hirudin	
2.3.3	Haemadin	
2.4	Synthetic inhibitors of thrombin	51
2.4.1	Synthetic inhibitors	
2.4.2	Inhibitors of the catalytic site	
2.4.3	Inhibitors of the fibrinogen recognition site	
2.4.4	Multi-site inhibitors	
2.5	Rational design of new thrombin inhibitors	55
2.5.1	Peptide-functionalized tetraphenylporphyrin as potential inhibitor	
2.5.2	Design of new porphyrin-based thrombin inhibitors	
Chapter 3 Synthesis of the tetraphenylporphyrin scaffolds		59
Introduction		
3.1	Results	62
3.1.1	Synthesis of the porphyrin scaffolds	
3.1.2	Synthesis of <i>trans</i> di-substituted porphyrin	
3.1.3	Synthesis of <i>cis</i> di-substituted porphyrin	
3.1.4	Synthesis of tetrakis(<i>p</i> -(aminomethyl)phenyl)porphyrin	
3.1.5	Protection of the amine function	
3.2	Discussion	64
3.3	Experimental section	72
3.3.1	Materials and methods	
3.3.2	Synthesis of intermediates	
3.3.3	Synthesis of the porphyrin scaffolds	
3.3.4	Synthesis of <i>trans</i> di-substituted porphyrin: 2+2 condensation	
3.3.5	Synthesis of <i>cis</i> di-substituted porphyrin: modified ABCD-porphyrin synthesis	
3.3.6	Synthesis of tetrakis(<i>p</i> -(aminomethyl)phenyl)porphyrin	
3.3.7	Partial protection with Boc	
Chapter 4 Functionalization of the scaffolds		88
Introduction		
4.1	Results	90
4.1.1	Synthesis of the peptides	
4.1.2	Activation of the peptides	
4.1.3	Functionalization of the scaffolds	
4.1.4	Insertion of manganese in the peptide-porphyrin compounds	
4.2	Discussion	96

4.3	Experimental section	97
4.3.1	Materials and methods	
4.3.2	Synthesis of the peptides	
4.3.3	Activation of the peptides	
4.3.4	Coupling of the peptides to porphyrin scaffolds	
4.3.5	Insertion of manganese	
Chapter 5	Tests of inhibition of α-thrombin	118
	Introduction	
5.1	Results	121
5.1.1	Calculation of K_m	
5.1.2	Inhibition of the catalytic site	
5.1.3	Stability of the inhibitors	
5.1.4	Selectivity of the inhibitors	
5.1.5	Interaction with the exo site	
5.1.6	Inhibition of clot-bound thrombin	
5.2	Discussion	128
5.3	Experimental section	129
5.3.1	Materials and methods	
5.3.2	Inhibition tests	
Chapter 6	General discussion and future prospects	132
	Introduction	
6.1	Functionalized tetraphenylporphyrins as versatile scaffold	132
6.2	New inhibitors of thrombin	133
6.2	Suggestions for further research	134
	References	135

List of abbreviations

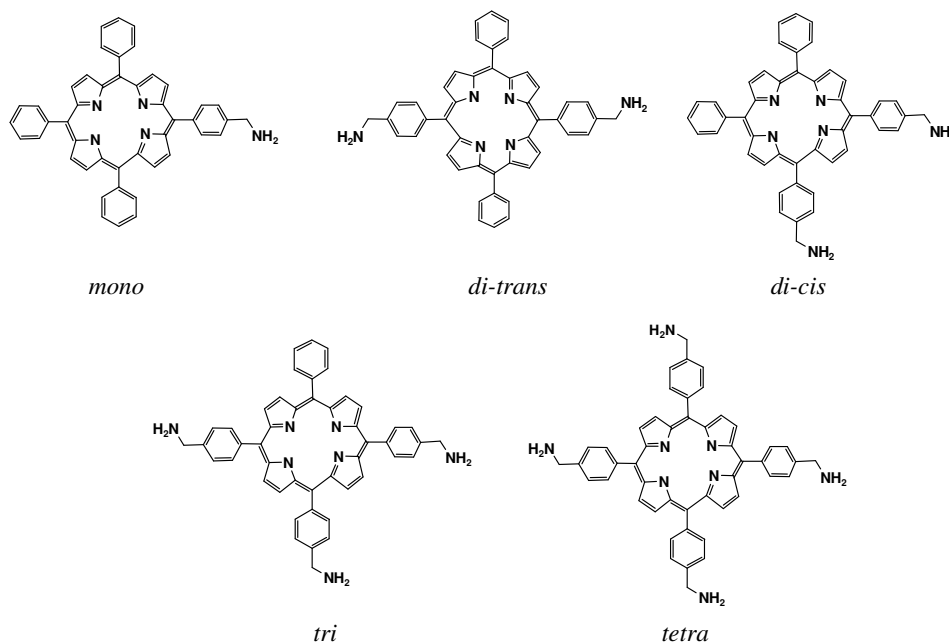
Aib	Aminoisobutyric acid
APC	Activated Protein C
Arg	Arginine
Asn	Asparagine
Asp	Aspartic acid
AT	Antithrombin
BAEE	Benzoylarginine ethyl ester
Boc	t-Butoxycarbonyl
Bz	Benzoyl
Cbz	Carbobenzyloxy
Cha	Cyclohexylalanine
Chg	Cyclohexylglycine
CS	Catalytic Site
Cys	Cysteine
DCC	Dicyclohexylcarbodiimide
DCM	Dichloromethane
DDQ	2,3-Dichloro-5,6-dicyano-1,4-benzoquinone
DIBAL	Diisobutylaluminiumhydride
DIEA	Diisopropylethylamine
DMF	Dimethylformamide
DMSO	Dimethylsulfoxide
DNA	Deoxyribose Nucleic Acid
EDT	Ethanedithiol
ES	Exo Site
EtOH	Ethanol
FDP	Fibrin Degradation Product
Fmoc	9-Fluorenylmethoxycarbonyl
Gln	Glutamine
Glu	Glutamic acid
Gly	Glycine
HATU	<i>N</i> -[(dimethylamino)-1 <i>H</i> -1,2,3-triazolo[4,5- <i>b</i>]pyridin-1-ylmethylene]- <i>N</i> -methylmethanaminium hexafluorophosphate <i>N</i> -oxide

HBTU	2-(1H-Benzotriazole-1-yl)-1,1,3,3-tetramethyluronium hexafluorophosphate
HC	Heparin Cofactor
His	Histidine
HOBt	N-hydroxybenzotriazole
Ile	Isoleucine
IRU-1	N-acetyl-hirudin ^{54'-65'}
K _i	Inhibition constant
K _m	Michaelis-Menten constant
Leu	Leucine
LMHW	Low Molecular Weight Heparin
Lys	Lysine
MALDI	Matrix Assisted Laser Desorption Ionization
MeOH	Methanol
Met	Methionine
MRI	Magnetic Resonance Imaging
Nal	Naphtylalanine
NIH	National Institute of Health
Noa	Naphtyloxyacetic acid
Pbf	2,2,4,6,7-Pentamethyldihydrobenzofurane-5-sulfonyl
PDT	Photodynamic Therapy
PEG	Polyethyleneglycol
Phe	Phenylalanine
PN-1	Protease nexin-1
<i>p</i> -NA	<i>para</i> -nitroanilide
PPACK	D-Phe-Pro-Arg chloromethylketone
Pro	Proline
PyBop	Benzotriazole-1-yl-oxy-tris-pyrrolidino-phosphonium hexafluorophosphate
R _F	Retention Factor
RP-HPLC	Reverse Phase High Pressure Liquid Chromatography
Ser	Serine
SPPS	Solid Phase Peptide Synthesis
TAMPP	Tetrakis(<i>p</i> -(aminomethyl)phenyl)porphyrin
TAP	Tetraarylporphyrin
TASP	Template Assembled Synthetic Protein

t-Bu	tert-Butyl
TEA	Triethylamine
TF	Tissue Factor
TFA	Trifluoroacetic acid
TFPI	Tissue Factor Pathway Inhibitor
THF	Tetrahydrofuran
Thr	Threonine
TLC	Thin Layer Chromatography
TM	Thrombomodulin
Tos	Tosyl
Tween 80	Polyoxyethylene (20) sorbitan monooleate
t-PA	Tissue Plasminogen Activator
TPP	Tetraphenylporphyrin
Tris	Tris(hydroxymethyl)aminomethane
Trp	Tryptophan
Tyr	Tyrosine
Val	Valine
Z	Benzyloxycarbonyl

Summary

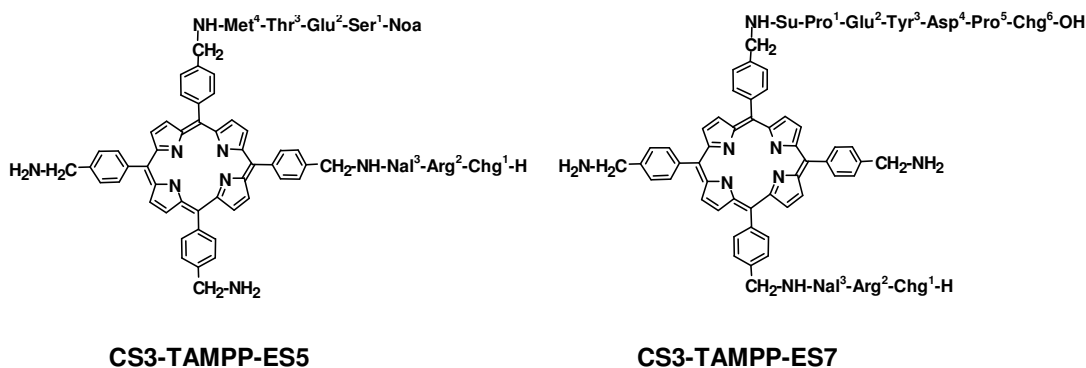
In the course of this thesis, new molecular scaffolds based on tetraphenylporphyrin have been designed and synthesized, and their versatility has been studied by functionalization with various peptides.



The porphyrin scaffolds were successfully functionalized with peptides. Activation of the peptides required the use of N-hydroxysuccinimide, since other activants, such as PyBop, HOBt, HATU did not produce the desired results. The functionalization reaction can take place either in solution, or with the activated peptide still attached to the resin. Both Fmoc and Boc protected peptides could be used for functionalization of the scaffolds, as the porphyrin scaffolds proved to be stable in both deprotection protocols. No alteration of the peptide-porphyrin compound was observed during the synthesis. When stored at -20 °C, the peptide-functionalized porphyrin compounds could be kept for a prolonged period of time. Stable Mn^{III}-porphyrin complexes were obtained by insertion of manganese using Mn^{II}Ac₂ in a 50% acetic acid/MeOH solution.

An application of the functionalized scaffolds has been found in the design and synthesis of new inhibitors of thrombin, an enzyme of fundamental importance in the blood coagulation process. These inhibitors consist of a central porphyrin macrocycle bearing two different peptides; one of them is designed to interact with the thrombin catalytic site, while the other is designed to bind to the fibrinogen recognition site or exosite. The peptide sequences were designed using the structure of Hirunorm IV as

template, a synthetic peptide-based thrombin inhibitor that faithfully mimics the specific binding mode of hirudin, and is considered the most potent synthetic thrombin inhibitor known so far. The sequence of the N-terminal tripeptide of Hirunorm IV, responsible for the interaction with the catalytic site, was left unaltered. The fibrinogen recognition site was accessible from the *cis* position as well as from the *trans* position, therefore, two new potential inhibitors have been proposed:



The porphyrin ring offers many advantages, of which the insertion of a (paramagnetic or radio-active) metal ion in its centre could be of great interest for diagnostic purposes. The inhibitors CS3-TAMPP-ES5 and CS3-TAMPP-ES7, as well as their Mn^{III} -complexes, were able to interact with both the catalytic site and the exo site of thrombin. CS3-TAMPP, CS3-TAMPP-ES5, CS3-TAMPP-ES7 all had a K_i value of 1.0 μM , whereas Mn^{III} -CS3-TAMPP-ES5 had a slightly higher K_i of 1.6 μM . The presence of the peptides ES5 and ES7 did not affect the value of the inhibition constant.

The inhibitors resulted to be very resistant against enzymatic degradation by thrombin, as after 24 h 85% of the original compound was still intact. Assays of inhibition of trypsin with the substrate BAEE proved the high selectivity of the new inhibitors. Even at elevated concentrations (up to 10 μM) the inhibitors did not affect the hydrolysis rate of the reaction. The interaction of the new inhibitors with the thrombin exo site by the peptides ES5 and ES7 was proved by fluorescence spectroscopy. The fluorescence of residue Trp¹⁴⁸, in close proximity of the exo site, was quenched when the porphyrin-based inhibitors were added. Addition of N-acetyl-hirudin^{54'-65'}, an inhibitor of the exosite only with a high affinity for thrombin, displaced the inhibitor from the exo site, thus allowing the fluorescence intensity to return to almost its original level.

The manganese complexes of the new inhibitors were capable of interacting with clot-bound thrombin, and partially inhibited clot-growth in the presence of fresh fibrinogen. After 1h pre-incubation with a 10 μM inhibitor solution, clot growth was decreased to

60% compared to the uninhibited clots. The change of colour of the fibrin clot from white to yellow proved the presence of the inhibitors on the fibrin clot.

To the best of our knowledge, the compounds Mn^{III}-CS3-TAMPP-ES5 and Mn^{III}-CS3-TAMPP-ES7 are the first specific inhibitors of thrombin that might be employed for diagnostic purposes, due to the presence of a paramagnetic metal ion inside the porphyrin structure. The high stability against degradation by thrombin, and the high selectivity of these compounds make them extremely interesting for various applications.

Chapter 1 Porphyrins as scaffold

Introduction

Porphyrins and porphyrin-related structures are widely diffused in nature, where they play important roles in various biological processes. They are most abundant in the so-called heme proteins, proteins that contain one of the four naturally occurring hemes as prosthetic group¹. The most common heme is heme *b*, the iron(II) complex of protoporphyrin-IX (shown in figure 1). The other hemes present slightly different substituents on the porphyrin ring.

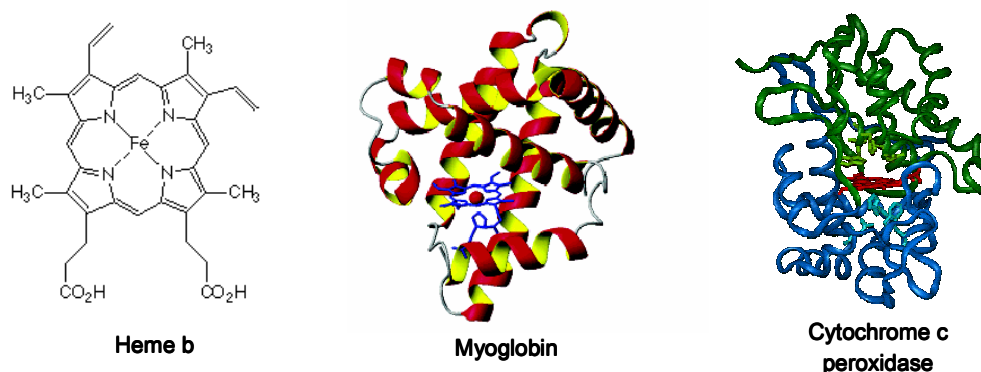


Figure 1: Structure of heme and two heme-proteins: myoglobin and cytochrome c peroxidase.

Heme proteins carry out many different biological functions. The main function of the heme group is the retention of O₂ and delivering it for enzymatic reactions. The iron atom of every heme group can bind one molecule of O₂. For example, hemoglobin is a transporter of dioxygen, myoglobin is responsible for oxygen storage in living tissues, and peroxidases catalyze the breakdown of hydrogen peroxide to water. Other heme-containing proteins include the catalases, oxidases, mono- and dioxygenases and the cytochromes, involved in electron transfer processes where the heme centres serve as one-electron carriers.

Given the biological importance of these proteins, a large number of artificial model systems for their active sites has been developed in an attempt to (i) provide further insights for structure-activity relationships, (ii) understand the minimal requirements for function, (iii) reproduce the properties of the parent natural proteins in smaller molecules, and (iv) most importantly construct new, tailor-made molecules useful for biomedical, pharmaceutical, biological, and environmental applications^{2,3}. In the search for these so-called low molecular weight heme-protein mimetics, the heme centre and

related porphyrin structures have been extensively studied. From these studies has emerged that the porphyrin macrocycle presents several characteristics (mentioned in detail hereafter), that render it extremely suitable as building block for the design of larger molecular structures.

The goal of this thesis is therefore to describe the synthesis of a multifunctional, porphyrin-based scaffold, carrying from one to four functional groups that allow a selective functionalization. Since we are mostly interested in the functionalization of these scaffolds with biomolecules, especially peptides, different peptides have been synthesized and linked to the porphyrin scaffolds. A possible application of these peptide-functionalized porphyrins can be found in the interaction with larger biomolecules such as proteins, enzymes or DNA, for example to interfere with certain biological processes. In our case, the peptides have been designed to interact with the active site of thrombin, an enzyme that is of fundamental importance for the blood coagulation process. The presence of the porphyrin scaffold should help to position the peptides in the correct orientation to bind simultaneously two different parts of the protein: the catalytic site and the substrate binding site. Moreover, the porphyrin ring can be a host for a variety of metal ions, including paramagnetic or radio-active metal ions, which allow the detection of the porphyrin-thrombin complex.

1.1 Porphyrins

1.1.1 Properties of the porphyrin macrocycle

The basic structure of porphyrin (shown in figure 2) consists of four pyrrole-like five-membered units, A, B, C and D, which are linked by four methine bridges, 5, 10, 15, 20 (*meso* positions). The porphyrin macrocycle is an aromatic system containing 22 π electrons, but only 18 of them are involved in a delocalization pathway. Porphyrin obeys Huckel's rule of aromaticity ($4n + 2 \pi$ electrons, $n = 4$) and is shown by X-ray crystallography to be planar. The aromatic character of porphyrins can also be seen by NMR spectroscopy. Due to the anisotropic effect from the porphyrin ring current, the NMR signals for the deshielded *meso* protons appear at low field (8 to 10 ppm), whereas the signals for the shielded protons (on the inner nitrogen atoms) appear at very high field (-2 to -4 ppm).

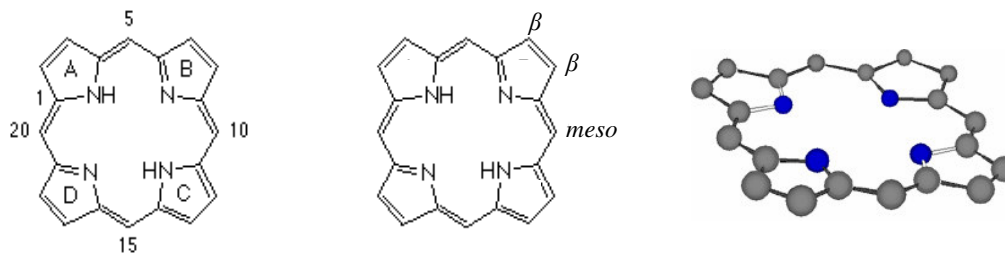


Figure 2: Basic structure of the porphyrin macrocycle: numbering, functionalization sites and planarity.

Meso-hydrogenated porphyrin derivatives, such as porphodimethanes and porphyrinogens (figure 3), are thermodynamically unfavourable, but their preparation by reduction of porphyrin is possible under anaerobic conditions and in the absence of light. Reduction of one of the pyrrole units on the porphyrin ring leads to a class of porphyrin derivatives called chlorins. Further reduction of chlorins gives another type of porphyrin derivative called bacteriochlorins, in which the reduced pyrrole units can be either diagonally opposite, or next to each other.

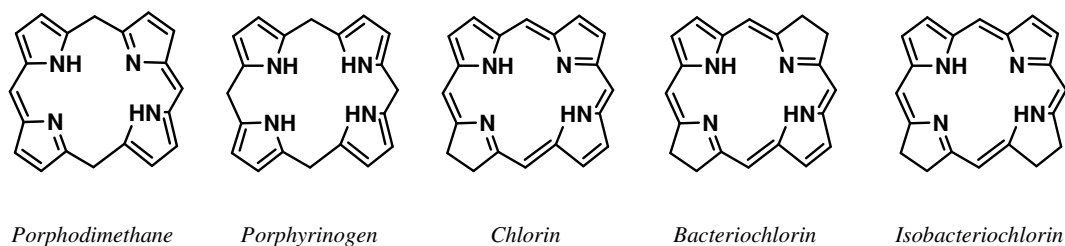


Figure 3: Hydroporphyrins.

The porphyrin ring is very stable to concentrated acids (e.g. sulphuric acid), and can act both as an acid and a base. Strong bases such as alkoxides can remove the two protons ($pK_a \sim 16$) on the inner nitrogen atoms of a porphyrin to form a di-anion. On the other hand, the two free pyrroline nitrogen atoms ($pK_b \sim 9$) can be protonated easily with acids such as trifluoroacetic acid.

Porphyrins can undergo a number of chemical reactions typical of aromatic compounds. For example, electrophilic substitution reactions are often performed on porphyrins. The *meso* carbons and the β -pyrrolic carbons participate in these reactions. Furthermore, certain substituents on a porphyrin molecule can be modified. This leads to the availability of a variety of different porphyrins.

1.1.2 Tetraphenylporphyrins

Tetraphenylporphyrins (usually called TPP, 3D-structure shown in figure 4) are one of the most commonly used porphyrinic systems. They are easy to prepare, chemically very stable and their derivation has been well studied. Functional groups are usually placed on the *ortho*, *meta* and/or *para* positions of the phenyl groups. Because of steric hindrance the phenyl rings are positioned almost orthogonal to the equatorial porphyrin plane.

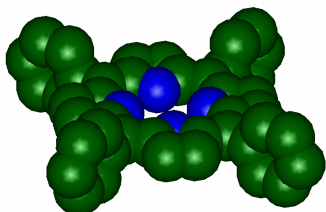


Figure 4: 3D-structure of *meso*-tetraphenylporphyrin showing the phenyl rings orthogonal to the porphyrin plane.

The presence of the phenyl groups enhances the rigidity of the overall complex, whereas functional groups on specific positions of the phenyl groups have defined orientations in space. Also, the tetraphenylporphyrin itself is soluble in various organic solvents, but anchoring of polar substituents to the functional groups dramatically enhances the solubility in polar solvents. The free porphyrin base has a deep red colour, whereas the corresponding acid has an intense green colour.

1.1.3 Metalloporphyrins

The porphyrin nucleus is a tetradentate ligand, in which the space available for a coordinated metal has a maximum diameter of approximately 3.7 Å. Upon coordination, the two protons on the pyrrolic nitrogen atoms are removed, leaving two negative charges⁴. Almost all metal ions form 1:1 complexes with porphyrin, only Na⁺, K⁺ and Li⁺ are known to form 2:1 complexes with one metal ion incorporated slightly below and the other above the porphyrin macrocycle plane. The geometry of the resulting porphyrin-metal complex and the presence or not of additional ligands depend on the metal ion⁵. For example, when Cu^{II} and Ni^{II} are incorporated in the porphyrin macrocycle, they generally display low affinity for additional ligands forming square planar complexes, whereas the chelates with Mg^{II}, Cd^{II} and Zn^{II} readily combine with one more exogenous ligand (often corresponding to a solvent molecule) to form penta-coordinated complexes with a square-pyramidal structure. Since these ions are slightly too large to fit perfectly into the porphyrin hole, they are positioned slightly out of the equatorial plane. Metalloporphyrins containing Fe^{II}, Co^{II} or Mn^{II} are able to form distorted octahedral structures with two extra ligands. The coordination type, geometry and symmetry of several metalloporphyrin-complexes are summarized in table 1.

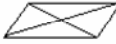

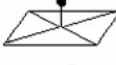
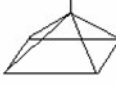

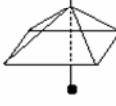

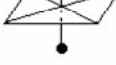
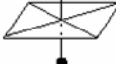
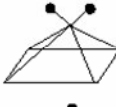
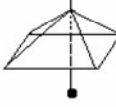
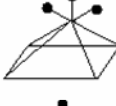
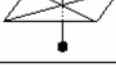
Formal charge (n) of M^{n+} cation	CN	Atomic arrangement in coordination entity	Symmetry	Example of entity and molecule
2	4		D_{4h}	$(MN)_4$, CuP
	4		C_{4v}	$(MN)_4$, BaP
	5		C_{4v}	XMN_4 , (NO)CoTPhP
3	5		C_{4v}	XMN_4 , (Cl)MnTPhP
	5		C_{4v}	XMN_4 , (Cl)AuP
	6		C_{4v}	$XYMN_4$, (Cl)(Py)MnP
4	5		C_{4v}	$O=MN_4$, $O=VP$
	6		D_{4h}	X_2MN_4 , (Cl) $_2$ SnTPhP
	6		C_{4v}	$XYMN_4$, (Cl)(Ph)RhP
	6			X_2MN_4 , (Ac) $_2$ ZrOEP
5	6		C_{4v}	$O=M(X)N_4$, $O=Mo(OPh)OEP$
	7			X_3MN_4 , (F) $_3$ TaOEP
6	6		D_{4h}	O_2MN_4 , (O) $_2$ OsTPhP

Table 1²: Coordination, geometry and symmetry of metalloporphyrins. CN = Coordination Number, P = porphyrin, PhP = tetraphenylporphyrin, OEP = 2,3,7,8,12,13,17,18-octaethyl-21H,23H-porphin.

1.1.4 UV-VIS spectrum of porphyrin

In the UV-visible absorption spectrum, the highly conjugated porphyrin macrocycle shows intense absorption (extinction coefficient $> 10^5$) around 400 nm (the "Soret" band, B band or γ band), followed by several weaker absorption bands (Q bands or β - α bands) in the visible region^{6,7}. The α band corresponds to the lowest porphyrin π - π^* transition Q_0 , the β band to the vibronic envelope Q_v . Since these transitions are polarized in the xy -plane of the porphyrin, both bands are split into two distinct bands, resulting in four Q bands, named I-IV in increasing intensity. Variations of the peripheral substituents on the porphyrin ring often cause minor changes in the intensity and wavelength of these absorptions. The UV-VIS spectra of *meso*-substituted porphyrins in which the substituent is an aromatic group, as is the case for tetraphenylporphyrins, display bathochromical shifts (even up to 20 nm) for all bands, as well as a change in the intensity sequence from Soret $\gg \alpha > \beta$ to Soret $\gg \beta > \alpha$.

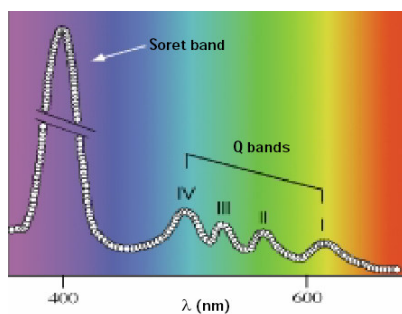


Figure 5: Typical UV-VIS absorption spectrum of a porphyrin

Upon formation of a metalloporphyrin, the two protons of the inner nitrogen atoms are lost. Due to the new D_{4h} symmetry, the dipole transitions in the x and y directions are equivalent and both the Q_0 and Q_v transitions are doubly degenerate. As a result, the absorption spectrum of a metalloporphyrin usually displays only two bands in the visible region, whereas the Soret band can remain at its original position or shift to higher or lower energy. In some cases the insertion of a metal may cause new bands. The absorption spectra of metalloporphyrins can be classified into three types: regular or normal, hypso and hyper spectra.

The 'normal' absorption spectrum

Normal-type spectra are observed for a majority of metalloporphyrins where the relevant π orbitals of the porphyrin macrocycle do not interact significantly with the

metal π orbitals (p_z , d_{xz} , d_{yz} orbitals). The colour of these metalloporphyrins is deep purple. All closed-shell metal ions (d^0 or d^{10}) display this normal spectrum, in which the position of the α -band is around 570 nm, the β -band around 530 nm and the Soret band at 400 nm. In most cases the intensity sequence is Soret \gg α $>$ β . Increasing atomic number of the metal within a given coordination type and set of axial ligands causes an additional small bathochromic shift. Also some lanthanoid ions (f^n) display this normal-type spectrum, apparently the extra electrons of these ions are too deeply buried to disturb the normal type. Almost all other metal ions with open electron shells give rise to 'abnormal' spectra.

The 'hypso' spectrum

The absorption spectra of d^6 - d^9 metal ions follow the regular absorption pattern, but are blue shifted due to filled metal d (π) to porphyrin e_g (π^*) back donation. This shift increases with increasing atomic number, as the back-bonding is more pronounced with heavier transition metals. The colour of these metal-porphyrin complexes varies from red to orange.

The 'hyper' spectrum

The hyper spectrum consists of more or less red-shifted α , β and Soret bands, and one or more additional bands. These spectra are caused by charge transfer transitions, more or less mixed with the porphyrin π - π^* transitions. The number of extra bands varies from metal to metal, and the positions of the bands are far more dependent on the axial ligands than in the other spectrum types. The metal ions causing the hyper type spectra have the configurations d^1 - d^5 , the metalloporphyrin complexes are usually brown or green. Most of the metal ions belonging to this class can also have lower oxidation states within in the porphyrin, causing a normal or hypso spectrum (Cr, Mo, Mn, Fe, Os).

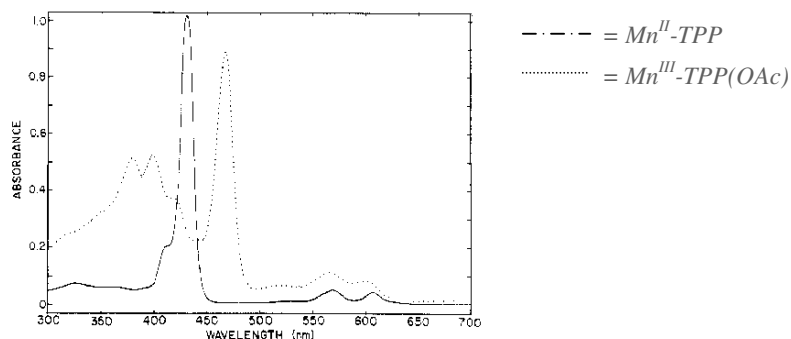


Figure 6: Hypso (Mn^{II}) and hyper (Mn^{III}) type spectra of Mn-tetraphenylporphyrin complexes⁸

The metalloporphyrin complexes with their metal oxidation numbers and corresponding spectral absorption types are summarized in table 2.

Li I-n												B III-n		
Na I-n	Mg II-n											Al III-n	Si IV-n	P III-h V-h
K I-n	Ca II-n	Sc III-n	Ti IV-n	V IV-n	Cr II-h III-h IV-o	Mn II-y III-h IV-o	Fe I-y II-y III-h	Co I-h II-y III-y	Ni II-y III-y	Cu II-y	Zn II-n	Ga III-n	Ge IV-n	As III-h V-n
Rb I-n	Sr II-n	Y III-n	Zr IV-n	Nb V-n	Mo IV-n V-h VI-h	Tc I-n	Ru II-y III-y	Rh I-y II-y III-y	Pd II-y	Ag II-y III-y	Cd II-n	In III-n	Sn IV-n	Sb III-h V-n
Cs I-n	Ba II-n	La III-n	Hf IV-n	Ta V-n	W V-h	Re I-n V-h	Os II-y III-y IV-h VI-h	Ir III-y	Pt II-y IV-y	Au III-y	Hg II-n	Tl III-n	Pb II-h IV-n	Bi III-h
		Ln III-n	Th IV-n											

Table 2: Periodic table of metalloporphyrins. Spectral type: n = normal, h = hyper, y = hypso, o = no spectrum reported. Ln = lanthanoids. The normal spectrum is bathochromically shifted in monovalent metal ions as well as in B, Sr and Ba.

1.1.5 Photochemistry

Porphyrins and certain metalloporphyrins are excellent photosensitizers (light-absorbing molecules) because of similar energies of the singlet and triplet excited levels, high intersystem crossing yield and long triplet lifetime. The excited state porphyrins can be both donors and acceptors and form exciplexes [$*\text{Por}^+\text{D}^-$] or [$*\text{Por}^+\text{A}^-$], which then relax to the ground state or undergo chemical reaction. In acidic media or in the presence of reductants, porphyrins can be photoreduced to the dihydro, tetrahydro and hexahydro derivatives mentioned in paragraph 1.1.1. If an appropriate electron acceptor is available, the photo-excited porphyrin can transfer an electron. The acceptor may be an organic molecule, a metal complex or another porphyrin molecule. Since the reaction creates a charged species, polar media accelerate the process. The back reaction or other photosensitization processes such as $^1\text{O}_2$ generation become favourable in nonpolar solvents.

1.2 Synthesis of porphyrins

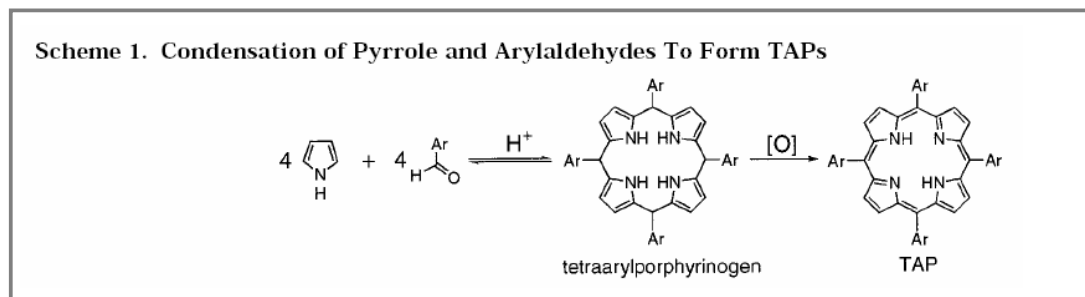
1.2.1 General synthesis

There are two general approaches to obtain a desired porphyrin: (1) by modification of a naturally occurring porphyrin (e.g. heme); or (2) by total synthesis. Although convenient, modification of naturally occurring porphyrins poses great limitations on the choice of peripheral substituents because certain substituents cannot be easily modified. In most cases, such limitations can be overcome by total synthesis, which involves the syntheses of the pyrrole subunits having the required substituents. The following are the methods commonly used in porphyrin total synthesis^{9,10,11}:

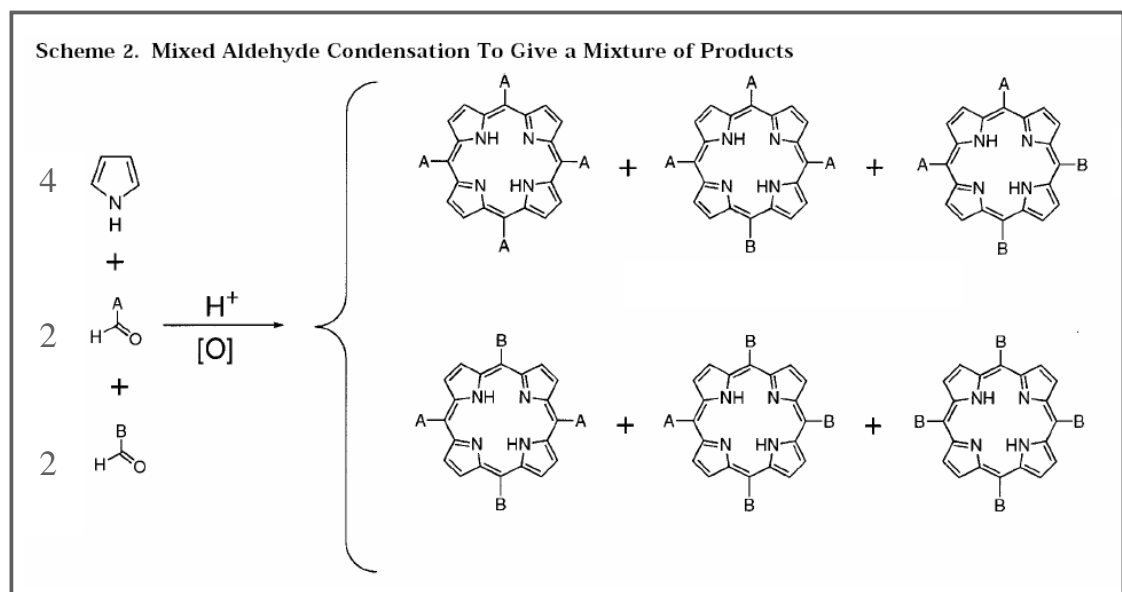
- Condensation of pyrrole and (aryl)aldehydes
- Mixed aldehyde condensation to give a mixture of porphyrins
- 2 + 2 condensation of dipyrromethanes
- 3 + 1 condensation of tripyrranes with diformylpyrroles
- Stepwise synthesis leading to porphyrins bearing four different substituents
- Cyclization of linear tetrapyrroles

The simplest procedure to synthesize symmetrical meso-substituted porphyrins (e.g. tetraphenylporphyrin) consists of the acid-catalyzed condensation of pyrrole with a suitable aldehyde (scheme 1). The porphyrinogen formed in this reaction is subsequently oxidized to the corresponding porphyrin. This procedure was originally developed by Rothmund and Menotti in 1941 with an initial yield of 10%, reacting benzaldehyde and pyrrole in pyridine in a sealed tube at 150 °C for 24 h¹². The conditions were so severe that few substituted benzaldehydes could be converted to the corresponding porphyrin. An improvement were the modifications made by Adler and Longo, allowing benzaldehyde and pyrrole to react for 30 min in refluxing propionic acid (141 °C) open to air¹³. These comparatively milder reaction conditions allowed a wider selection of substituted benzaldehydes to be converted to the corresponding porphyrins, in yields of up to 20%. β -substituted porphyrins could be obtained by using β -substituted pyrroles in the initial condensation reaction. However, this method still presented some problems, as the harsh conditions prevented the use of benzaldehydes bearing sensitive functional groups. Also, the product is invariably contaminated by the presence of reduced porphyrin (chlorin) in the reaction mixture, and the purification of the desired product can be complicated if it does not spontaneously crystallize or precipitate at the end of the reaction. A procedure with milder reaction conditions and

higher yield has been developed by Lindsey and co-workers^{14,15}, consisting of the reaction of pyrrole and (substituted) benzaldehydes in dichloromethane in the presence of a catalytic amount of acid, at room temperature and under nitrogen¹⁶. The resulting porphyrinogen is oxidized to the corresponding porphyrin by addition of 2,3-dichloro-5,6-dicyano-1,4-benzoquinone (DDQ). Yields up to 45% can be obtained, depending on the type of substituent on the benzaldehyde.

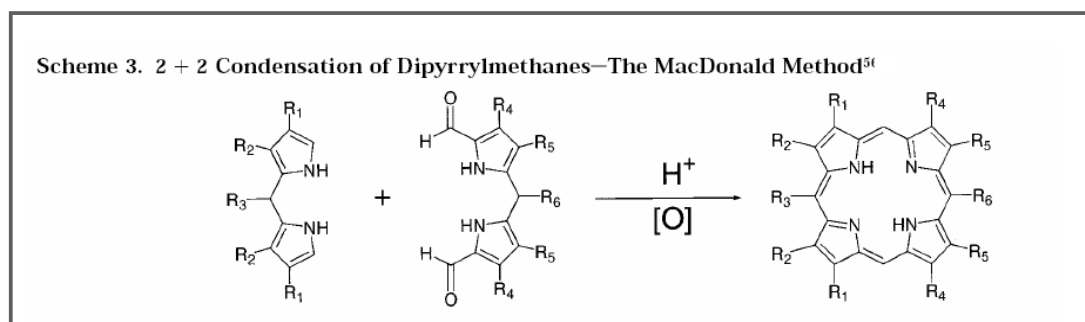


Asymmetrically substituted porphyrins can be synthesized by mixed aldehyde condensations. If a mixture of two different aldehyde starting products is employed in the Adler or Lindsey syntheses, a statistical mixture of porphyrin products is obtained (scheme 2). The obvious problem is the separation of the many products, which can include up to six different compounds that make large-scale syntheses virtually impossible. However, by varying the stoichiometry of the reagents, the yield of the desired product can be maximized.

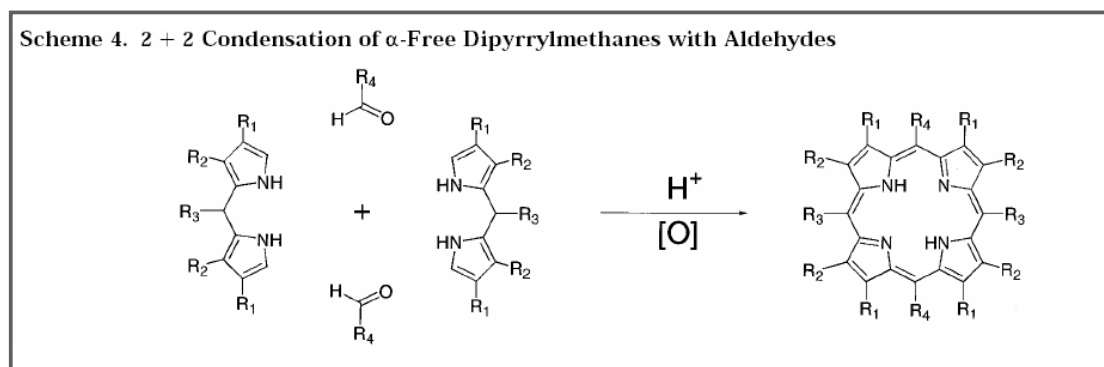


An alternative approach to the synthesis of substituted porphyrins is the 2 + 2 condensation of dipyrrolic starting materials that can be dipyrromethenes, dipyrrolylketones or dipyrrolyl-methanes. The first use of dipyrrolylmethenes in porphyrin

synthesis was reported by Fisher in 1934, involving the self-condensation of 1-bromo-9-methyldipyrrromethenes in an organic acid melt (e.g. succinic acid) at temperatures up to 200 °C. Although the yield of porphyrin was relatively high, only few substituted dipyrromethenes could withstand the severe reaction conditions. Dipyrromethanes were initially considered too unstable to be useful intermediates in porphyrin synthesis, but the milder reaction conditions developed by MacDonald and co-workers in 1960 led to the publication of the first dipyrromethane-based porphyrin synthesis (scheme 3)¹⁷. The condensation of a free dipyrromethane with a dipyrromethane dialdehyde was catalyzed by an acid catalyst, and the intermediate porphyrinogen oxidized by exposure to air to give the desired porphyrin. This route is widely used today also because the dipyrromethanes required for the MacDonald synthesis are often more easily prepared and purified than the corresponding dipyrromethenes.

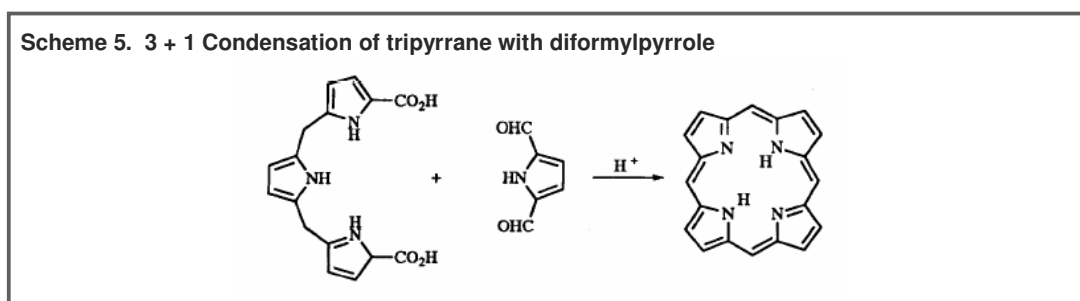


Variations on this method include the acid-catalyzed condensation of free dipyrromethanes with aldehydes to form porphyrinogens, which are subsequently oxidized to give the corresponding porphyrins (scheme 4). This route is widely used today due to its flexibility, and there are many reports of porphyrin synthesis based on this methodology. It is, however, very dependent on the availability of suitable dipyrromethane building blocks.



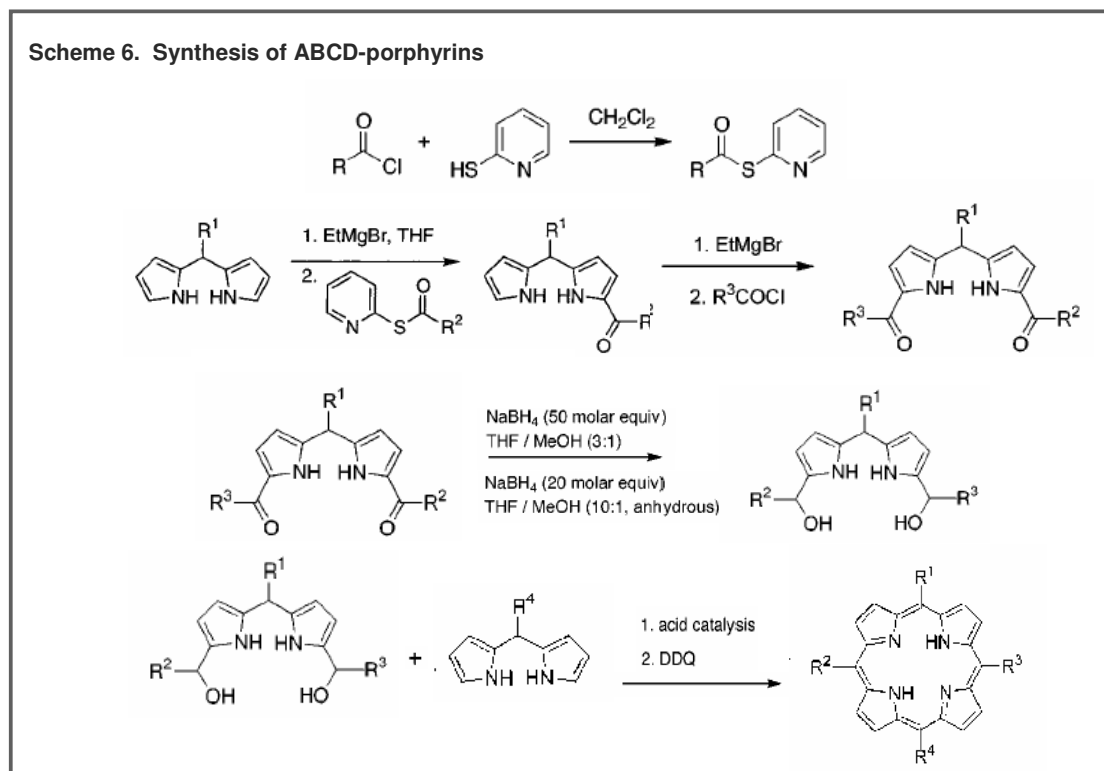
The principal limitation of MacDonald's '2+2' approach is that one of the condensing units must be symmetrical, or two isomeric porphyrins will be produced. To overcome

this limitation, the 3+1 synthetic route has been developed by Momenteau and co-workers^{18,19}. The 3+1 condensation involves the condensation of a tripyrrane (the tripyrrolic analogue of dipyrromethane, a compound containing three pyrrole groups linked alpha to the ring nitrogen atoms by two saturated carbons) with a diformylpyrrole in the presence of an acidic catalyst (scheme 5). Until the development of this 3+1 method, tripyrranes had seen little application in the synthesis of porphyrin structures, although they had been widely utilized in the preparation of porphyrinoid derivatives in which a thiophene, furan or pyridine ring replaces one of the pyrrole rings²⁰, as well as in the preparation of extended macrocycles such as sapphyrins²¹. The 3+1 procedure is particularly convenient if one of the components, either the tripyrrane or the diformylpyrrole, is symmetrical, or when the traditional 2+2 condensation encounters problems during the synthesis of the required dipyrromethanes²². This is, for example, the case for porphyrins bearing exocyclic rings such as phenanthrolinoporphyrins²³ and acenaphthoporphyrins²⁴.

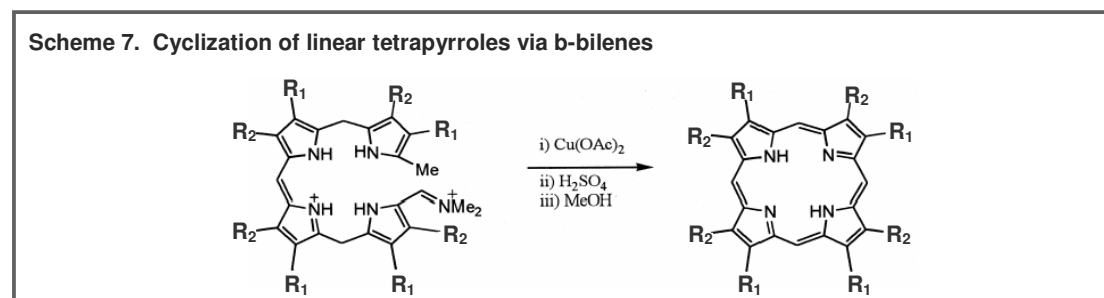


The stepwise synthesis of porphyrins bearing four different *meso* substituents (ABCD-porphyrins) from dipyrromethanes was recently developed by Lindsey and co-workers^{25,26}. The procedure involves a total of 4 steps (scheme 6): *a*) preparation of a S-2-pyridyl-substituted benzothiate; *b*) preparation of an unsymmetrical diacyl dipyrromethane by sequential acylation of a dipyrromethane with the S-2-pyridyl-substituted benzothiate obtained in step a; *c*) reduction of the diacyl dipyrromethane to the corresponding dipyrromethane-dicarbiniol using NaBH₄; *d*) condensation of the dipyrromethane-dicarbiniol with a new dipyrromethane followed by oxidation with DDQ to give the desired porphyrin. Although the yields for this type of reaction may vary from 15% to 40%, depending on the substituents on the *meso*-positions, the main advantage of this procedure is the absence of detectable scrambling in almost all cases. This greatly diminishes the usually extensive chromatography required for purification, and thus allows the production of significant quantities. Apart from the formation of ABCD-porphyrins, this rational synthesis can also be applied to the formation of A₃B-

trans-AB₂C-, cis-A₂B₂- and cis-A₂BC-porphyrins. The only drawback is, again, the availability of suitable dipyrromethane building blocks.



Linear tetrapyrroles (bilanes, bilenes or biladienes) can be cyclized to produce porphyrins (scheme 7)²⁷. This procedure involves the multi-step condensation of pyrroles, after which the cyclization of the tetrapyrroles takes place in the presence of a transition metal. This strategy is mostly used when there is a need to synthesize porphyrins that are asymmetrical and contain a variety of substituents at the β -position. The most common tetrapyrroles used for porphyrin synthesis are 1,19-dimethyl-a,c-biladienes and 1,19-dimethyl-b-bilenes.



Instead of preparing the porphyrin macrocycle from reactants that already contain functional groups, another possibility is to introduce functional groups on a preformed

porphyrin macrocycle. These functionalization reactions can be classified according to the reaction site on the porphyrin:

- reactions at the *meso*-position
- reactions at the β position

The *meso*- and β -positions of the porphyrin macrocycle have similar reactivity towards electrophilic substitution, so the selective introduction of substituents at the *meso*-positions commonly requires the use of β -substituted porphyrins. Formylation at the *meso*-position is one of the most common reactions, but nitration and halogenation reactions are also known. The same reactions can be performed to functionalize the β -position, but again, to avoid a mixture of products, the *meso*-positions should be protected. Also, the exocyclic double bonds of porphyrins will undergo addition reactions, providing another method for the introduction of groups at the β -positions. Oxidation of the β -position leads to the formation of 1,2-diols. Depending on the functional groups introduced at the β - and/or *meso*-positions of the porphyrin, further reactions can take place; these include intramolecular cyclization, functional group interconversions and functionalization of the phenyl groups of arylporphyrins.

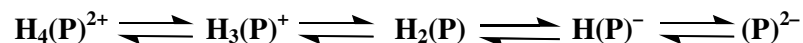
As is clear from the many different synthesis routes described above, there is not one perfect method to synthesize a specific porphyrin. The choice of the most convenient procedure depends heavily on the type of substituents required, as well as on the desired quantity needed.

1.2.2 Insertion of metal ions

Basically, the reaction between the metal ion and a porphyrinic compound consists of *a*) the formation of the equatorial MN_4 plane; and *b*) the completion of the axial coordination sphere. However, certain considerations have to be made concerning the metalation procedure:

1. The solvent for the reaction should be able to dissolve the porphyrin as well as the metal compound, but without coordinating the metal ion with high affinity in order to avoid competition with the porphyrin.
2. The porphyrin has to be deprotonated in order to produce the negative P^{2-} ion that is present in the metal-porphyrin complex. The presence of strong acids in

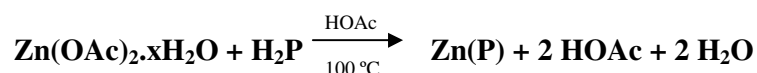
the reaction media will impede or even reverse metalation by shifting the protonation/ deprotonation equilibrium to the left.



3. To be able to react with the porphyrin macrocycle, the metal compound which carries the metal ion should dissociate, yielding an active (coordinatively unsaturated) species. Therefore, the metal complex should not be too stable otherwise it will not react with the porphyrin present in the reaction mixture. Other considerations are the availability, ease of handling, and solubility of the metal complexes in organic solvents.
4. After the incorporation of a metal ion with a positive charge greater than +2, it will bind one or more anions from the reaction medium to form a neutral species. Some metal ions prefer certain defined geometries, which require the addition of a neutral ligand (solvent, H₂O, O₂) to complete their coordination sphere.

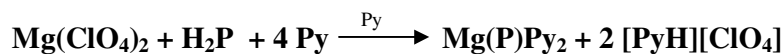
The methods commonly used for the insertion of metal ions in the porphyrin macrocycle are listed below. The systems are characterized either by the solvent or the metal carrier used, depending on the more essential component. Since metalloporphyrins have characteristic UV-VIS properties, the reaction is usually monitored by spectrophotometry.

The acetate method



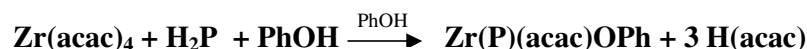
The acetate method includes all metalation reactions in which the protons of the porphyrin are transferred to acetate or propionate ions of the metal acetates/propionates. The solvents can be glacial acetic acid, or mixtures of CHCl₃/MeOH. This method can be applied to all divalent metals, except those which are unstable in acetic acid, and to some tri- and tetravalent metal ions. Often sodium acetate is added to further buffer the solution and to enhance deprotonation of the porphyrins. This method is considered the method of choice for the synthesis of manganese-porphyrin complexes.

The pyridine method



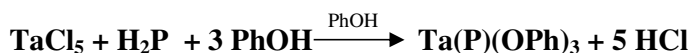
In those cases where the metalloporphyrin is very labile towards acids, the basic solvent pyridine is used for divalent metal ions. Pyridine is capable of dissolving the porphyrins as well as the metal salts, and the good complexing properties of pyridine allow the direct isolation of metalloporphyrin pyridinates. The same properties, however, impede the incorporation of metal ions with higher charges by forming pyridine complexes with the metal carrier, thus retarding the dissociation of the metal ion.

The acetylacetonate method



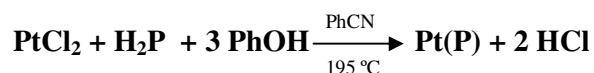
The advantages of metal acetylacetonates as metal carriers are the ready availability, good solubility in organic solvents, easy manipulation, and the weakness of the acid liberated. Their only disadvantage lies in the stability of the chelated coordination sphere when metal ions of high charge and small size are used. Therefore, in many cases weakly acidic solvents like phenol or imidazole are necessary to generate more labile metal carriers. Nevertheless, this method is the method of choice to incorporate metal ions belonging to groups IIIa, IIIb, the lanthanides, and the early transition metal group.

The phenoxide method



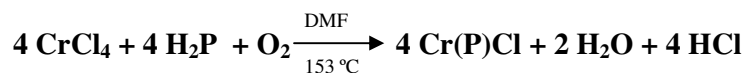
In some cases the acetylacetonates of early transition metals are missing. They can be incorporated using the metal oxides or chlorides in boiling phenol, as can acetylacetonates that are not reactive by themselves and need the phenoxides as intermediates. This method is especially recommended for the incorporation of Ta, Mo, W, and Re.

The benzonitrile method



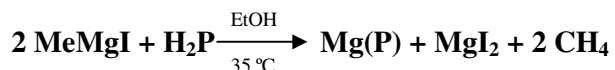
Benzonitrile dissolves porphyrins at its boiling point, it is weakly coordinating and basic, and the high temperature assists in dissociating the high molecular aggregates of some anhydrous metal halides that are otherwise unreactive or sparingly soluble. This method is excellent for Pd^{II}, Pt^{II} and Nb.

The dimethylformamide method



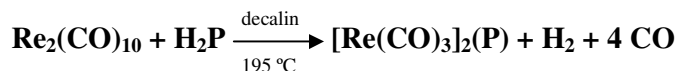
Weakly coordinating, high boiling oxygen-donor solvents such as dimethylformamide, tetramethylurea and sulfolan are excellent solvents for the metal carriers and porphyrins. The best results have been obtained with anhydrous metal chlorides (although they can be difficult to obtain and to handle), as the high boiling temperature forces the formed HCl to escape.

The metal organyl method



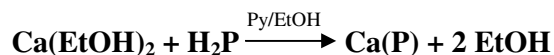
Metal alkyls are the ideal metal carriers. In most cases they are Lewis acids, thereby promoting association with the porphyrin nitrogen atoms, but at the same time they provide very strong bases that easily accept the protons from the porphyrin. The reaction can therefore take place at rather low temperatures. The only disadvantage of this method is the problem concerning the synthesis and manipulation of the air- and moist sensitive metal alkyls and the related metal halides.

The metal carbonyl method



In metal carbonyls some of the CO groups may be eliminated, resulting in a coordinatively unsaturated species. This species acts as a Lewis acid, attacking the lone pairs of the porphyrin nitrogen atoms. This method is especially useful for the preparation of porphyrins containing the metals of groups VI to VIII.

The metal alkoxide method



The very acid-labile metalloporphyrins containing Ca^{II} , Sr^{II} , Ba^{II} or alkali metal ions require a strongly basic medium.

Obviously, the choice of an appropriate metalation procedure depends strongly on the type of functional groups and/or substituents present on the porphyrin macrocycle, and their sensitivity towards strong reagents and high temperatures. Especially for porphyrins functionalized with biomolecules, a less aggressive method should be followed in order not to disrupt the molecular structure.

1.3 Applications of porphyrins

1.3.1 Porphyrins as scaffold

In many areas of organic, bioorganic and bioinorganic chemistry, small molecules are designed and synthesized to interact with large biomolecules such as proteins or DNA, or to perform and/or imitate certain enzymatic reactions. Whether the goal is to mimic a certain biological function or to design a potential new pharmaceutical compound, one of the major problems is reducing the flexibility of the new molecule, forcing it in the desired conformation. A rigid framework or scaffold is often used as a basic structure, upon which different substituents are introduced at the functional groups present on the scaffold. The use of macrocycles as scaffold is widely diffused, since their limited flexibility determines at least in part the orientation of the anchored molecules. Examples are cyclic peptides, peptide-based templates or organic macrocycles²⁸ (figure 7).

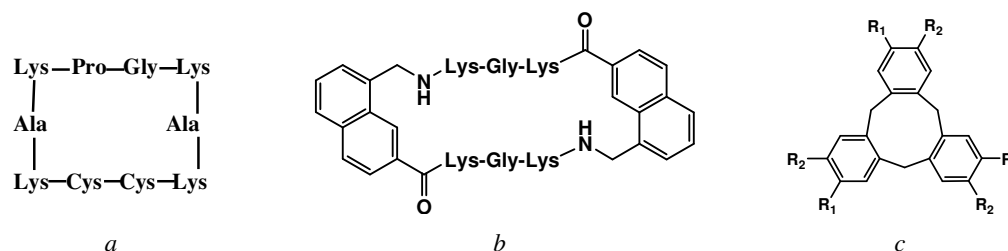


Figure 7: Examples of macrocyclic scaffolds: a) cyclic peptide; b) peptide based template; c) cyclotribenzylene, an organic macrocycle ($R_{1,2}$ = functional group).

The porphyrin macrocycle has several features that render it unique as potential scaffold²⁹:

- The rigidity of the porphyrin ring, allowing the design of a preorganized structure in which the groups anchored to the porphyrin framework display geometrically defined orientations.
- The spectroscopic characteristics of the porphyrin ring, allowing the detection of small changes in the interaction with other molecules using UV-VIS spectroscopy, circular dichroism, NMR, fluorescence and Raman spectroscopy.
- The presence of several distinct functionalization sites: the *meso* position, the β position and the inner nitrogens.
- The possibility to incorporate various metal ions inside the planar structure, with characteristic redox chemistry at both metal and ligand.

Due to their well-studied synthesis in combination with their many useful characteristics, porphyrins have found many applications in numerous research areas.

1.3.2 MRI and photodynamic therapy

Magnetic Resonance Imaging (MRI) is a non-invasive diagnostic technique, based on the generation of images of tissue hydrogen atoms (of water protons). To enhance the resolution of an MRI image, contrast agents are used, of which the unpaired electrons increase the velocity of relaxation of the water protons^{30,31}. Usually paramagnetic metals such as Gd^{III} and Mn^{III} are used in contrast agent preparations, because of their elevated number of unpaired electrons. Although high concentrations of manganese are toxic for the organism, Mn^{III} ions form strong chelates with porphyrins to give stable complexes with reduced toxicity. Synthetic tetraarylporphyrins incorporate the Mn ions tightly and are slowly metabolized; therefore they are good candidates for MRI. Several water-soluble metalloporphyrins have been developed as potential contrast agents for MRI and/or therapeutic purposes. Examples are Mn^{III} -TPPS (tetraphenylporphyrin sulphate)³² and ^{99m}Tc -CAP (cyclam acid porphyrin)³³.

Furthermore, it is known that several porphyrins and porphyrin derivatives can accumulate in malignant tumor tissue, even though the tumor-localizing activity of these compounds is not completely understood^{34,35,36}. Besides using tumor-selective agents for localization and characterization purposes (diagnostics), they can also be of great importance for photodynamic therapy (also called PDT, photoirradiation therapy, phototherapy, or photochemotherapy), the treatment of cancer using the combination of light with a photosensitizing drug in an oxygen-rich environment³⁷. Instead of light acting directly on tissue, a light-absorbing molecule (photosensitizer) is activated, upon which a photochemical reaction takes place. The photodynamic action is initiated by the absorption of a photon, bringing the photosensitizer in the excited singlet state, as shown in the Jablonski diagram (figure 8). From there, various relaxation processes are possible. The chromophore can relax back to the ground state by emitting a fluorescent photon [B], or to excited triplet states via intersystem crossing (ISC) [C]. From triplet excited states the chromophore can relax back to the ground state by emitting a phosphorescent photon [D] or transferring energy to another molecule via a radiationless transition [E]. Additionally, the chromophore can also lose energy through internal conversion or radiation-less transitions during collisions with other molecules [G]. In oxygenated environments the chromophore readily transfers its energy to

ground-state molecular oxygen ($^3\text{O}_2$) to produce singlet oxygen ($^1\text{O}_2$), which can form adducts with organic substrates $\text{S}(\text{O})$ [F]. This often results in oxidation and degradation of vital biomolecules and eventually cell death³⁸. Molecular oxygen thus plays a key role in propagation of the initial molecular damage. Ideally, a photosensitizer should display a high degree of selective accumulation in malignant tissue, in order to destroy the tumor tissue without effecting healthy tissues.

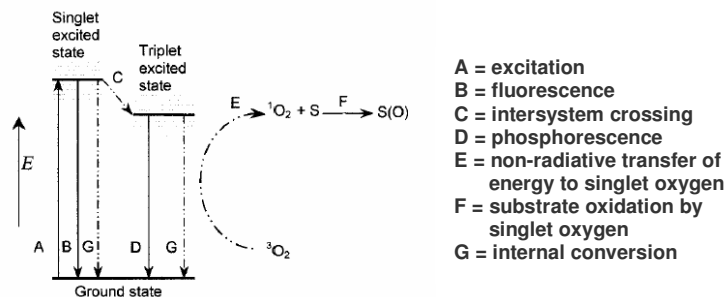


Figure 8: Jablonski diagram showing the various modes of excitation and relaxation in a chromophore.

Porphyrins, just as chlorins and bacteriochlorins, are very interesting as potential photosensitizers because, apart from their accumulation in tumor tissue, they are efficient singlet oxygen generators and have absorption maxima in the red portion of the electromagnetic spectrum (the Q-bands)³⁹. Red absorption maxima allow activating light to penetrate deeper into tissue. The most commonly used and studied porphyrin-based photosensitizer to date is Photofrin[®], a hematoporphyrin derivative⁴⁰. Clinically Photofrin[®] has exhibited no systemic toxicity and does not appear to be carcinogenic or mutagenic at the doses used. Photofrin[®] has been used successfully against a wide variety of cancers, does not appear to succumb to multidrug resistance, and Photofrin[®]-PDT has no known cumulative dose ceiling as do radiation and chemotherapy. New porphyrin-based compounds have been synthesized in an attempt to create new and better photosensitizers. Even though many of them are photodynamically more active than Photofrin[®], their pharmacological profile is usually less favourable and none of them have been legalized yet for clinical use.

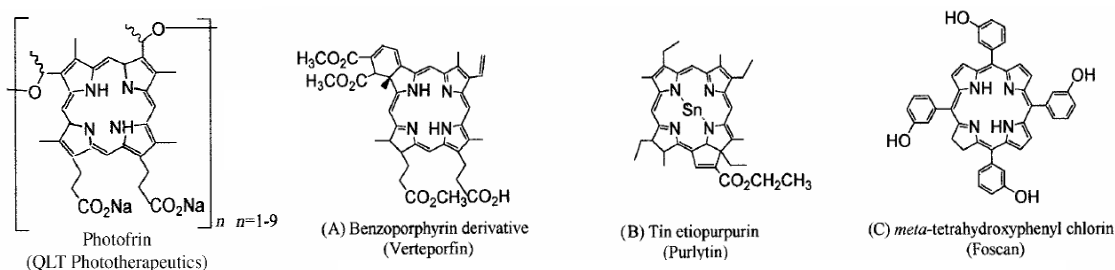


Figure 9: Structure of Photofrin[®] and new photosensitizers candidates.

1.3.3 Interaction with DNA

Chemical agents that bind and cleave nucleic acids are potentially useful as reagents for accessing structural and genetic information, as well as for development of efficient chemical nucleases. Such compounds may also be useful as drugs for treatment of cancer, genetic diseases, and viral infections. In general, free porphyrin bases and Cu^{2+} and Ni^{2+} complexes of meso-substituted cationic porphyrins are able to intercalate between the base pairs of the DNA (mostly at GC-rich regions), or bind in the minor groove by an outside binding mode (AT-rich regions). For Mn^{3+} , Fe^{3+} , Zn^{2+} , and Co^{2+} complexes of these porphyrins, intercalation is blocked due to the presence of axially bound ligands and only outside binding occurs (AT-rich regions)⁴¹. Upon activation with light, porphyrins such as *meso*-tetra-(4-*N*-methylpyridyl)porphyrin (T4MPyP, figure 10) and related analogues also display the ability to irreversibly cleave DNA^{42,43}.

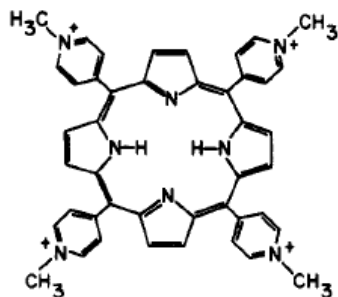


Figure 10: Structure of T4MpyP.

The high affinity of these complexes for DNA and their ability to cleave single strand as well as double strand DNA, combined with the many useful characteristics of the porphyrin macrocycle, makes them highly interesting as a starting point for the development of new chemical nucleases. Recently, new compounds consisting of a porphyrin-anthraquinone conjugate have been synthesized that display wavelength dependent photonuclease activity⁴⁴.

1.3.4 Molecular recognition

Molecular recognition, the ability of molecules to recognize and interact with each other, is a key element not only in many vital biological processes but also in current research areas, including drug design and synthesis, disease prevention, biomimetic chemistry, molecular catalysis, and the development of biomaterials and analytical sensors^{45,46}. A striking feature of many of these biological and abiological processes is the very high selectivity between the 'host' and 'guest' molecules. Porphyrins are very

attractive as potential sensors, since the binding of the analyte to a porphyrin (metal) center usually results in a detectable optical change, thus allowing a rapid analysis. Furthermore, the possibility to introduce polar groups on the hydrophobic surface of the porphyrin allows the use of the receptors in organic as well as aqueous media. The selectivity of the receptor can be increased by so-called multipoint recognition, where there is more contact area between host and guest and/or more interacting pairs of recognition groups. Once the first interaction has been established, the second and possibly even third interaction can take place easily. Multiple weak interactions are favoured over one strong interaction, because they result in high selectivity and fast association / dissociation kinetics. In case of a porphyrin receptor, the design of such a multipoint recognition is facilitated by the rigid framework, allowing the placement of suitable recognition groups on the periphery of the porphyrin macrocycle.

One of the research topics in this area has focused on the incorporation of synthetic porphyrins and metalloporphyrins into a variety of material matrices, and substantial work has been done in the areas of solution and gas phase sensing. Considering the well-understood ability of heme to bind a variety of gases, such as NO, CO₂ and O₂, porphyrins are a suitable choice for the detection of gaseous species. Other applications of porphyrins as chemical sensors, besides the straightforward recognition of metal ions, involve the recognition of small biomolecules, such as amino acids, oligopeptides, nucleotides, saccharides and other small organic compounds^{47,48}.

1.3.5 Super-molecular assembly of porphyrins

Super-molecular chemistry involves the assembly of organized entities, by means of the association of two or more molecular entities, for example through covalent bonds, electrostatic forces, or weak van der Waals interactions⁴⁹. Due to their attractive structural features as well as their structure-sensitive spectroscopic, photophysical and electrochemical properties, porphyrins, porphyrin analogues and their corresponding metal / metalloid derivatives provide an extremely versatile synthetic building block for a variety of materials applications⁵⁰. Synthetic multiporphyrin assemblies are mostly involved in materials science and nanotechnology (e.g. molecular-scale electronics, molecular wires, optical devices, sensors, data-storage)⁵¹. In particular, light-induced functions have attracted a great deal of interest, not in the least because of the potential of such aggregates to mimic the energy and electron transfer processes of the photosynthetic reaction center, providing better understanding of the photosynthesis.

The super-molecular structures can vary from dimers to trimers to entire networks of porphyrins, in which the repeating units can be linked by a variety of bonds. These linkers can be subdivided in three types: nonmetallic covalent linkers (e.g. carbon-nitrogen, carbon-oxygen, and carbon-carbon bonds), metal-ligand coordination⁵² (e.g., metal-oxygen and metal-nitrogen), and noncovalent linkers (e.g., hydrogen bonding, electrostatic, hydrophobic, hydrophilic, δ - δ , and van der Waals interactions)¹³. The linkages can be created between *meso*- or β - pyrrolic carbons of each porphyrin, or between the substituents at these positions. An infinite number of complicated, highly organized three-dimensional structures can be synthesized, of which a few are reported in figure 11 to show some of the many possible variations.

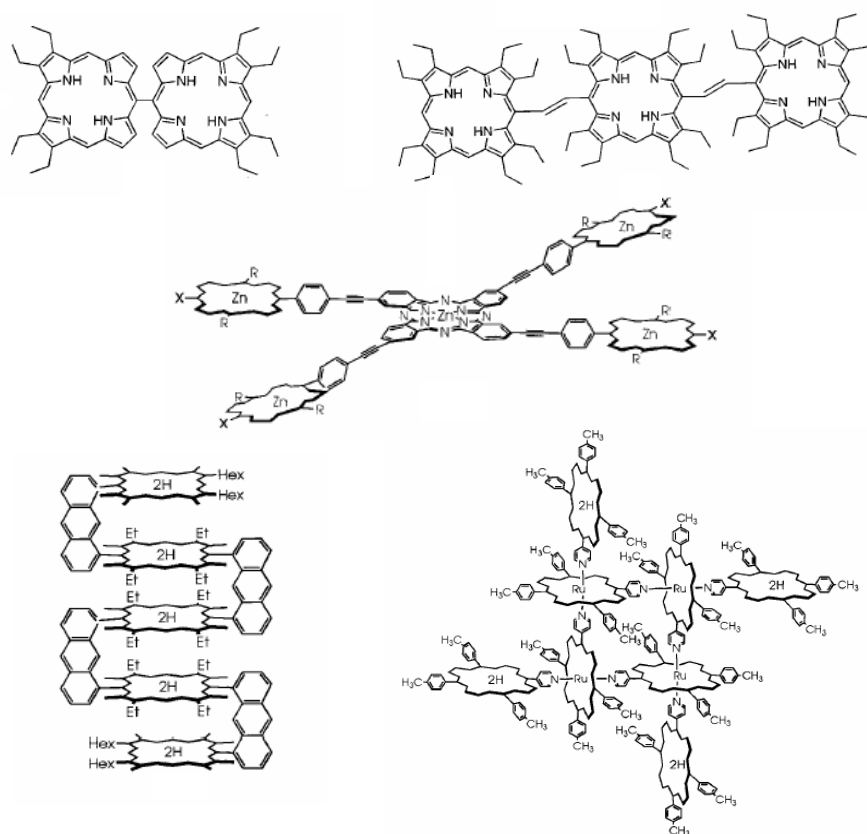


Figure 11: From dimer and trimer to highly organized three-dimensional porphyrin networks^{53,54,55,56,57}.

1.3.6 Porphyrins as templates in *de novo* design

The construction of novel proteins exhibiting functional properties similar to natural proteins represents one of the most challenging goals in biomimetic chemistry. The major problem is determining how to induce the desired three-dimensional structure in the polypeptide chain (the so-called ‘protein-folding problem’)^{58,59}. To overcome the potentially complex folding patterns available to a polypeptide, peptides with

predetermined secondary structures such as α -helices or β -sheets can be linked to a template⁶⁰. The result is a ‘template-assembled synthetic protein’ or TASP. Many porphyrin-based templates are known to induce an α -helical folding in certain amino acid sequences⁶¹. A commonly encountered motif in many proteins is the four helix bundle, found in native enzymes like ferritin, tobacco mosaic virus, myohaemerythrin, haemerythrin, cytochrome *c*, cytochrome *b562*, as well as in methane mono-oxygenase. Extensive research has been done to imitate this particular type of folding. The stabilizing effect of porphyrin structures on helical bundles does not solely stem from the axial ligation of coordinating histidines. It has been shown that hydrophobic interactions between the (hydrophobic) surface of the porphyrin and the hydrophobic face of the helices also stabilize hemoproteins^{62,63}. Examples are ‘helichrome’⁶⁴, consisting of four identical 15-residue peptide chains linked to the four propionic groups of coporphyrin I, designed to mimic the hydroxylase activity of cytochrome P-450, and ‘tetraphilin’, four 21-residue ion-channel forming peptides linked to a tetraphenylporphyrin, designed to serve as ion channel across the cell membrane (figure 12).

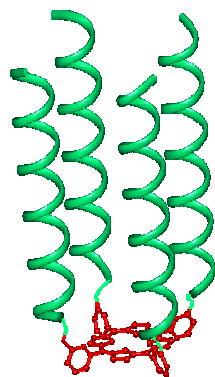


Figure 12: Tetraphilin, a porphyrin-template-induced four helix bundle.

1.4 Design of new porphyrin scaffolds

1.4.1 Tetraphenylporphyrins bearing functional groups

As basic structure for a new multifunctional scaffold that is to interact with biomolecules, we have chosen a tetraphenylporphyrin. This choice offers various advantages, among which the easy preparation and high stability of tetraphenylporphyrins, as well as the well-defined orientation of the substituents on the phenyl rings. The scaffolds bear from one to four functional groups (figure 13) on the para positions of the *meso* phenyl substituents, which is as far away from the porphyrin macrocycle as possible to avoid excessive steric hindrance in case of bulky substituents. Also, substitution on the para position has the advantage that the substituents occupy a defined position in space, whereas the orientation of the substituents on the ortho and meta positions are less defined due to rotation of the phenyl rings.

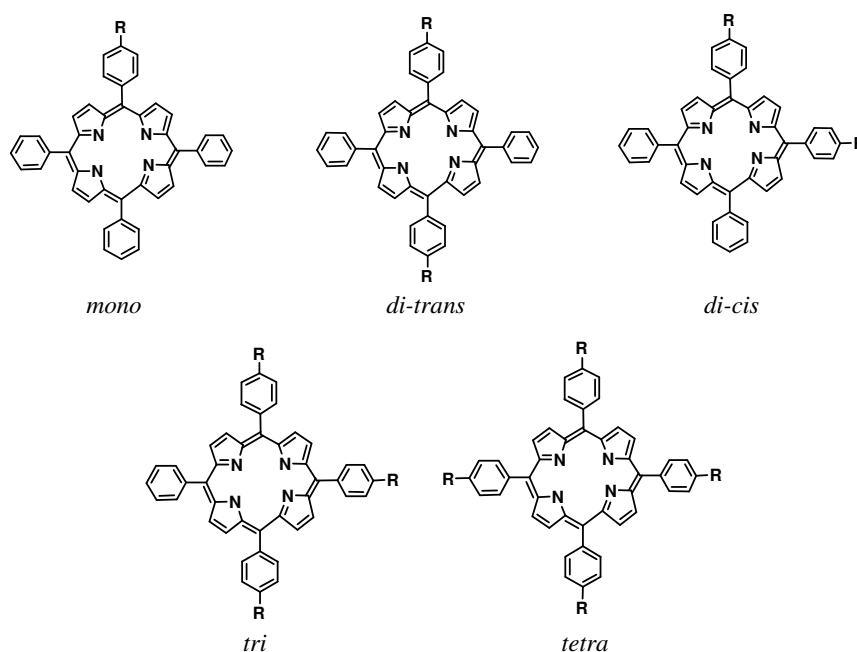


Figure 13: Tetraphenylporphyrin scaffolds bearing from one to four functional groups.

1.4.2 Choice of $-\text{CH}_2-\text{NH}_2$ as functional group

There are various characteristics that make the amine group extremely suitable as functional group on the porphyrin scaffold. First of all, the easy introduction of the $-\text{NH}_2$ group on the commercially available α -bromo-*o*-tolualdehyde using the well-known Gabriel synthesis makes it an excellent precursor in porphyrin synthesis. The

Gabriel synthesis consists of three steps: 1) the reaction of phthalimide with KOH removes the N-H proton giving an imide ion, a good nucleophile, 2) the nucleophilic substitution by the imide ion on the alkyl halide generates the intermediate, N-alkyl phthalimide, 3) hydrolysis or hydrazinolysis liberates the primary alkyl amine.

Since the object of these scaffolds is the functionalization with biomolecules, specifically with peptides, the presence of the amine groups is particularly useful because of the well-known coupling reaction with free carboxyl groups. Numerous activants are known for the formation of a peptide bond, but for these particular molecules the activation of the carboxyl group with N-hydroxysuccinimide in the presence of dicyclohexylcarbodiimide (DCC) appears to be the best choice (figure 14). Even though the activation reaction takes several hours, the activated peptide can be purified using HPLC, and stored for long periods of time at $-20\text{ }^{\circ}\text{C}$ without losing its reactivity^{65,66}. Also, the activated peptide is capable of reacting with the amine group even in presence of H_2O , while most activators, for example PyBop, HOBt, HATU, are de-activated in these conditions. Since porphyrins bearing amine groups tend to be quite hygroscopic, it is difficult to keep them in a completely dry environment.

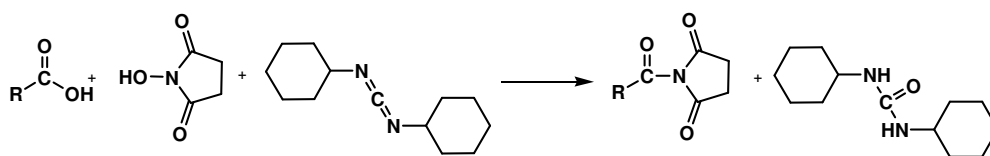


Figure 14: Activation of the carboxyl group of a peptide (R) with N-hydroxysuccinimide in the presence of dicyclohexylcarbodiimide.

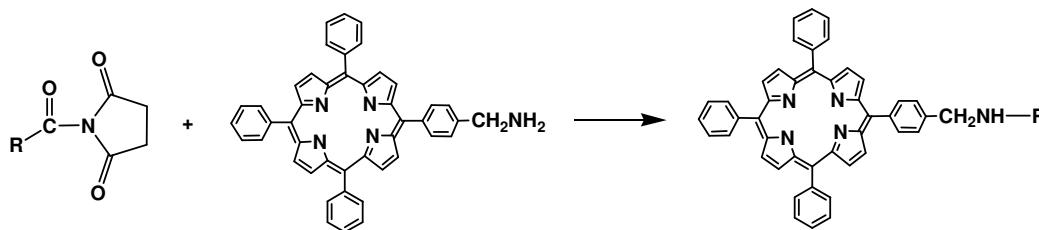


Figure 15: Reaction of the activated peptide with the amine group of the porphyrin scaffold

If the peptide is supposed to bind with the N-terminal end to the scaffold instead of the C-terminus, a carboxyl group can be easily introduced either on the scaffold or on the N-terminus of the peptide using an appropriate spacer. An example is the reaction of the amine group with succinic anhydride in the presence of pyridine (shown in figure 16).

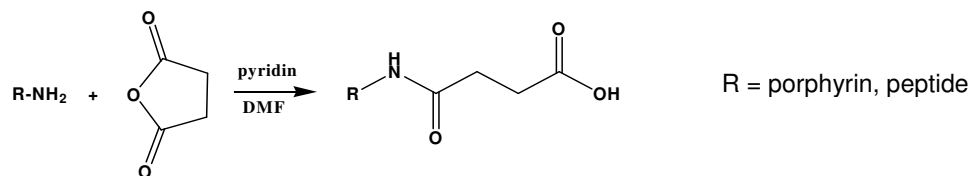
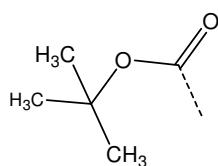


Figure 16: Reaction between the N-terminal of the peptide with succinic anhydride.

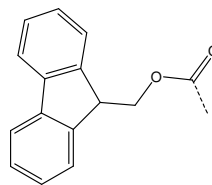
When the porphyrin scaffold is designed to carry different peptides, it can be opportune to temporarily protect the remaining free amine groups during the coupling reaction with the first peptide. Although it is possible to obtain a large amount of the desired peptide-porphyrin compound by adding a deficient amount of the peptide, it is almost impossible to overcome the formation of small amounts of di, tri, and even tetrakis substituted porphyrin. Since this reaction is irreversible and would thus signify loss of the peptide as well as the scaffold, a preventive protection of the orthogonal groups is advisable, with subsequent deprotection after the reaction with the peptide has taken place. In peptide synthesis, the most widely used protection groups of the amine function are Boc and Fmoc, because of their straightforward synthesis, introduction and deprotection (figure 17).



Boc

Introduction: Boc-O-Su in DIEA/DMF

Deprotection: 50% TFA in DCM



Fmoc

Introduction: Fmoc-O-Su in DIEA/DMF

Deprotection: 20% piperidine in DCM

Figure 17: Protecting groups for the amine function^{67,68}.

The choice of the protecting group depends on the peptide sequence, since it is advisable to avoid deprotection of other functional groups present in the sequence before finalization of the functionalized scaffold. For Fmoc-protected peptides a Boc protection of the scaffold is advised, and vice versa. The protection reaction takes place using Fmoc-O-Su or Boc-O-Su in DIEA, and usually produces a mixture of porphyrins, each containing a different number of protection groups. However, the desired porphyrin can be easily detected by mass spectroscopy and purified by HPLC or column chromatography. The protected scaffolds can easily be deprotected to obtain the original scaffold without loss of product, since the scaffolds are stable in both Fmoc and Boc deprotection protocols.

Chapter 2 Thrombin

2.1 Biological function of thrombin

2.1.1 The coagulation cascade

Blood coagulation involves a series of enzymatic reactions known as the coagulation cascade⁶⁹. In each of these reactions, an inactive pro-enzyme (also called coagulation factor) is converted to an active form, which then activates the next pro-enzyme in the series. The ultimate product of the coagulation process is thrombin, a highly specific serine protease of the chymotrypsin family. It is generated by proteolytic activation of the zymogen prothrombin, and plays a central role in the process of blood coagulation.

Initiation of coagulation (also known as the *extrinsic pathway* of blood coagulation) is triggered by tissue factor (TF), a non-enzymatic lipoprotein constitutively expressed on the surface of cells that are not normally in contact with plasma. Upon injury, platelets start to aggregate at the site of injury and tissue factor is exposed to blood, where it functions as a receptor for activated coagulation factor VIIa (FVIIa) that circulates in plasma at a very low concentration. The complex formed between TF and FVIIa will then activate FIX and FX to FIXa and FXa, respectively. Although FXa is a poor activator of prothrombin (also called coagulation factor II or FII), enough thrombin is generated to initiate a series of new activation steps. Thrombin converts a small amount of fibrinogen (factor I) into fibrin strands that start to ‘precipitate’, stabilizing the primary platelet plug bound to the site of injury. The initial phase of the coagulation system generates only a small amount of thrombin, which, however, is sufficient to initiate fibrin formation and to start several thrombin-mediated feedback activations.

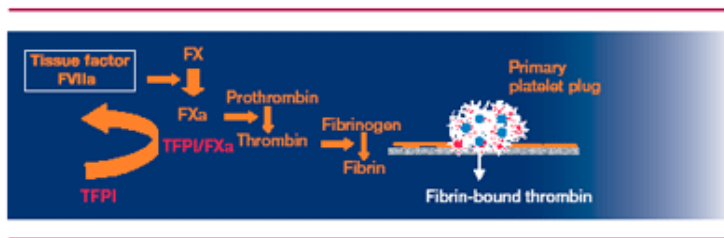


Figure 1. The **initiation phase** of coagulation which, in the final stage, generates fibrin, which reinforces the primary platelet plug. Tissue factor (TF) in the subendothelium is exposed and binds to and forms a complex with FVIIa that circulates in plasma. This complex can activate FX to FXa, which converts prothrombin (FII) to thrombin (FIIa). Thrombin cleaves fibrinogen into fibrin for clot formation. This part of the coagulation system is also known as the extrinsic pathway.

Thrombin generated during the initiation phase will then activate additional platelets and the coagulation factors V, VIII and XI. Activation of FV and FVIII is a very important step, as it will result in a huge amplification of thrombin generation. In order to localize thrombin generation to the site of injury, coagulation factor IXa (which has been activated by FXIa) is bound to phospholipids that are exposed on the membrane of activated platelets in the primary platelet plug. IXa on the platelet membrane will then bind to its cofactor, FVIIIa, and form the tenase complex that is a potent activator of FX. Thus, FX can be activated via two pathways, first during the early initiation phase by FVIIa/TF complex, and then during the amplification phase (previously known as the *intrinsic pathway*) by the tenase complex. Activated FX will also, like FIXa, bind to the platelet membrane and together with its cofactor, FVa, form the prothrombinase complex which is a much more potent activator of prothrombin than FXa alone. More than 90% of the thrombin that is formed during coagulation is generated via the action of the tenase and prothrombinase complexes.

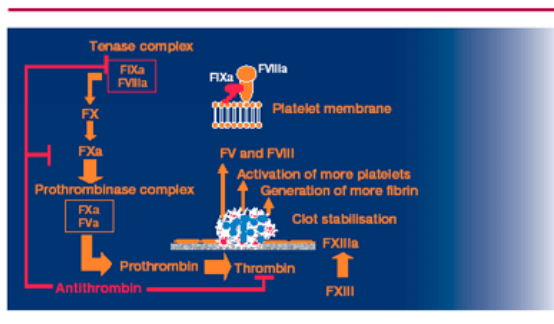


Figure 2. The **amplification phase** of coagulation: In this phase, a number of new platelets are recruited, via thrombin activation, to the primary platelet plug. At the same time, thrombin generation is sharply amplified when the thrombin that was produced during the initial phase activates new coagulation factors in the amplification loop (FXI, FVIII and FV).

In addition to fibrinogen activation, thrombin converts factor XIII to factor XIIIa, a highly specific transglutaminase that introduces cross-links composed of covalent bonds between the amide nitrogen of glutamines and the ϵ -amine group of lysines in the fibrin monomers, thus reinforcing the initial fibrin clot.

2.1.2. Reaction of thrombin with fibrinogen

The main function of thrombin in the coagulation cascade is the conversion of soluble fibrinogen to insoluble fibrin, thus forming a clot. The reaction between thrombin and fibrinogen is highly selective, as thrombin cleaves only 4 of the present 376 Arg/Lys-Xaa peptide bonds. Fibrinogen consists of three pairs of polypeptide chains $[(A\alpha, B\beta, \gamma)_2]$

covalently linked by disulfide bonds, and has a molecular weight of approximately 340 kDa. Thrombin converts fibrinogen to fibrin monomers by cleaving fibrinopeptides A (16 amino acid residues) and B (14 amino acid residues) from the N-terminal ends of the A α and B β chains, respectively. Removal of the fibrinopeptides allows the fibrin monomers to form a gel consisting of long polymers.

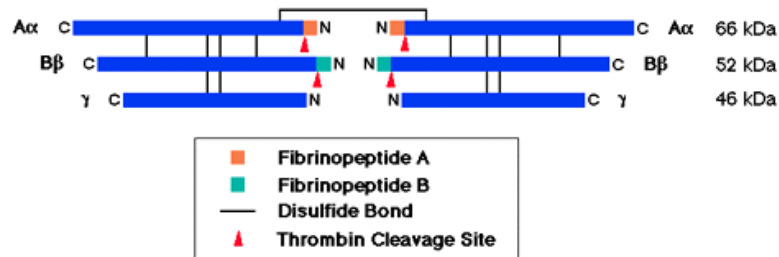


Figure 3: Structure of fibrinogen

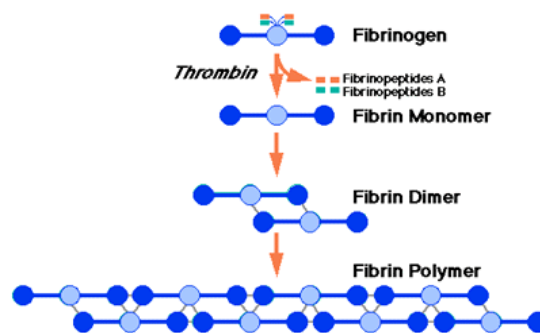


Figure 4: Fibrin polymerization

Besides the conversion of fibrinogen to fibrin, thrombin also initiates further reactions that are of importance for blood coagulation⁷⁰. It activates the clotting factors V and VIII required for prothrombin conversion and factor XIII, which stabilizes the formed fibrin clot⁷¹. Furthermore, thrombin induces the aggregation of platelets and is shown to have direct effects on the vascular endothelium and to mediate other nonhemostatic cellular events. Therefore, the inhibition of thrombin represents an effective interference in the coagulation process.

2.1.3 Regulation of the coagulation cascade

The coagulation system is regulated by the action of two endogenous plasma inhibitors:

- TF pathway inhibitor (TFPI) inhibits the action of FXa via formation of a TFPI/FXa complex. This complex can also inhibit the TF/FVIIa complex, whereby the first step in the coagulation cascade is blocked.
- The second inhibitor is antithrombin III (AT or ATIII), which despite its name is also a potent inhibitor of FXa. Antithrombin is a protein synthesized by liver and endothelial cells which binds and directly inactivates thrombin and other serine proteases (factors IXa, Xa and XIa). The uncatalyzed reaction between the serine proteases and AT is relatively slow. The serine proteases still have time to generate thrombin and fibrin before becoming inactivated. However, in the presence of heparin or similar sulphated glycosaminoglycans, the reaction between AT and the serine proteases is virtually instantaneous resulting in the immediate blockage of fibrin formation. Normal endothelial cells express heparan sulphate (a sulphated glycosaminoglycan). Upon binding to this glycosaminoglycan, AT is able to inactivate any nearby serine proteases, thus preventing the formation of fibrin clot in undamaged areas. In the presence of heparin, thrombin is the primary target of AT.
- Finally, coagulation and thrombin generation are also regulated by thrombin itself. Thrombomodulin (TM) is an endothelial cell protein that binds thrombin with high affinity. When thrombomodulin and thrombin form a complex, the conformation of the thrombin molecule is changed. This altered thrombin molecule now readily activates protein C to activated protein C (APC) and loses its platelet activating and protease activities. Protein C, together with its cofactor protein S, inhibits the formation of factors Va and VIIIa. Therefore, the binding of thrombomodulin to thrombin converts thrombin from a tremendously potent procoagulant into an anticoagulant. This is important in the normal physiological state because normal endothelial cells produce thrombomodulin that binds any circulating thrombin, thus preventing clot formation in undamaged vessels. APC finally degrades FVa and FVIIIa into inactive forms (FVai and FVIIIai) and the formation of tenase and thrombinase is terminated.

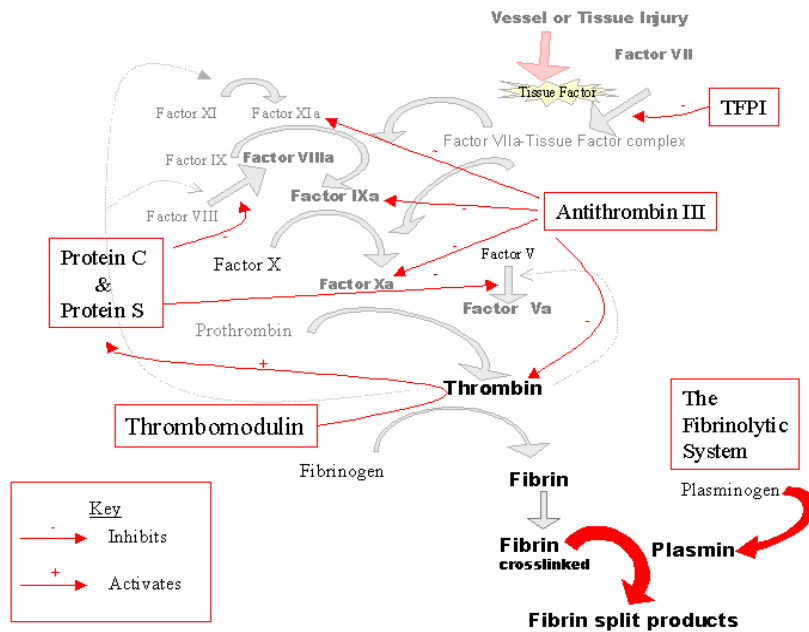


Figure 5: Regulation of the coagulation cascade

The fibrinolytic system is responsible for dissolving fibrin and the eventual removal of the blood clot⁷². In the presence of fibrin and an enzyme called tissue plasminogen activator (t-PA), the pro-enzyme plasminogen is converted to plasmin. Streptokinase and urokinase plasminogen activator are also able to catalyze this conversion. Formation of plasmin is strictly located to the thrombus as both t-PA and plasminogen are bound to lysine residues that are exposed on partially degraded fibrin in a clot. Plasmin breaks fibrin into small soluble fractions known as fibrin degradation products (FDPs). There are several types of FDPs, since plasmin cleaves at multiple sites in the fibrin structure. Like coagulation, fibrinolysis is also carefully regulated. Alpha-2-antiplasmin and alpha-2-macroglobulin are both proteins that bind to and inactivate plasmin.

At any stage in the life of a blood clot, the amount of clot depends on the balance between the activity of coagulation and fibrinolysis. Excessive fibrinolysis can lead to haemorrhage (uncontrolled bleeding), whereas insufficient fibrinolysis and/or excessive thrombin activity could cause thrombosis: the formation of a fibrin clot (thrombus) capable of obstructing normal blood flow. The three phases of the haemostatic system, platelet aggregation, coagulation and fibrinolysis, are also termed primary, secondary and tertiary hemostasis.

2.2 Structure of thrombin

2.2.1 α , β , γ thrombin

The predominant form of thrombin *in vivo* is its zymogen, prothrombin (factor II), which is produced in the liver. The concentration of prothrombin in normal human plasma is ~5-10 mg/dl. Prothrombin is a glycoprotein with a glycan content of ~12%. It is cleaved *in vivo* by activated factor X, releasing the activation peptide and cleaving thrombin into light and heavy chains yielding catalytically active α -thrombin. Alpha-thrombin consists of two peptide chains, where the A-chain of 36 amino acids is linked by a disulfide bridge to the B-chain consisting of 259 amino acids. Alpha-thrombin is known to undergo autolysis upon long-term storage or proteolysis by trypsin or other enzymes, resulting in less active forms. These proteolyzed forms of α -thrombin have been termed β -thrombin and γ -thrombin^{73,74}. β -thrombin is produced by the cleavage of the Arg-70 or the Arg-73 bond in the thrombin B-chain, whereas another form of proteolyzed thrombin, termed β' -thrombin, is formed by the single cleavage of thrombin at Arg-154⁷⁵. γ -thrombin is produced by proteolytic cleavage at both of these sites (Arg70/73 and Arg-154) in the B-chain. These cleavages cause the release of peptides that are no longer covalently attached to the thrombin molecule, but remain associated through ion exchange and gel filtration chromatography. However, eventually also β and γ -thrombin are degraded into smaller peptides. Only naturally occurring α -thrombin possesses the ability to clot fibrinogen and induce the aggregation of platelets, but the proteolyzed forms of thrombin retain their ability to cleave small synthetic substrates, suggesting the active site remains essentially intact within both β and γ thrombin⁷⁶.

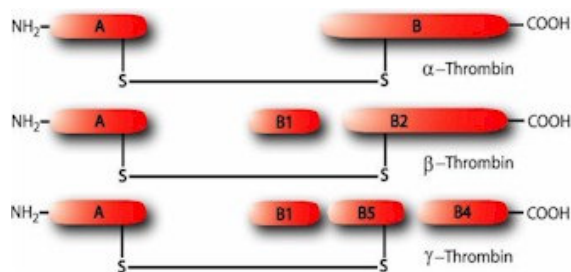


Figure 6: Proteolyzed forms of α -thrombin. The degradation of α -thrombin to less active forms, either by autoproteolysis or limited trypsin digestion, is illustrated above. β -thrombin is generated by cleavage at Arg-70/73 in the thrombin B-chain, giving rise to the B1 and B2 peptides. γ -thrombin is generated from β -thrombin by the additional cleavage at Arg-154 of the B-chain, giving rise to the B4 and B5 peptides from the B2 peptide.

2.2.2 Crystal structure of human α -thrombin

Serine proteases are proteolytic enzymes that all contain the characteristic serine-histidine-aspartate catalytic triad [Ser195, His57, and Asp102 in thrombin]. The hydroxyl group of the serine acts as a nucleophile, targeting the scissile amide bond of the substrate. Thrombin is a glycosylated trypsin-like serine protease and, like trypsin, cleaves peptide bonds involving basic amino acid residues, most often arginine. However, unlike trypsin, it exhibits a marked specificity in cleaving only a very limited number of bonds in macromolecular substrates^{77,78}. Although various three-dimensional models have been proposed for the thrombin B-chain based on sequence homology with bovine chymotrypsin and trypsin, the understanding of the specific and unique function of thrombin has been possible only since the determination of the first crystal structure in 1989 of the complex of α -thrombin with the specific inhibitor D-Phe-Pro-Arg chloromethylketone (PPACK)^{79,80}, and the subsequently obtained crystal structures of thrombin complexes with various other inhibitors and/or substrates⁸¹.

Thrombin can be described as an almost spherical molecule of approximate dimensions 45Å x 45Å x 50Å, where the A- and B-chain are not organized in separate domains but form a single body, in which the A-chain is arranged in a boomerang like shape against the B-chain globule. The B-chain exhibits the characteristic polypeptide fold of trypsin-like serine proteases, consisting essentially of two interacting six-stranded barrel-like domains of five helical segments, one helical turn and various surface-located turn structures. Though absent in other serine proteases, the A-chain, containing several turns and a helical segment at the C-terminal, resembles the propeptide of chymotrypsinogen and is similarly not involved in substrate and inhibitor binding. Because of the homology with the chymotrypsinogen sequence, the thrombin amino acid residues have been numbered according to the chymotrypsin sequence numbering. Insertion of amino acid residues is indicated by alphabetical subscripts. Also, for a better understanding of the various regions of the thrombin molecule, the amino acid residues of the substrate or inhibitor are named in respect to the peptide bond that is cleaved by the enzyme⁸². The residues on the N-terminal end of the cleavage site are indicated with P1, P2, P3, etc, whereas the residues on the C-terminal end are defined P1', P2', P3'. Consequently, the regions of the thrombin surface that interact with the respective residues are named S1, S2, S3 and S1', S2', S3'.

The most remarkable difference with trypsin and chymotrypsin, apart from several inserted residues forming specific bulges or loops on the surface, lies in the high

number of charged residues, many of which are involved in internal as well as surface located salt-bridges. The negatively and positively charged residues are not distributed uniformly over the entire molecule, but are clustered to form a sandwich-like electric field distribution where the positive charges are mostly concentrated at two poles, whereas the negative charges are found in a ring-like arrangement, particularly around the active site. Furthermore, the catalytic site of human thrombin is deeper and more prominent than the trypsin catalytic site, due to the presence of two loops, the relatively rigid Trp^{60D} loop and the slightly more flexible Trp¹⁴⁸ loop. These loops physically restrict access to the active site pocket and stabilize interactions with appropriate substrates, thus explaining the exceptionally high specificity of thrombin for macromolecular substrates. In fact, mutants of human thrombin without the residues Glu¹⁴⁶-Trp¹⁴⁸ are definitely less specific in their interactions with serine protease inhibitors, emphasizing the fundamental role of this loop in substrate recognition⁸³.

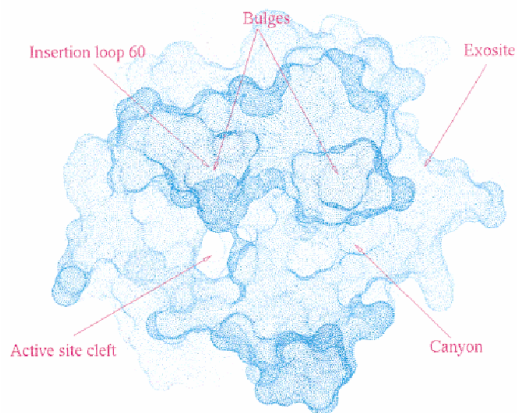


Figure 7: Connolly surface of human α -thrombin with indication of the major interaction sites.

Of the previously mentioned positively charged area's, the region around loop Lys⁷⁰-Glu⁸⁰ is of particular interest, containing nine positively charged residues in close proximity (Arg⁷³, Arg⁷⁵, Arg^{77A}, Arg³⁵, Lys^{149E}, Lys⁸¹, Lys¹¹⁰, Lys¹⁰⁹ and Lys³⁶). The overall positive charge is only partially compensated by the presence of the negative charges of two Glu residues, Glu⁷⁷ and Glu⁸⁰, just beneath the surface. This region, also called exosite 1 or fibrinogen recognition site, not only binds fibrin and fibrinogen but is also known to bind negatively charged parts of several thrombin inhibitors such as hirudin and thrombomodulin, as well as the thrombin receptor. The electrostatic attraction makes sure the reactive (positively charged) domain of fibrinogen is in the right orientation to enter the catalytic site. The second positively charged region is centered around the residues Arg⁹³, Arg¹²⁶, Lys²³⁶ and Lys²⁴⁰, including the basic

residues Arg⁹⁷, Arg¹⁰¹, Arg¹⁶⁵, Lys¹⁶⁹, Arg¹⁷³, Arg¹⁷⁵, Arg²³³ and Lys²³⁵. In this region there are no negatively charged residues present below the surface to counteract the very strong positive electrostatic field. This site is also called the heparin-binding site, as it seems to be particularly suited to bind polyanions like the glycosaminoglycan heparin, a known thrombin inhibitor. Another interesting region in the human thrombin structure is the RGD segment (Arg¹⁸⁷-Gly¹⁸⁸-Asp¹⁸⁹) beneath the specificity pocket, that probably plays an important part as docking site in platelet binding through the platelet specific integrin receptor GPIIb/IIIa.

The complex of thrombin with the specific inhibitor D-Phe-Pro-Arg chloromethylketone has provided detailed information on the thrombin catalytic site. Analysis of the crystal structure of thrombin-PACKK complex shows the interaction of the S1-S3 sites of the enzyme with the various residues of the tripeptide inhibitor to be in an antiparallel fashion. The primary specificity site S1 of the enzyme, Asp¹⁸⁹, forms a salt bridge with the basic residue in position P1 of the inhibitor (Arg^{3'}) and is practically identical to the corresponding trypsin site, the only difference being the substitution of Ser¹⁹⁰ in Ala, which renders the active site slightly less polar. The S2 site consists of two hydrophobic regions, both capable of hosting non polar residues of medium dimensions. The first hydrophobic region, formed by the residues His⁵⁷, Ser²¹⁴, Leu⁹⁹, Tyr^{60A} and Trp^{60D}, accommodates the pyrrolidonic ring of P2 (Pro^{2'}), whereas the second region, consisting of residues Ile¹⁷⁴, Trp²¹⁵ and the peptide segment 97-99, is occupied by the benzylic side chain of P3 (D-Phe^{1'}). This second hydrophobic region, which is particularly adapted to accommodate aromatic residues, is usually called the aryl binding site to distinguish it from the first S2 site.

2.2.3 Specific binding of fibrinogen

Thrombin recognizes a number of natural substrates that are responsible for important physiologic functions. Its high specificity is controlled by residues within the active site, and by separate recognition sites located on the surface of the enzyme. As mentioned before, fibrinogen is the main substrate of thrombin. After removal of the fibrinopeptides A and B, the fibrin monomer remains and subsequently undergoes polymerization. The high specificity of thrombin for this substrate lies in the particular binding mode of fibrinogen to thrombin. The exosite 1 (also called fibrinogen recognition site) is the regulator of thrombin specificity and is believed to direct the reactive domain of the substrate to the active site of thrombin by electrostatic interactions. In fact, the positively charged exosite 1 interacts with the negatively

charged C-terminal end of fibrinogen, as shown in figure 8. Besides interacting with fibrinogen, the exosite 1 is known to interact with numerous thrombin substrates, including FVIII, FV and the thrombin receptor. Other interactions with exosite 1 mediate anticoagulant functions.

The crystal structure of the complex of thrombin with a fibrinopeptide A analogue shows that the N-terminus of this peptide folds in a compact manner, bringing together hydrophobic residues so they can interact with the apolar region S2⁸⁴. In fact, fibrinogen residue Phe⁸ occupies the aryl-binding site of thrombin, adjacent to fibrinogen residues Leu⁹ and Val¹⁵ in the S2 subsite. The multiple hydrophobic interactions between fibrinogen and the thrombin surface provide an explanation for the narrow specificity of thrombin.

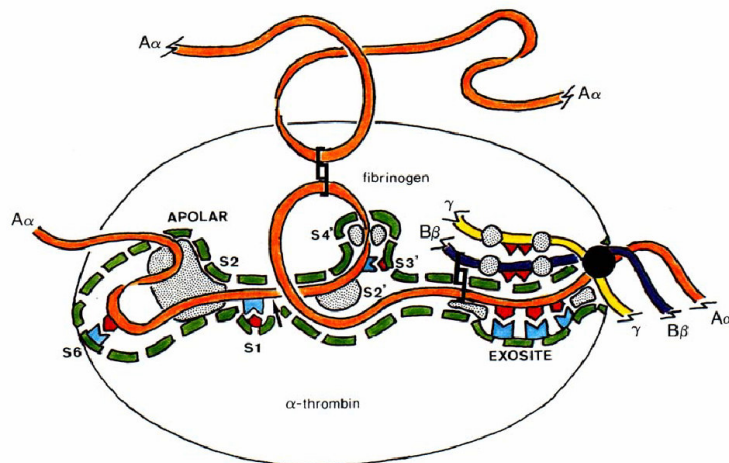


Fig. 8: Schematic diagram showing the major interactions of the fibrinogen A α chain (orange) with thrombin. The boundary of the active-site cleft is depicted by a green dashed line. Hydrophobic interactions are dotted, acidic groups are depicted by red and basic groups by blue. The cleavage point is marked by an arrow. The B β (blue) and γ (yellow) chains, linked by a disulphide knot (●) are shown in the neighbourhood of the fibrinogen-recognition exosite.

2.2.4 Thrombin and fibrin

Apart from binding fibrinogen, thrombin is also capable of specifically binding its product, fibrin, thereby limiting the amount of active protease that can reach the general circulation^{85,86}. Fibrin serves as a reservoir of active thrombin, and has therefore historically been termed antithrombin I. Upon fibrinolysis, the bound thrombin is released while retaining its clotting activity. Thrombin that is bound to fibrin is protected from inhibition by antithrombin and heparin cofactor II, and still capable of cleaving fibrinogen, thus maintaining local procoagulant activity. Also, it can amplify its own generation by activating factors V, VIII and XI. The fibrin-binding ability of thrombin is thought to serve several purposes⁸⁷. Clot forming is initially slowed, because the concentration of thrombin in solution is lowered. However, since most of the free thrombin is rapidly inactivated by several anticoagulant mechanisms, the bound thrombin secures a slow but constant activity around the site of injury. Degradation of the fibrin clot sets the bound thrombin free, resulting in new thrombin activity. The removal of the clot is therefore not rapidly, but slowly and gradually in order to avoid uncontrolled bleeding.

2.3 Natural inhibitors

2.3.1 Inhibitors of thrombin in the coagulation cascade

Generally speaking, serpins (*serine proteinase inhibitors*), a family of homologous, large (glyco)proteins, inhibit the action of their respective serine protease by mimicking the three-dimensional structure of the normal substrate of the protease. As a result, the serine protease binds the serpin instead of its normal substrate, blocking any further activity by the protease⁸⁸.

As mentioned before, the main direct inhibitors of thrombin in the coagulation cascade are thrombomodulin and antithrombin III. Other known inactivators are heparin cofactor II, protease nexin-1 and α 2-macroglobulins.

Of these inhibitors, antithrombin III (ATIII, also called heparin cofactor) is thought to be the most important physiological inhibitor of thrombin, even though it inhibits thrombin at a relatively slow rate. In fact, the glycosaminoglycans heparin and heparan sulphate accelerate the reaction by forming a trimolecular complex with thrombin and ATIII, thus increasing the inhibition rate at least a 1000-fold⁸⁹. The binding to heparin induces a conformational change in the inhibitor, which renders its reactive site arginine more accessible to the active center serine residue of thrombin⁹⁰. Despite the fact that this inhibitor is known as antithrombin III, it is known to inhibit also other enzymes of the coagulation cascade, specifically factor Xa and IXa. The same dependence on the presence of glycosaminoglycans has been seen for a second inhibitor, heparin cofactor II (HCII), although the affinity of heparin for HCII is about ten-fold lower than for ATIII and the binding mechanisms are slightly different⁹¹. However, HCII is unique among serine protease inhibitors in its ability to be activated also by dermatan sulphate. In the absence of a glycosaminoglycan, HCII inhibits chymotrypsin more rapidly than thrombin, and does not inhibit other trypsin-like proteases of the coagulation pathway. This protease specificity is probably due to the presence of a leucine residue at the P1 position of the reactive site, which is unusual for a thrombin substrate but seems to be essential for its inhibition of chymotrypsin⁹². The effective antithrombotic part of the heparin molecule is a pentasaccharide, crucial for the binding of antithrombin and for the fast anticoagulant activity of heparin. The heparin-inhibitor complex inhibits free circulating thrombin. Due to its large size, however, the complex is not able to inhibit thrombin that is already clot-bound.

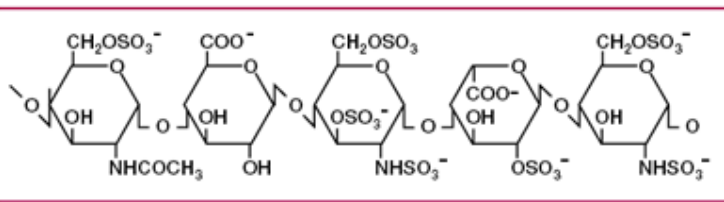


Figure 9: Structure of the pentasaccharide of heparin responsible for the binding to thrombin.

Protease nexin-1 (PN-1) is a potent inhibitor of serine proteases present in vascular cells, and forms complexes with trypsin, thrombin, plasminogen activators, and plasmin⁹³. PN-1 forms carboxylic ester links with serine proteases at their active site serine residues, a reaction that is characteristic of inhibitors in the antithrombin III/ α 1-antitrypsin family. Also, like antithrombin III, heparin and heparan sulphate bind PN-1 with high affinity, thus accelerating its binding to and inhibition of thrombin. A difference between these two proteases however lies in their site of action, whereas antithrombin III is active in plasma, PN-1 appears to be active mostly in non-vascular tissues⁹⁴.

Thrombomodulin is an endothelial cell surface glycoprotein that forms a 1:1 complex with thrombin. Binding of thrombin to this high-affinity receptor alters its specificity toward several substrates⁹⁵. The key contacts with thrombin are hydrophobic interactions between the side chains of residues Ile⁴¹⁴ and Ile⁴²⁴ of thrombomodulin and the hydrophobic pocket on the thrombin surface⁹⁶. A thrombin-thrombomodulin complex activates protein C approximately 1000-fold faster than thrombin alone. Activated protein C, together with cofactor protein S, degrades clotting factors Va and VIIIa, thus interfering in the coagulation cascade.

The α 2-macroglobulins are known to inhibit α - as well as β -thrombin⁹⁷. Besides being able to bind and inactivate thrombin, α 2-macroglobulins are also capable of inducing the degradation of the subchains of fibrinogen. This fibrinolytic activity results in the formation of products whose structure resembles that of circulation fibrinogen catabolites⁹⁸.

2.3.2 Hirudin

Several natural anticoagulant agents have been found in haematophagous (blood-sucking) parasites such as leeches and ticks, since they require to maintain blood fluidity during feeding and digestion. Hirudin, isolated from the salivary gland of the medicinal leech *Hirudo medicinalis*, is found to be one of the most potent natural

inhibitors of thrombin ($K_i = 0.3 \text{ pM}$), and certainly the most widely studied. Hirudin is a polypeptide of 65 amino acids that selectively binds thrombin in a 1:1 fashion, at the catalytic site as well as the fibrinogen recognition site. Because of the specificity of binding, hirudin does not inhibit other enzymes in the coagulation or fibrinolytic pathways, such as factor Xa, factor IXa, kallikrein, activated protein C, plasmin or tissue-type plasminogen activator. In contrast to heparin, hirudin: a) does not require antithrombin as a cofactor, b) is not inactivated by anti-heparin protein, c) has no direct effect on platelets, and d) is also capable of inactivating thrombin bound to clots or to subendothelium.

Structural studies indicate that this inhibitor is composed of a compact N-terminal region, including residues 1-47 and cross-linked by three disulfide bridges, and a flexible negatively charged C-terminal tail that binds to the positively charged fibrinogen recognition site (exosite I) of thrombin^{99,100}. The N-terminal domain covers the active site of thrombin and through its first three amino acids extensively penetrates into the specificity pockets of the enzyme, forming a parallel β -sheet with thrombin segment Ser²¹⁴-Gly²¹⁹. The formation of the parallel β -sheet by the N-terminal residues is the most remarkable feature of this particular binding, as opposed to the antiparallel binding fashion of fibrinogen and most thrombin inhibitors¹⁰¹. Also of great importance are the non-polar interactions with the hydrophobic regions of the thrombin surface, especially of the aromatic ring of Tyr³ that is buried in the aryl binding site. The many hirudin analogues that have been synthesized, containing one or more modified residues, have proven the importance of the N-terminal region¹⁰². In fact, the N-terminal tripeptide makes approximately half of the total contacts observed for the binding of fragment 1-47 to thrombin¹⁰³. The residues of the compact core, from Cys⁶ to Lys⁴⁷, make only few contacts with thrombin when compared with the N- and C-terminal segments¹⁰⁴. Of this central region, only 10 residues interact with the thrombin surface, with a total of 56 interactions. In contrast, the N-terminal pentapeptide and the C-terminal tail are involved in 47 and 93 interactions with thrombin, respectively.

The particular and highly specific binding mode of hirudin has been of great importance in the design of new, low molecular weight thrombin inhibitors.

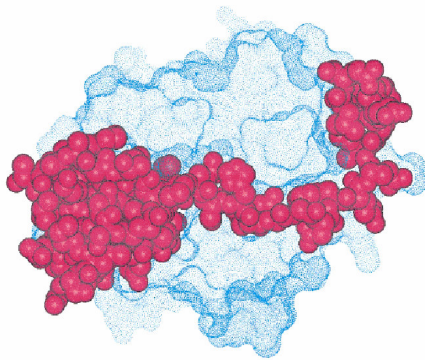


Figure 10: Interaction mode of hirudin (variant 2, Lys⁴⁷) with human α -thrombin, as obtained by X-ray analysis (PDB code 4htc). The thrombin Connolly surface is displayed in blue.

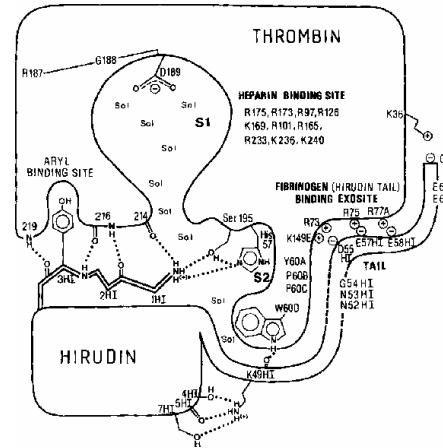


Figure 11¹⁸: Schematic representation of the thrombin-hirudin complex. The three N-terminal residues (1HI - 3HI) align with thrombin segment Ser²¹⁴-Gly²¹⁹ through formation of a parallel β -sheet. The reactive Ser¹⁹⁵ is not blocked and the specificity pocket is filled with water molecules. The C-terminal tail loops around the characteristic thrombin insertion loop (Tyr^{60A}- Trp^{60D}) and binds to the fibrinogen binding exosite of thrombin via several salt bridges.

2.3.3 Haemadin

Haemadin, a 57-amino acid peptide first identified in the saliva of the land-living leech *Haemadipsa sylvestris*, is very similar to hirudin^{105,106}. The main difference between these two peptides lies in the binding location of their acidic C-terminal region¹⁰⁷: whereas hirudin binds to the exosite I of thrombin, haemadin binds to the heparin binding site or exosite II. Haemadin binds tightly to thrombin, and at physiological ionic strength is found to be a slightly stronger inhibitor of thrombin than hirudin. At infinite ionic strength, haemadin is even a six-fold stronger inhibitor, indicating that the formation of the human α -thrombin-haemadin complex is less dependent on ionic forces than it is for the human α -thrombin-hirudin complex. Like hirudin, haemadin binds to the active site of thrombin, with its N-terminus forming a parallel β -sheet with thrombin residues Ser²¹⁴-Gly²¹⁶. Additionally, haemadin makes many other contacts with the active site, including a salt bridge between Arg²⁷ and Asp¹⁸⁹ of thrombin in the S1 pocket. The compact core of haemadin (residues 10-37) makes further interactions mainly through its A and C loops with the 60- and 96-loops of thrombin, while the acidic C-terminal tail covers the heparin binding site of thrombin (exosite II). As hirudin, haemadin is a very specific inhibitor of thrombin as it does not inhibit other proteinases.

2.4 Synthetic inhibitors of thrombin

2.4.1 Synthetic inhibitors

Since thrombin is one of the central enzymes of the coagulation cascade, it is also the most desirable target for interference in the blood coagulation process. Comparison of various crystal structures of thrombin and its complexes with low molecular weight inhibitors has indicated that the active site region changes but little upon binding of different ligands. Thus the thrombin structure provides an ideal starting point for computer graphics aided molecular design of structure based antithrombotic agents.

Heparin and low molecular weight heparins (LMWH's) inhibit both thrombin formation and thrombin activity by the activation of the natural inhibitor antithrombin III. Heparin is the most widely used anticoagulant in the treatment and prevention of thrombotic disorders, but it has limitations that reduce its clinical efficacy and safety^{108,109}. The non-specific binding of heparin reduces its anticoagulant effect by binding to plasma proteins, platelet proteins, matrix proteins and endothelial cells, requiring constant monitoring of the patient to avoid undesired effects. Also, the heparin-ATIII complex is not able to inhibit thrombin bound to fibrin. Although the LMWH's are more specific and do not bind proteins and subendothelial surfaces to the same amount as heparin, they are still unable to access clot-bound thrombin. The intensive search for new, specific inhibitors of thrombin has led to the development of numerous synthetic inhibitors. These inhibitors can be divided into three distinct classes, based on their mechanism of action:

- Inhibitors of the catalytic site
- Inhibitors of the fibrinogen recognition site
- Multi-site inhibitors

To be useful in the treatment of thrombotic disorders, a thrombin inhibitor has to be specific as it should not interfere with the activity of other serine proteases, which often have a structural homology to thrombin. Hirudin, being a highly specific inhibitor of thrombin with a unique binding mode, is therefore usually a starting point in the development of new inhibitors.

2.4.2 Inhibitors of the catalytic site

Inhibitors of the catalytic site can be sub-divided in inhibitors of peptidic nature and inhibitors of non-peptidic nature. Inhibitors of peptidic nature can interact with the active site in a substrate mode, with their backbone antiparallel to the thrombin segment Ser²¹⁴-Glu²¹⁷, or in a non-substrate mode, in which their backbone is aligned parallel to this segment.

Of the inhibitors of peptidic nature, the tripeptide D-Phe-Pro-Arg-H and its derivatives are the most widely studied. This tripeptide binds to the catalytic site of thrombin in an antiparallel fashion, in which the side-chain of Arg^{3'} is covalently linked to S1 residue Asp¹⁸⁹, and residues Pro^{2'} and Phe^{1'} are found in the hydrophobic binding sites S2 and S3 respectively. The specificity of this short peptide for thrombin can be explained by the perfect fit of the three residues in the different sites the enzyme, resulting in a minor accessibility of the hydrophobic surface to the solvent as well as an optimal coupling between polar and charged residues. Although a very potent and selective inhibitor of thrombin, the peptide itself is rather unstable in neutral aqueous solution since it tends to cyclize and is thus inactivated. Therefore, numerous derivatives have been synthesized in which either the N- or the C-terminus is protected to prevent cyclization. The compound Boc-D-Phe-Pro-Arg-H is more stable than its parent peptide, but is less specific for thrombin since it inhibits plasmin as well. To maintain specificity, a series of N-alkyl derivatives have been synthesized of which the methyl derivative D-MePhe-Pro-Arg-H has been found to be a potent and selective inhibitor of thrombin. The tripeptide chloromethyl ketone D-Phe-Pro-Arg-CH₂Cl (PPACK) is one of the most widely known inhibitors, and its antithrombotic effects have been extensively studied. Other derivatives include D-Phe-Pro-Arg-CN and D-Phe-Pro-Arg-CF₃.

Peptides that bind in the parallel (hirudin-like) mode include BMS-186282 and BMS-189090¹¹⁰. Among the the inhibitors of non-peptidic nature, NAPAP¹¹¹, 4-TAPAP, 3-TAPAP¹¹² and MQPA¹¹³ all have inhibition constants in the nanomolar range.

2.4.2 Inhibitors of the fibrinogen recognition site

Inhibitors of the fibrinogen recognition site (exosite 1) have also been of great importance for the development of medicinal antithrombotics. These inhibitors block the binding site of fibrinogen, and thus inhibit its hydrolysis to fibrin. Since this type of inhibitor does not occupy the catalytic site, the enzyme retains the ability to cleave

small substrates¹¹⁴. The starting compound for most exosite-1 inhibitors is the C-terminal end of hirudin, more specifically the residues 53-65. Hirugen, N-acetyl-hirudin^{53'-64'} with sulfatoTyr⁶³, is a competitive inhibitor and has K_i values in the submicromolar range¹¹⁵. The desulfated hirugen still inhibits thrombin activity, but the binding affinity is decreased by an order of magnitude because the sulfate group is involved in an extended hydrogen bonding network utilizing all three sulfato oxygen atoms¹¹⁶. Derivatives of hirugen and of the C-terminal end of hirullin¹¹⁷, a hirudin-related protein, have been extensively studied to increase the inhibition potential of these exosite 1 inhibitors.

2.4.3 Multi-site inhibitors

Multi-site inhibitors of thrombin combine the characteristics of the previously mentioned inhibitors, and bind the catalytic site as well as exosite 1. Not only do they block the conversion of fibrinogen to fibrin, but they also inhibit thrombin's activity towards small substrates. These bifunctional inhibitors consist of an exosite 1 inhibitor linked by a flexible spacer to an inhibitor of the catalytic site, thus mimicking the interaction thrombin-hirudin. Hirulogs are a class of peptides in which an inhibitor of the catalytic site (the tripeptide D-Phe-Pro-Arg-H) and an inhibitor of exosite-1 (residues 54-64 of hirudin) are linked by a poly-glycine spacer^{118,119}. Various hirulogs have been synthesized, with different spacer lengths. The most promising inhibitor, hirulog1, presents a linker consisting of 4 glycine residues and has an inhibition constant in the nanomolar range. Hirutonins have a similar mechanism of binding, consisting of desolfo hirudin⁴⁵⁻⁶⁵ with amino acid modifications at the N-terminal end¹²⁰.

Hirunorms are peptide-based thrombin inhibitors consisting of 26 amino acids, rationally designed to mimic hirudins specific binding mode to thrombin¹²¹. The N-terminal end interacts with the thrombin catalytic site in a non-substrate manner, connected by a three amino acid spacer to the C-terminal end, which specifically binds the fibrinogen recognition site. The crystal structures of the hirunorm-thrombin complexes confirm that their inhibitor binding mode is distinctive of a true hirudin mimetic¹²². The most potent hirunorms, IV and V, have inhibition constants in the picomolar range.

Hirudin ^a	Hirunorm I	Hirunorm II ^b	Hirunorm III	Hirunorm IV	Hirunorm V
Ile ^{1'}	Ile ^{1'}	Ile ^{1'}	Ile ^{1'}	Chg ^{1'}	Chg ^{1'}
Thr ^{2'}	Arg ^{2'}	Arg ^{2'}	Arg ^{2'}	Arg ^{2'}	Val ^{2'}
Tyr ^{3'}	Tyr ^{3'}	Phe ^{3'}	Phe ^{3'}	2-Nal ^{3'}	2-Nal ^{3'}
Thr ^{4'}	Thr ^{4'}	Thr ^{4'}	Thr ^{4'}	Thr ^{4'}	Thr ^{4'}
Asp ^{5'}	Asp ^{5'}	Asp ^{5'}	Asp ^{5'}	Asp ^{5'}	Asp ^{5'}
	D-Ala ^{6'}	D-Ala ^{6'}	D-Ala ^{6'}	D-Ala ^{6'}	D-Ala ^{6'}
Globular Domain	β -Ala ^{7'}	Gly ^{7'}	β -Ala ^{7'}	Gly ^{7'}	Gly ^{7'}
	β -Ala ^{8'}	β -Ala ^{8'}	β -Ala ^{8'}	β -Ala ^{8'}	β -Ala ^{8'}
Pro ^{48'}	Pro ^{9'}	Pro ^{9'}	Pro ^{9'}	Pro ^{9'}	Pro ^{9'}
Glu ^{49'}	Glu ^{10'}	Glu ^{10'}	Glu ^{10'}	Glu ^{10'}	Glu ^{10'}
Ser ^{50'}	Asn ^{11'}	Ser ^{11'}	Ser ^{11'}	Ser ^{11'}	Ser ^{11'}
His ^{51'}	His ^{12'}	His ^{12'}	His ^{12'}	His ^{12'}	His ^{12'}
Asn ^{52'}	Asn ^{13'}	h-Phe ^{13'}	h-Phe ^{13'}	h-Phe ^{13'}	h-Phe ^{13'}
Asx ^{53'}	Asn ^{14'}	Gly ^{14'}	Gly ^{14'}	Gly ^{14'}	Gly ^{14'}
Gly ^{54'}	Gly ^{15'}	Gly ^{15'}	Gly ^{15'}	Gly ^{15'}	Gly ^{15'}
Asp ^{55'}	Asp ^{16'}	Asp ^{16'}	Asp ^{16'}	Asp ^{16'}	Asp ^{16'}
Phe ^{56'}	Phe ^{17'}	Tyr ^{17'}	Tyr ^{17'}	Tyr ^{17'}	Tyr ^{17'}
Glu ^{57'}	Glu ^{18'}	Glu ^{18'}	Glu ^{18'}	Glu ^{18'}	Glu ^{18'}
Glu ^{58'}	Glu ^{19'}	Glu ^{19'}	Glu ^{19'}	Glu ^{19'}	Glu ^{19'}
Ile ^{59'}	Ile ^{20'}	Ile ^{20'}	Ile ^{20'}	Ile ^{20'}	Ile ^{20'}
Pro ^{60'}	Pro ^{21'}	Pro ^{21'}	Pro ^{21'}	Pro ^{21'}	Pro ^{21'}
Glu ^{61'}	Aib ^{22'}	Aib ^{22'}	Aib ^{22'}	Aib ^{22'}	Aib ^{22'}
Glu ^{62'}	Aib ^{23'}	Aib ^{23'}	Aib ^{23'}	Aib ^{23'}	Aib ^{23'}
Tyr ^{63'}	Tyr ^{24'}	Tyr ^{24'}	Tyr ^{24'}	Tyr ^{24'}	Tyr ^{24'}
Leu ^{64'}	Leu ^{25'}	Cha ^{25'}	Cha ^{25'}	Cha ^{25'}	Cha ^{25'}
Gln ^{65'}	Glu ^{26'}	D-Glu ^{26'}	D-Glu ^{26'}	D-Glu ^{26'}	D-Glu ^{26'}

Table 1: Structure comparison of hirudin and hirunorms

2.5 Rational design of new thrombin inhibitors

2.5.1 Peptide-functionalized tetraphenylporphyrin as potential inhibitor

The most important interactions between hirudin and thrombin take place at the N- and C-terminal ends of hirudin, whereas its central part is mostly involved in hydrophobic interactions with the thrombin surface. This is shown by the development of many multi-site inhibitors of thrombin, of which the amino acids of the N-terminal part, responsible for the interaction with the catalytic site, are linked by an appropriate spacer to the amino acids of the C-terminal part, responsible for the interaction with exosite 1. Therefore, the replacement of the central part of the peptide-chain with a porphyrin scaffold should not have a large impact on the interaction with thrombin. The hydrophobic pocket that is present on the thrombin surface should be able to accommodate and interact with the porphyrin macrocycle. The porphyrin ring offers many advantages, of which the insertion of a (paramagnetic or radio-active) metal ion in its centre could be of great interest for diagnostic purposes. Although many synthetic inhibitors of thrombin are known, to the best of our knowledge no specific inhibitor of clot-bound thrombin has been developed that allows identification by non-invasive techniques, offering a unique chance to monitor and prevent excessive and possibly dangerous clot formation in the bloodstream. The binding to clot-bound thrombin is important not only to allow detection of fibrin clots, but also because the presence of thrombin circulating freely in blood is usually extremely low, and not enough to trigger a measurable response.

2.5.2 Design of new porphyrin-based thrombin inhibitors

Since hirunorms are considered the most potent synthetic thrombin inhibitors known, it has been a logical choice to use their amino acid sequence as template for the rational design of new thrombin inhibitors. Also, since the crystal structures of several thrombin-hirunorm complexes have been obtained and the specific binding mode of the hirunorms to thrombin has been extensively studied, computer graphics programmes can be of great help in the molecular design of new inhibitors. From the hirunorms I-V synthesized so far, hirunorm IV is proved to be the strongest inhibitor of thrombin, having an inhibition constant K_i in the picomolar range. The three amino acid sequence at the N-terminus (H-Chg-Arg-2Nal-), responsible for the interaction with the catalytic site, has therefore been left unaltered. Starting from the crystal structure of the

thrombin-hirunorm IV complex, the tetrakis(*p*-(aminomethyl)phenyl)porphyrin has been introduced by the formation of a peptide bond between the carboxyl group of the N-terminal tripeptide and one of the porphyrin amine groups. It was observed that the fibrinogen recognition site was accessible from the *cis* position as well as from the *trans* position. Therefore, two new potential inhibitors have been proposed, the structures of which are shown in figure 12. Both inhibitors have the same amino acid sequence at the N-terminus, but differ in the peptide sequence that is supposed to interact with the fibrinogen recognition site.

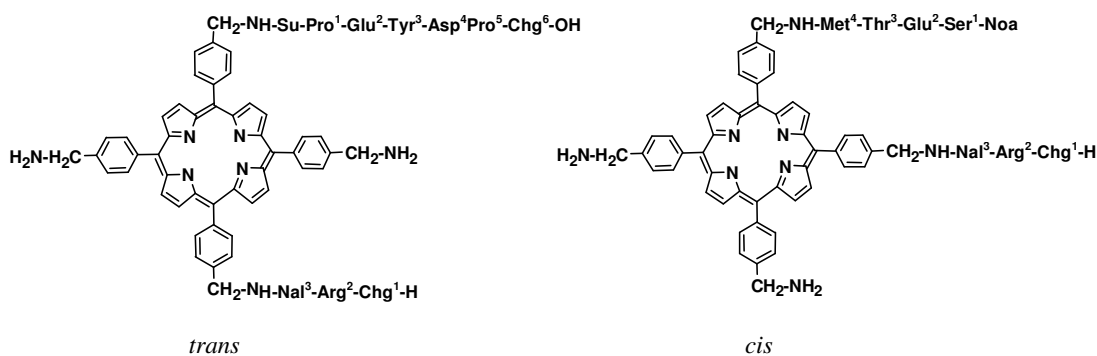


Figure 12: Structures of the newly designed porphyrin-based potential inhibitors of thrombin.

The tripeptide H-Chg-Arg-Nal- is supposed to interact with the catalytic site just like hirunorm IV: The backbone of the tripeptide forms a short β -strand parallel to thrombin main-chain residues Ser²¹⁴-Gly²¹⁹, with the Chg¹ side chain filling the S2 subsite, Arg² located at the entrance of S1, and the 2-Nal³ side chain occupying the aryl binding site. In case of the *trans* porphyrin, residue Trp¹⁴⁸ (shown in figure 13) is involved in hydrophobic interactions with the porphyrin macrocycle. Also, one of the free amine groups has ionic interactions with Glu¹⁹², occupying the position of a water molecule in the original crystal structure. For the *cis* porphyrin these interactions are absent, as the porphyrin is positioned slightly outside the hydrophobic pocket present on the thrombin surface. Since the *trans* amine group is positioned further away from the exosite, the peptide H-Glu-Tyr-Asp-Pro-Chg-OH, interacting with the fibrinogen recognition site, is linked to the porphyrin by a spacer consisting of the segment HO-Succ-Pro-OH. The presence of succinic acid has a double function as it also serves to introduce a carboxy group on the N-terminal end of the peptide for the formation of a peptide bond with the porphyrin scaffold. The second peptide of the *cis* inhibitor is linked to the porphyrin scaffold by its C-terminal end, therefore an additional spacer is not required.

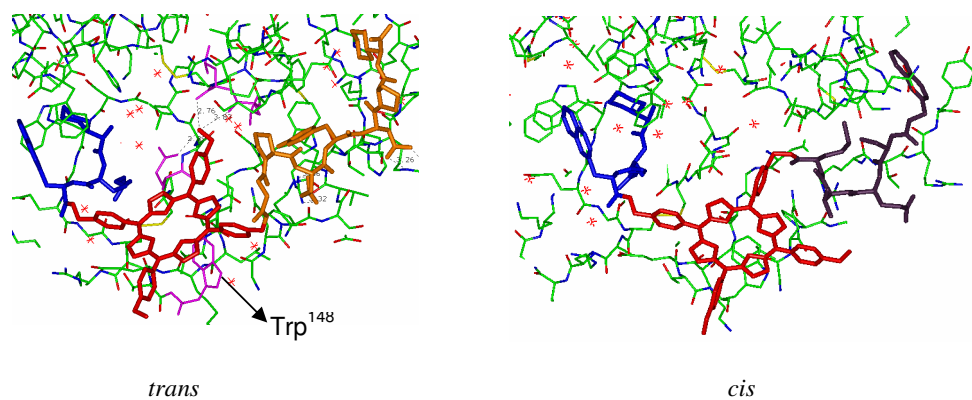


Figure 13: Specific interactions of the newly proposed inhibitors with the thrombin catalytic site and exosite 1. For the *trans* inhibitor: In pink the residues of particular interest for the binding of the inhibitor.

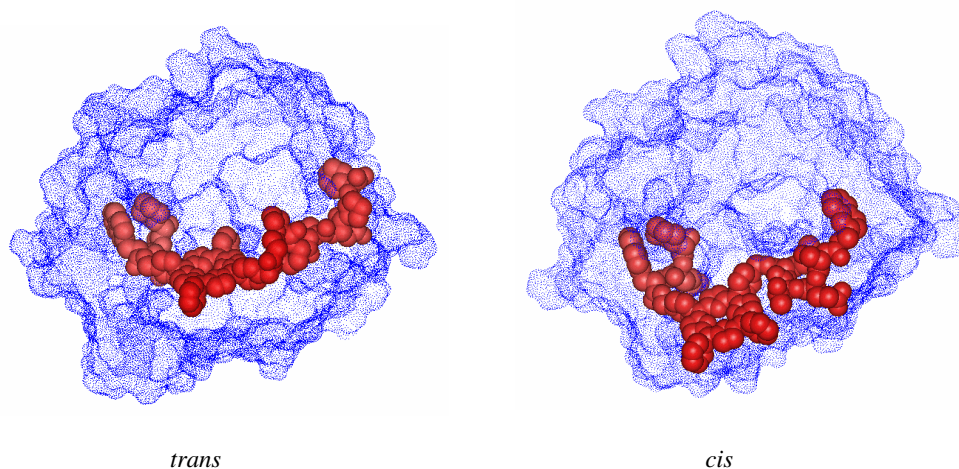


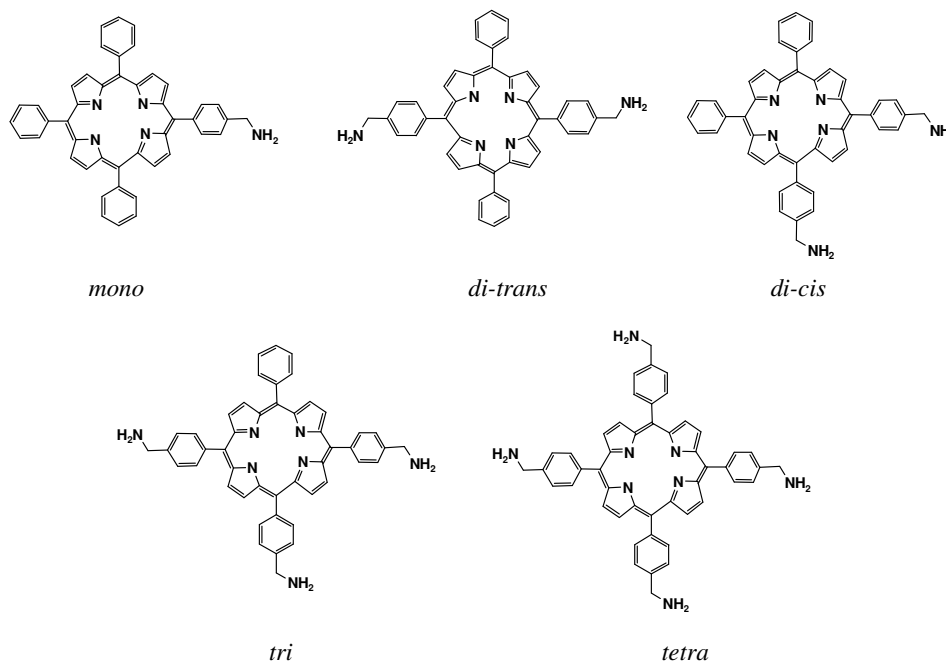
Figure 14: Space-filling model of the newly proposed inhibitors on the thrombin Connolly surface. For clarity the free aminomethyl groups on the porphyrin ring are omitted.

Both inhibitors were designed with TAMPP as starting compound, but can also be synthesized using the *cis* and *trans* disubstituted tetraphenylporphyrins discussed in paragraph 1.4.1, which lack the presence of additional free amine groups.

Chapter 3 Synthesis of the tetraphenylporphyrin scaffolds

Introduction

The following porphyrin scaffolds were synthesized, presenting from one to four aminomethyl groups on the *para* positions:



The porphyrins, containing different numbers of functional groups, were initially synthesized using the mixed aldehyde condensation discussed in paragraph 1.3.1, by the reaction of benzaldehyde and 4-(formylbenzyl)phthalimide with pyrrole in the presence of TFA. Since our interest lies specifically in the *cis* and *trans* di-functionalized porphyrins, two other strategies have been attempted, to enhance the overall yields of these porphyrins. For the *trans* porphyrin, a 2+2 condensation of dipyrromethanes has been applied, by reacting 5-(4-phthalimidomethyl)phenyldipyrromethane with pyrrole in the presence of TFA. The synthesis of the *cis* isomer proved to be slightly more complicated, therefore a modified version of the ABCD-porphyrin synthesis has been applied.

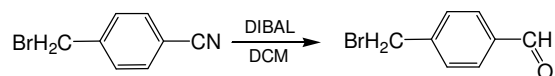
Furthermore, to obtain larger quantities of the tetrakis(*p*-(aminomethyl)phenyl)porphyrin, two different methods were applied to synthesize the precursor tetrakis(*p*-(phthalimidomethyl)phenyl)porphyrin: 1) direct synthesis by refluxing 4-(formylbenzyl)phthalimide and pyrrole in propionic acid, and 2) indirect synthesis by dissolving 4-(formylbenzyl)phthalimide and 5-(4-phthalimidomethyl)phenyldipyrromethane in THF,

followed by addition of TFA. In all cases, the phthalimidyl groups were hydrolyzed by hydrazin to yield free aminomethyl groups. In case of the tetrakis-(*p*-(aminomethyl)-phenyl)porphyrin scaffold, the aminomethyl groups were partially protected with the Boc protecting group in order to allow a selective functionalization of the scaffold.

3.1 Results

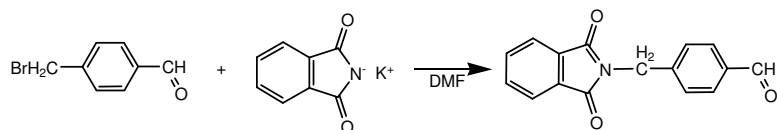
3.1.1 Synthesis of the porphyrin scaffolds

The mixed aldehyde condensation of benzaldehyde and 4-(formylbenzyl)phthalimide was performed to obtain the porphyrins with different numbers of aminomethyl groups on the *para* positions of the *meso* phenyl groups. The intermediate 4-(formylbenzyl)-bromide was synthesized on a 25 mmol scale by the reduction of α -bromo-*p*-tolunitrile under anaerobic conditions, using diisobutylaluminiumhydride (DIBAL) as reducing agent.



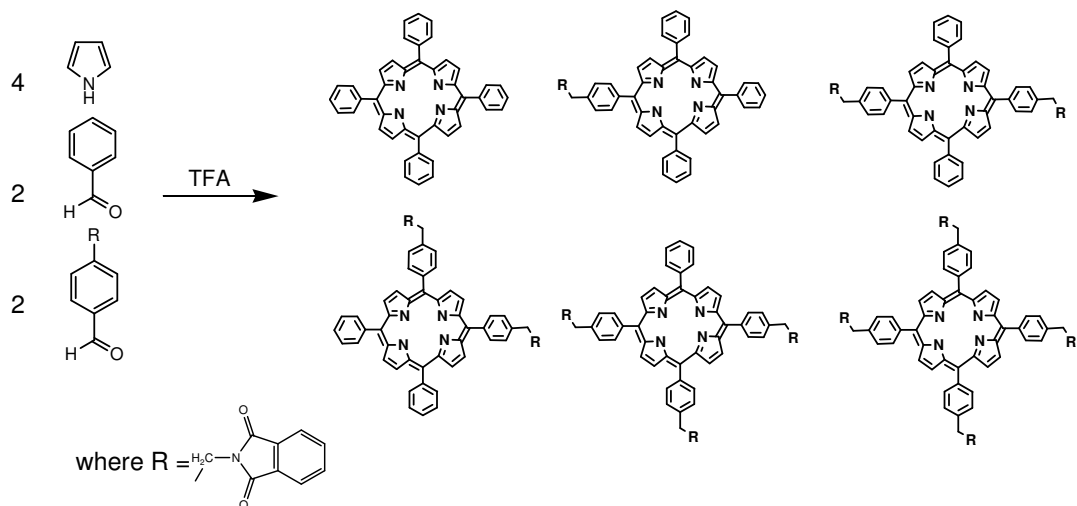
The product, still containing traces of the starting material α -bromo-*p*-tolunitrile, was purified in part by recrystallization from hexane. The remainder was purified by column chromatography using eluent CHCl_3 , and characterized by NMR. The yield was 79%.

The intermediate 4-(formylbenzyl)phthalimide was formed by refluxing 4-(formylbenzyl)bromide with potassium phthalimide in DMF.



The crude product was recrystallized from a mixture of CH_2Cl_2 and hexane and characterized by NMR. The yield was 84%.

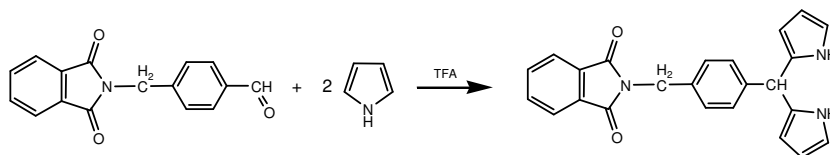
In the mixed aldehyde condensation, benzaldehyde and 4-(formylbenzyl)phthalimide reacted with pyrrole in the presence of TFA, to yield a mixture of porphyrins.



The products were separated by column chromatography using eluent CH₂Cl₂. The *cis* and *trans* isomers were inseparable by column chromatography and co-eluted with unreacted 4-(formylbenzyl)phtalimide, so a second purification step was needed, consisting of a second column chromatography using the eluent mixture hexane/ethyl acetate = 8/2. Separation of the isomers was possible by HPLC only after hydrolysis of the phtalimidyl groups. The identity of the products was determined by mass spectroscopy, the *cis* and *trans* isomers were distinguished by NMR. On a reaction scale of 0.2 mmol the following yields were obtained: TPP 3.9 %; mono 6.5 %; di-*trans* 4.0 %; di-*cis* 6.0 %; tri 3.6 %. Only a small amount of the tetra-substituted porphyrin was formed, and the purification resulted complicated. However, for this particular scaffold an alternative synthesis was performed (see paragraph 3.1.4).

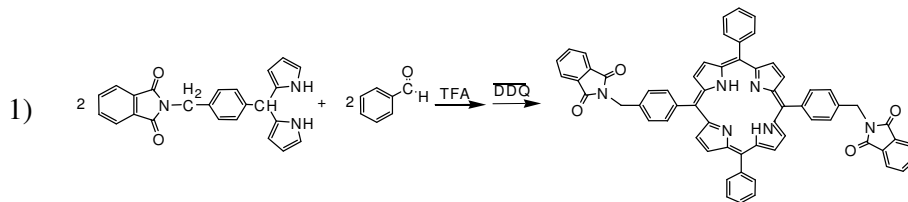
3.1.2 Synthesis of *trans* di-substituted porphyrin

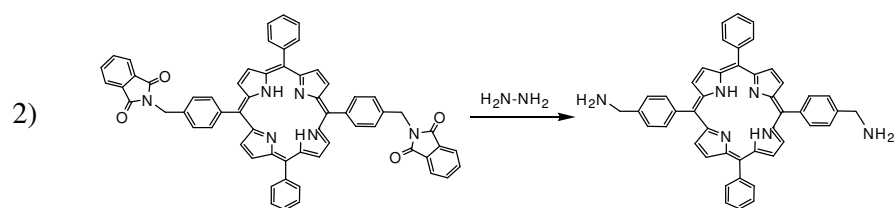
To obtain a higher yield of the *trans* di-substituted porphyrin, the 2+2 condensation of 5-(4-phtalimidomethyl)phenyldipyrromethane was applied. The intermediate 5-(4-phtalimidomethyl)phenyldipyrromethane was synthesized by the condensation under nitrogen of 4-(formylbenzyl)phtalimide with pyrrole, using TFA as catalyst.



The product was purified by flash chromatography to separate the dipyrromethane from polymeric byproducts, and characterized by NMR. The yield was 39%.

The 2+2 condensation of 5-(4-phtalimidomethyl)phenyldipyrromethane to form 10,20-di-phenyl-5,15-di(*p*-(aminomethyl)phenyl)porphyrin took place in two steps: 1) the condensation of 5-(4-phtalimidomethyl)phenyldipyrromethane with benzaldehyde in the presence of TFA; and 2) the hydrolysis of the phtalimidyl groups by hydrazine.



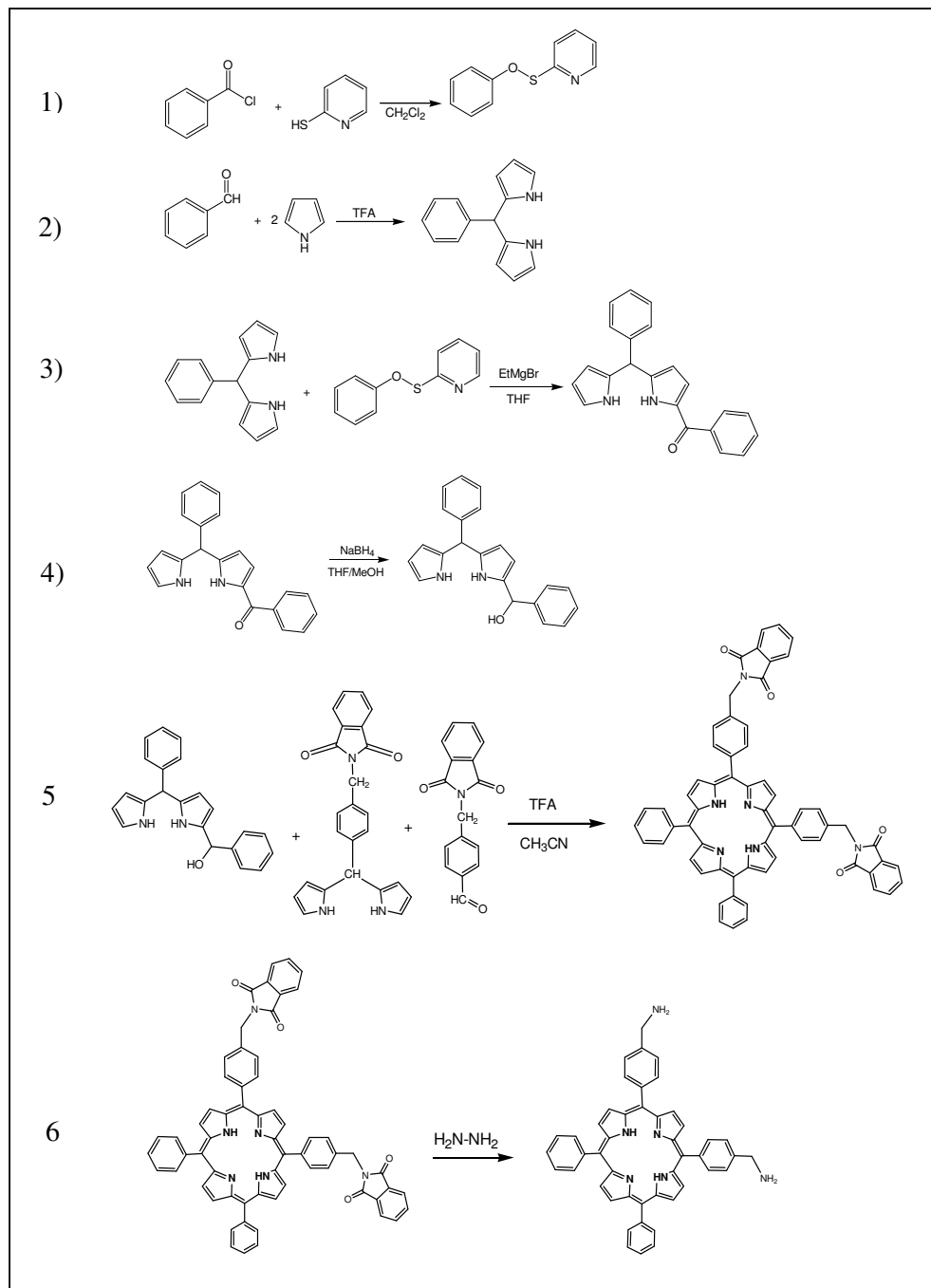


The product of the first reaction step was purified by column chromatography and identified by mass spectroscopy and NMR. The overall yield was 7 %. The hydrolysis of the phthalimidyl groups by hydrazin took place in TFE, the product was purified by centrifugation to remove the phthalimidyl salt. Mass spectroscopy confirmed the identity of the product, which was formed with a 91% yield.

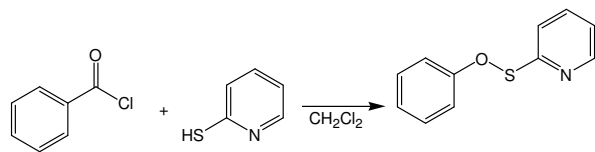
3.1.3 Synthesis of *cis* di-substituted porphyrin

It was also attempted to enhance the yield of the *cis* di-substituted porphyrin. However, this proved to be slightly more difficult than the synthesis of the *trans* isomer, due to the lesser symmetry of the molecule. A modified version of the classic ABCD-synthesis was developed, consisting of six steps (see scheme 1).

Scheme 1: Modified ABCD-synthesis of *cis*-disubstituted porphyrin.

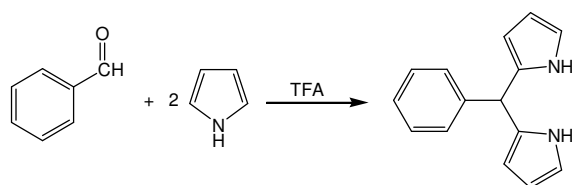


The first intermediate, S-2-pyridyl-4-benzothioate, was synthesized by mixing benzoyl chloride and 2-mercaptopyridine.



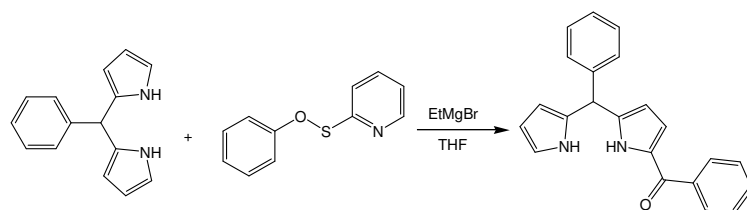
The product was purified by recrystallization from hexane with a 80% yield, and characterized by NMR.

The second reaction consisted of the condensation of benzaldehyde with pyrrole to form 5-phenyldipyrromethane.



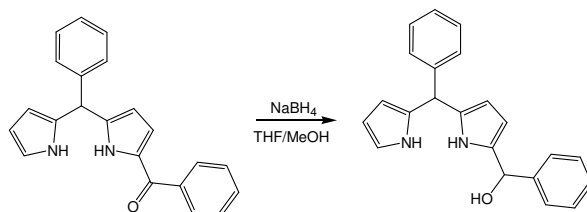
The product was purified by repeated column chromatography, and characterized by NMR. The yield after various purifications was 51%.

These two intermediates react in the presence of EtMgBr to form 1-benzoyl-5-phenyldipyrromethane, which was purified by flash chromatography.

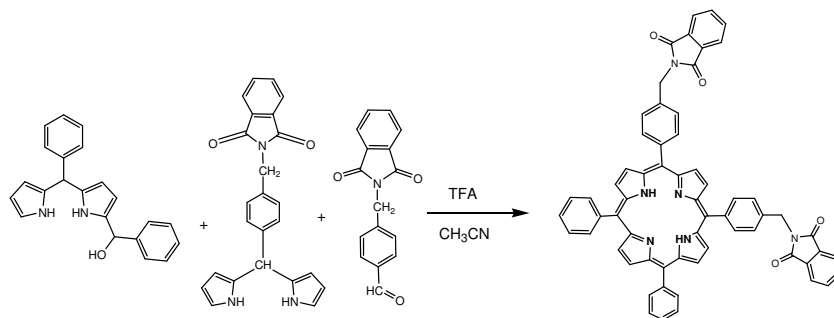


The product was characterized by NMR, the yield was 70%.

Reduction of 1-benzoyl-5-phenyldipyrromethane yielded 1-benzyl-5-phenyldipyrromethanecarbinol.



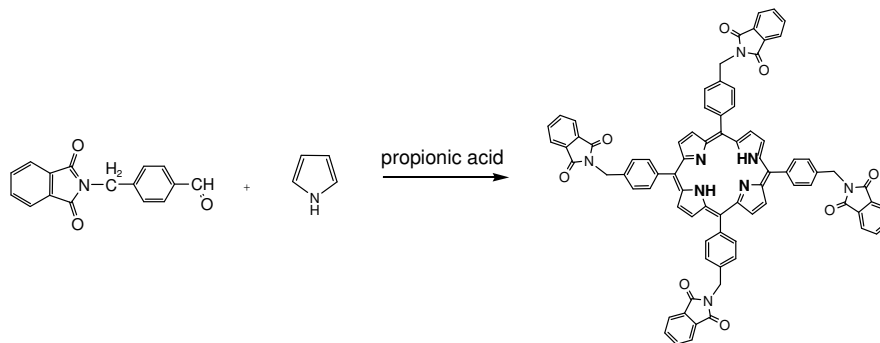
Since this product was highly reactive, it was decided not to attempt further purification and use it directly for the next reaction step: the synthesis of 5,10-diphenyl-15,20-bis(*p*-(phtalimidomethyl)phenyl)porphyrin by mixing the reactive carbinol, 4-(formyl-benzyl)phtalimide and 5-(4-phtalimidomethyl)phenyldipyrromethane in the presence of TFA.



This reaction yielded a mixture of porphyrins, which were purified by column chromatography and identified by mass spectroscopy. The formation of tetraphenylporphyrin and tetrakis(*p*-(phtalimidomethyl)phenyl)porphyrin, besides the desired 5,10-diphenyl-15,20-bis(*p*-(phtalimidomethyl)phenyl)porphyrin, was expected, but also small amounts of the mono and tri substituted porphyins were formed during this reaction. The overall yield of the *cis* substituted porphyrin was 8%. This product was hydrolyzed with hydrazine to give the final product, 5,10-diphenyl-15,20-bis(*p*-(aminomethyl)phenyl)porphyrin, which was purified by HPLC. The yield of this final step was 88%.

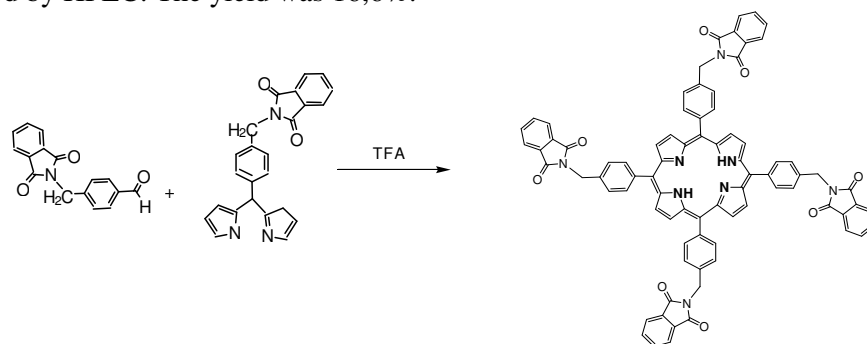
3.1.4 Synthesis of tetrakis(*p*-(aminomethyl)phenyl)porphyrin

Two different strategies were followed to synthesize tetrakis(*p*-(aminomethyl)phenyl)porphyrin. The first strategy consisted of the condensation of 4-(formyl-benzyl)phtalimide with pyrrole by refluxing in propionic acid.



The product was purified by repeated column chromatography, to remove all the polymeric byproducts that were formed during this reaction. The yield was 22%.

The second strategy involved the condensation of 4-(formylbenzyl)phthalimide and 4-(formylbenzyl)phthalimidyl dipyrromethane in the presence of acid. The product was purified by HPLC. The yield was 16,6%.



The phthalimidyl groups were hydrolyzed with hydrazin as described previously.

As mentioned before (see paragraph 1.1.2), the tetraphenylporphyrin base has a deep red colour in solution (absorption maximum 416 nm), whereas the corresponding acid has an intense green colour (absorption maximum 434 nm). The solutions of tetrakis-(*p*-(aminomethyl)phenyl)porphyrin acid and base in EtOH are shown in figure 1, as well as their corresponding UV-VIS spectra.

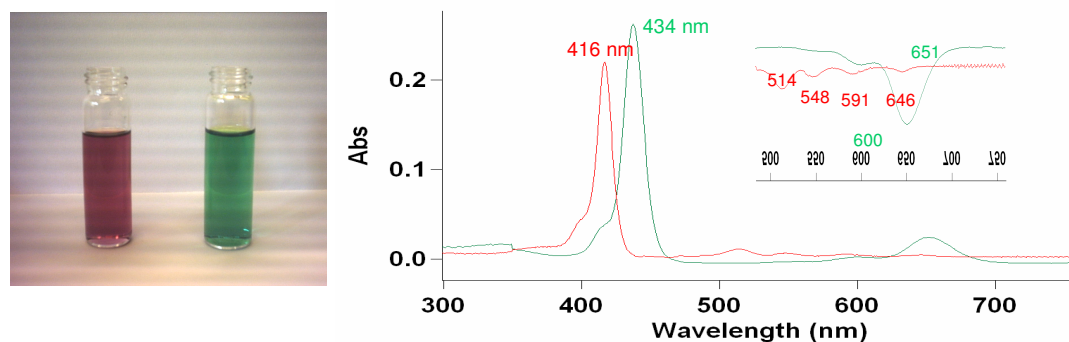
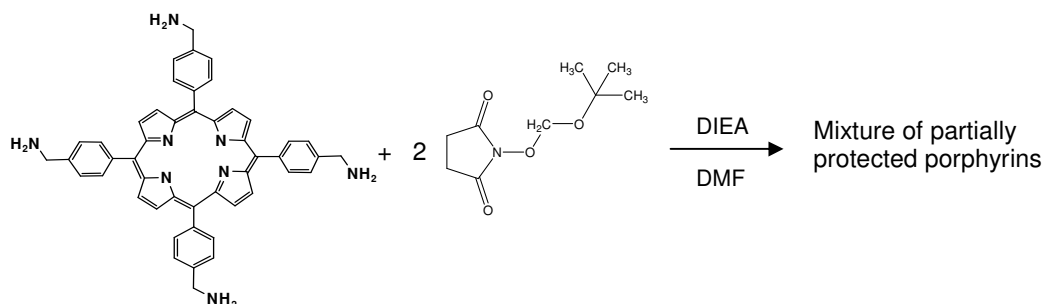


Figure 1: Solutions and UV-VIS spectra of tetrakis(*p*-(aminomethyl)phenyl)porphyrin in EtOH: Porphyrin base (red) and acid (green).

3.1.5 Protection of the amine function

The scaffolds were designed to be functionalized with Fmoc protected peptides, therefore the amine groups were partially protected with Boc. The tetrakis-(*p*-aminomethyl)porphyrin was protected by mixing 2 equivalents of Boc-O-Su in the presence of DIEA¹²³. The result was a mixture of porphyrins. The ratio between the various porphyrin compounds could be manipulated by changing the ratio porphyrin/Boc-O-Su.



The various porphyrins were purified by HPLC and the identity of the different products was determined by mass spectroscopy. NMR spectra were registered to establish the identity of the *cis* and *trans* isomers. The purified products were chemically stable and could be stored at -20 °C for an indefinite period of time.

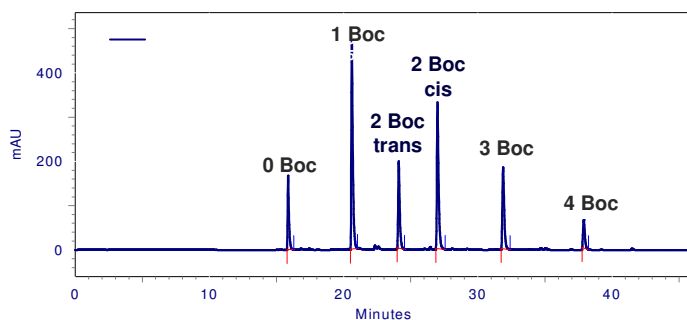


Figure 2: Chromatogram HPLC of the reaction between TAMPP and 2 eq Boc-O-Su.

3.2 Discussion

The mixed aldehyde condensation of benzaldehyde and 4-(formylbenzyl)phtalimide in pyrrole yielded mono, di-*trans*, di-*cis*, and tri-substituted porphyrins, with average yields of 4-6%. No particular problems were encountered in the syntheses of the intermediates. The *cis* and *trans* di-substituted porphyrins were especially of interest, because of their application in the synthesis of potential inhibitors of the active site of thrombin. The yields of these porphyrins in the mixed aldehyde condensation were relatively low and the purification steps laborious, so it has been attempted to enhance the yield of these products by alternative strategies. The *trans* porphyrin was synthesized by a 2+2 condensation of 5-(4-phtalimidomethyl)phenyldipyrromethane, with a yield of 7%. The workup of this reaction using column chromatography was relatively easy. The synthesis of the *cis* compound resulted more complicated due to the lesser symmetry of the molecule. A modified version of the ABCD-porphyrin synthesis, consisting of six steps, was applied. Although the final condensation reaction had a 8% yield of *cis* porphyrin, the entire six-step synthesis required several laborious purifications and presented elevated costs. Therefore, for the synthesis of this particular scaffold the mixed aldehyde condensation might be a better choice.

For the synthesis of tetrakis(*p*-(aminomethyl)phenyl)porphyrin, two different methods were applied: 1) the reaction of 4-(formylbenzyl)phtalimide and pyrrole in propionic acid, and 2) the TFA catalyzed condensation of 4-(formylbenzyl)phtalimide and 5-(4-phtalimidomethyl)phenyldipyrromethane. Although this latter method had a lower yield (16.6% versus 22%), the reaction was relatively clean with almost no polymeric byproducts. The product could therefore be purified by HPLC, as opposed to the extensive column chromatography that was required in the first strategy to obtain the pure product. Therefore, for the synthesis of tetrakis(*p*-(aminomethyl)phenyl)porphyrin the condensation of 4-(formylbenzyl)phtalimide and 5-(4-phtalimidomethyl)phenyldipyrromethane is recommended.

To allow a selective functionalization of the scaffolds, the aminomethyl groups were protected with the Boc protecting group by reacting the scaffold with Boc-O-Su in the presence of DIEA. The reaction was only performed for the tetrakis(*p*-(aminomethyl)phenyl)porphyrin, but could also be applied to the other scaffolds. The protected porphyrin scaffolds were stable and could easily be purified by HPLC. The Boc protecting groups could be removed with a 50% solution of TFA in CH₂Cl₂ to yield the original scaffold without loss of product.

All scaffolds were stable in a wide range of solvents, and at different values of pH. Storage at $-20\text{ }^{\circ}\text{C}$ for prolonged periods of time did not cause any alteration in the scaffolds.

3.3 Experimental section

3.3.1 Materials and methods

Unless otherwise stated, solvents of anhydroscale grade were used for all reactions. Reagents were obtained from commercial suppliers and used as received, with the exception of pyrrole that was distilled prior to use. All manipulations and reactions were carried out using standard Schlenk techniques. Analysis of reaction mixtures and products was performed by TLC on silica, or by using a RP-HPLC Shimadzu system LC-10AD VP with a spectrophotometric detector Diode Array SPD-M10A VP. Linear gradients were used of H₂O 0.1% TFA and CH₃CN 0.1% TFA. UV-VIS spectra were recorded on a Varian Cary 5000 spectrophotometer. ¹H-NMR spectra were recorded on a Varian 200 MHz spectrometer. All spectra were referenced using the residual solvent peak as an internal standard (chloroform-d₁ = 7.24, acetonitrile-d₃ = 1.94). Mass spectrometry was carried out on a Voyager DEPRO MALDI-TOF spectrometer (Applied Biosystems) in the linear mode, using bovine insulin as internal calibration standard. The matrix α -cyano-4-hydroxycinnamic acid was recrystallized from EtOH / H₂O prior to use.

3.3.2 Synthesis of the intermediates

Synthesis of 4-(formylbenzyl)bromide¹²⁴

A solution of 5.0 g (25 mmol) α -bromo-*p*-tolunitrile in 15 ml dry CH₂Cl₂ was degassed with nitrogen for 30 min. The reaction mixture was cooled to 0 °C and slowly 25 ml of a 1.0 M solution of diisobutylaluminiumhydride in CH₂Cl₂ was added. After refluxing for 5 h, the reaction mixture was acidified till pH ~ 3 with a 10% sulfuric acid solution and stirring was continued overnight. The water layer was extracted three times with CH₂Cl₂ after which the organic layers were collected and dried with Na₂SO₄. Evaporation of the solvent yielded a yellow solid, which according to TLC still contained traces of the starting product α -bromo-*p*-tolunitrile (eluent: CHCl₃, R_F tolunitrile = 9, R_F aldehyde = 8.5). After crystallization from hexane, 1.55 g (7.8 mmol, 31%) of pure white crystals was obtained. The remaining mixture of aldehyde and tolunitrile was purified by column chromatography (silica, eluent = CHCl₃). The overall yield was 3.9 g (19 mmol, 76%).

$^1\text{H-NMR}$ (200 MHz, CDCl_3): δ 10.01 (s, 1H, $\text{O}=\text{CH}_A$), 7.80 (d, 2H, Ar-H_B), 7.60 (d, 2H, Ar-H_C), 4.45 (s, 2H, Br-CH_2).

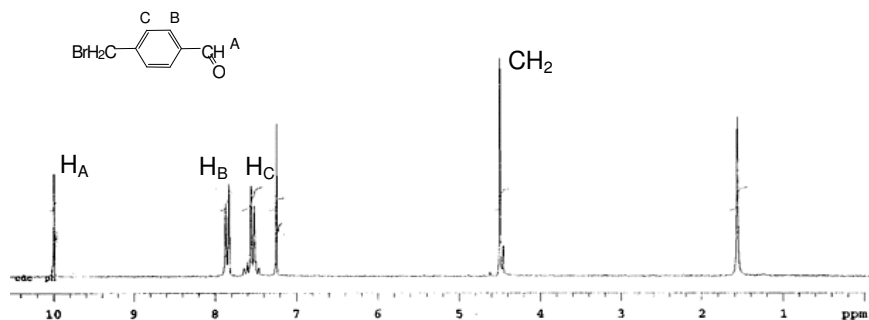


Figure 3: The $^1\text{H-NMR}$ spectrum of α -bromo-*p*-aldehyde in CD_3Cl .

Synthesis of 4-(formylbenzyl)phthalimide

In a reaction vessel, 1.5 g (7.5 mmol) 4-(formylbenzyl)bromide and 1.4 g (7.5 mmol) potassium phthalimide in 60 ml DMF were refluxed for 4 h. After cooling to room temperature and evaporation of the solvent, water and CH_2Cl_2 were added and the water layer was extracted three times. The organic layers were collected, dried with Na_2SO_4 and the solvent was evaporated. The resulting slightly yellow solid was recrystallized from a mixture of CH_2Cl_2 and hexane to yield 1.7 g of pure 4-(formylbenzyl)phthalimide (6.4 mmol, 84%).

$^1\text{H-NMR}$ (200 MHz, CDCl_3): δ 10.01 (s, 1H, $\text{O}=\text{CH}$), 7.90 (m, 4H, Ar-H_{B+E}), 7.60 (m, 4H, Ar-H_{C+F}), 4.90 (s, 2H, $\text{N-CH}_2\text{-Ar}$).

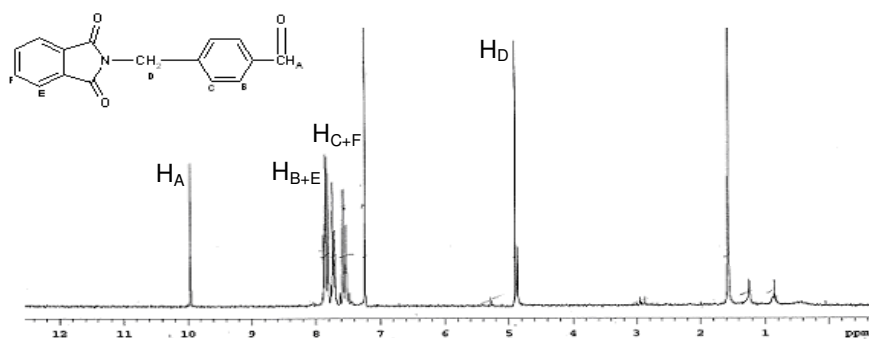


Figure 4: The $^1\text{H-NMR}$ spectrum of 4-(formylbenzyl)phthalimide in CD_3Cl .

Synthesis of 5-(4-phthalimidomethyl)phenyldipyrromethane¹²⁵

To a mixture of 0.53 g (2 mmol) 4-(formylbenzyl)phthalimide and 5.5 ml (80 mmol) pyrrole under nitrogen, 15 μ l (0.2 mmol) trifluoroacetic acid was added. The reaction was monitored by TLC (eluent: hexane/ethyl acetate = 1/1), where the 5-(4-phthalimidomethyl)phenyldipyrromethane appeared at $R_F = 0.9$. Byproducts (polymeric compounds) had minor R_F values of 0,65 and 0,45. After 45 min the reaction was stopped by addition of 70 ml CH_2Cl_2 and 40 ml 1 M NaOH. The organic phase was washed several times with water, dried with Na_2SO_4 and evaporated to dryness. The resulting dark oil was purified by flash chromatography (silica, eluent: hexane/ethyl acetate), where the dipyrromethane eluted at $\sim 40\%$ ethyl acetate. After evaporation, 0.29 g (0.76 mmol, 39%) of a yellow solid was obtained.

$^1\text{H-NMR}$ (200 MHz, CD_3CN): δ 7.89 (s, 2H, NH), 7.85-7.72 (2q, 4H, Ar- $\text{H}_{\text{A+B}}$), 7.38 (2d, 2H, Ar- H_{C}), 7.16 (2d, 2H, Ar- H_{D}), 6.66 (d, 2H, NH- CH_{G} -), 6.12 (t, 2H, NH- CH_{F} -CH), 5.88 (d, 2H, NH- CH_{E} -CH), 5.43 (s, 1H, meso), 4.83 (s, 2H, CH_2).

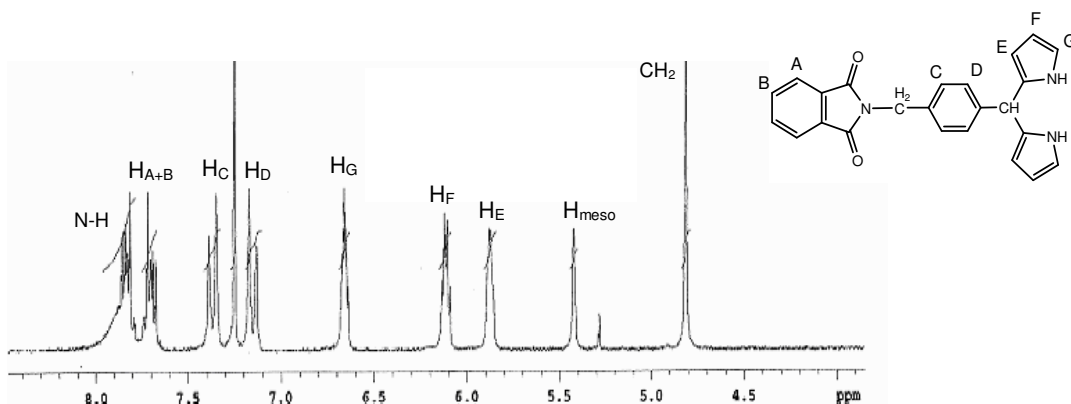


Figure 5: The $^1\text{H-NMR}$ spectrum of 5-(4-phthalimidomethyl)phenyldipyrromethane in CD_3Cl .

3.3.3 Synthesis of the porphyrin scaffolds

Mixed aldehyde condensation of benzaldehyde and 4-(formylbenzyl)phthalimide

40.7 μ l (0.4 mmol) benzaldehyde, 106 mg (0.4 mmol) 4-(formylbenzyl)phthalimide and 55.3 μ l (0.8 mmol) pyrrole were dissolved in 40 ml CH_2Cl_2 . TFA (30.6 μ l, 0.4 mmol) was slowly added, upon which the reaction mixture slowly turned deep red. After stirring for 3 h, DDQ (363 mg, 1.6 mmol) was added to oxidize the formed porphyrinogen to porphyrin. The reaction was stopped when the HPLC chromatogram showed that the porphyrinogen had been completely oxidized. The solvent was

evaporated, the residue dissolved in CH₂Cl₂ and extracted with H₂O. The crude product was purified first by filtration over alumina (eluent CH₂Cl₂, followed by MeOH), and subsequently by column chromatography using eluent CH₂Cl₂. The *cis* and *trans* isomers were inseparable and co-eluted with unreacted 4-(formylbenzyl)phtalimide. Therefore a second purification step was needed, consisting of another column chromatography using the eluent mixture hexane/ethyl acetate = 8/2. Separation of the isomers was possible by HPLC only after hydrolysis of the phtalimidyl groups with hydrazine. The identity of the products was determined by mass spectroscopy, the *cis* and *trans* isomers were distinguished by NMR. The yields of the products and their R_f values in 100% CH₂Cl₂ are summarized in table 1.

Compound	Mass (Da)	Yield (mg)	Yield (μmol)	Yield (%)	R _F (CH ₂ Cl ₂)
TPP	615.0	4.8	7.8	3.9	0.95
mono	775.6	11.6	15.0	6.5	0.85
di- <i>trans</i>	933.0	8.6	9.2	4.0	0.55
di- <i>cis</i>	933.0	12.8	13.8	6.0	0.55
tri	1093.7	7.9	7.2	3.6	0.25

Table 1: Products of the mixed aldehyde condensation.

3.3.4 Synthesis of *trans* di-substituted porphyrin: 2+2 condensation^{126,127}

Step 1: Synthesis of 10,20-diphenyl-5,15-di(*p*-(phtalimidomethyl)phenyl)porphyrin

To a solution of 381 mg (1.0 mmol) 5-(4-phtalimidomethyl)phenyldipyrromethane and 102 μl (1,0 mmol) benzaldehyde in 17 ml dry acetonitrile, 10 μl (0,13 mmol) TFA was added, upon which the reaction mixture immediately turned deep red. After stirring for 15 h, 0.345 g (1.52 mmol) DDQ was added to oxidize the formed porphyrinogen to porphyrin. The reaction was stopped when the HPLC chromatogram showed the complete oxidation of the porphyrinogen. The solvent was evaporated, the residue dissolved in CH₂Cl₂ and extracted with H₂O. The crude product was purified first by filtration over silica (eluent acetonitrile, followed by a solution MeOH/CH₂Cl₂ = 1/1), and subsequently by column chromatography using eluent CH₃CN/CH₂Cl₂. The HPLC chromatogram showed the pure product with a retention time of 28 min. The identity of the product was confirmed by the ¹H-NMR spectrum as well as by the mass spectrum (933.1 Da, calculated 933.0 Da). After evaporation of the solvent 31.2 mg (0.033 mmol) of a dark red solid was obtained. The overall yield was 7%.

$^1\text{H-NMR}$ (200 MHz, CDCl_3): δ 8.8 (s, 8H, $\underline{\text{H}}_{\text{F}}$), 8.2 (m, 8H, Ar- $\underline{\text{H}}_{\text{D+E}}$), 7.95 (m, 2H, Ar- $\underline{\text{H}}_{\text{B}}$), 7.8 (m, 2H, Ar- $\underline{\text{H}}_{\text{A}}$), 7.78 (m, 10H, Ar- $\underline{\text{H}}_{\text{G}}$), 5.10 (s, 4H, $\underline{\text{C}}\underline{\text{H}}_2$), -3.0 (s, 4H, $\underline{\text{N}}\underline{\text{H}}$).

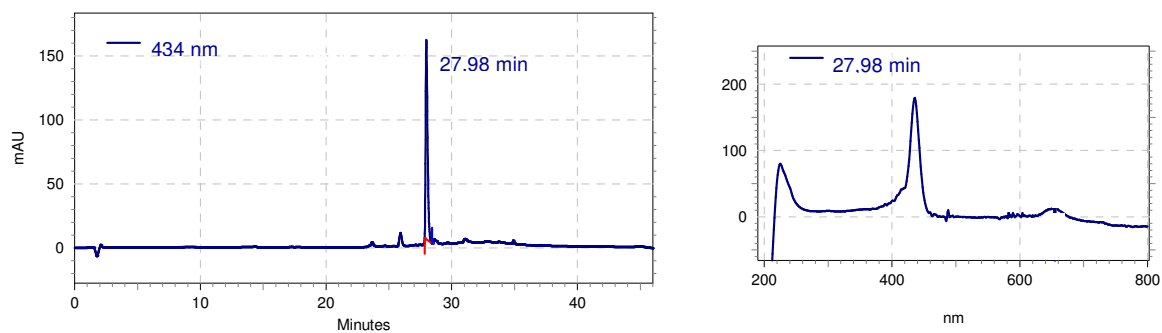


Figure 6: HPLC chromatogram and UV-VIS spectrum of 10,20-diphenyl-5,15-di(*p*-(phtalimidomethyl)phenyl)porphyrin.

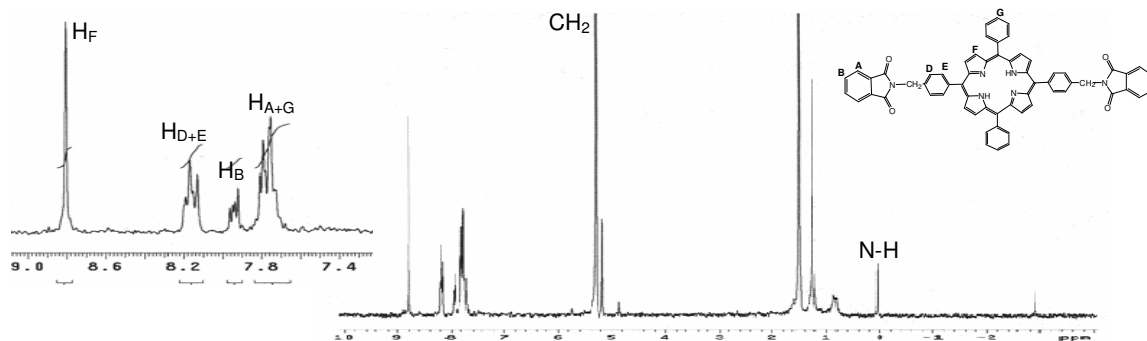


Figure 7: $^1\text{H-NMR}$ spectrum of 10,20-diphenyl-5,15-di(*p*-(phtalimidomethyl)phenyl)porphyrin.

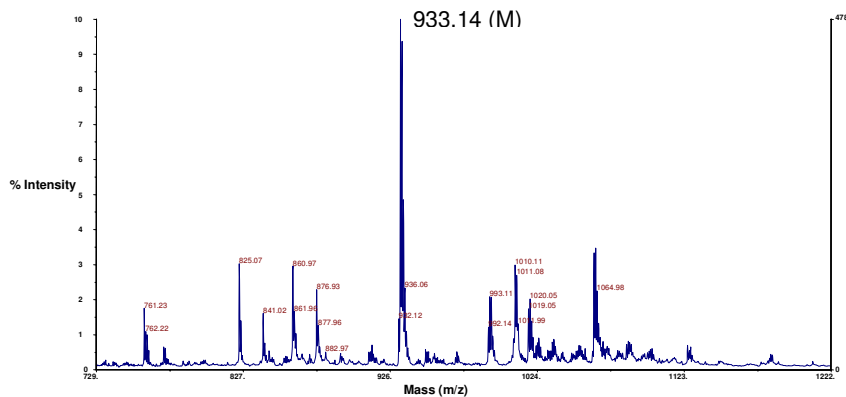


Figure 8: Mass spectrum of 10,20-diphenyl-5,15-di(*p*-(phtalimidomethyl)phenyl)porphyrin.

Step 2: Synthesis of 10,20-diphenyl-5,15-di(*p*-(aminomethyl)phenyl)porphyrin¹²⁸

The second step of this synthesis involved the hydrolysis of the phtalimidyl groups by hydrazine. The 10,20-diphenyl-5,15-di(*p*-(phtalimidomethyl)phenyl)porphyrin (31.2 mg, 33 μ mol) was dissolved in 7 ml THF and 243 μ l (5.0 μ mol) of hydrazine monohydrate was added. After stirring for 7 h, the solvent was evaporated and the residue dissolved in acetonitrile. The hydrazine salt was eliminated by centrifugation. The HPLC chromatogram showed the pure product with a retention time of 13.35 min. The mass spectrum confirmed the identity of the desired product (673.4 Da, calculated 672.8 Da). Yield: 20.4 mg (30 μ mol, 91%).

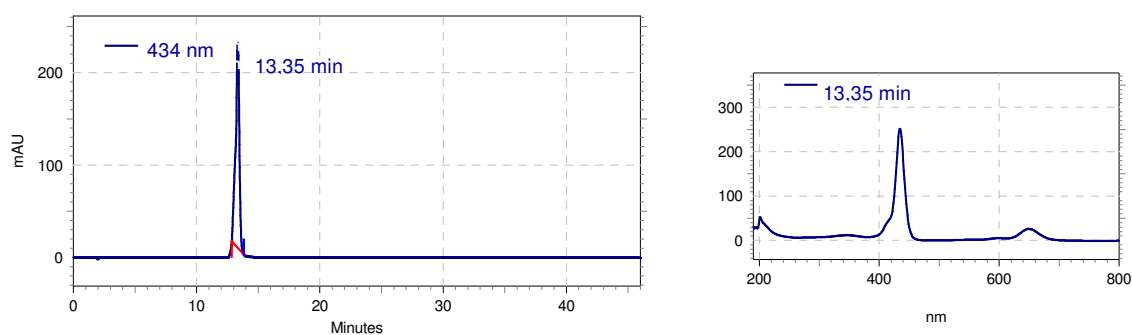


Figure 9: HPLC chromatogram and UV-VIS spectrum of 10,20-diphenyl-5,15-di(*p*-(aminomethyl)phenyl)porphyrin.

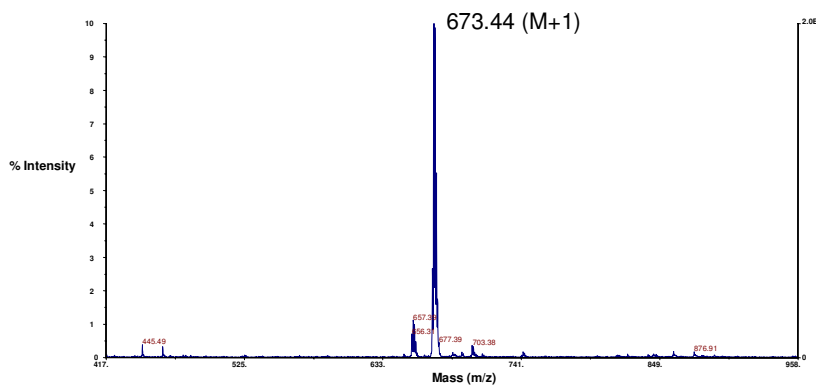


Figure 10: Mass spectrum of 10,20-diphenyl-5,15-di(*p*-(aminomethyl)phenyl)porphyrin.

3.3.5 Synthesis of *cis* di-substituted porphyrin: modified ABCD-porphyrin synthesis

Step 1: Synthesis of S-2-pyridyl-4-benzothioate^{129,130}

A solution of benzoyl chloride (581 μ l, 5.0 mmol) in 10 ml CH_2Cl_2 was slowly added to a stirred solution of 0.55 g (5 mmol) 2-mercaptopyridine in 25 ml CH_2Cl_2 . The reaction was monitored by TLC (eluent $\text{CHCl}_3/\text{MeOH} = 9/1$) where the product had $R_F = 0.9$. After circa 1 h the starting products had disappeared, and 30 ml 2.0 M NaOH was added to the reaction mixture. The organic phase was isolated, washed several times with water and dried over Na_2SO_4 . Evaporation of the solvent yielded an orange oil. A minimum of ethyl acetate was added to dissolve the oil, after which the S-2-pyridyl-4-benzothioate was precipitated with hexane. The resulting transparent crystals were washed several times with hexane and dried in vacuo. The $^1\text{H-NMR}$ spectrum confirmed the identity of the product. Yield: 0.862 g (4.0 mmol, 80%).

$^1\text{H-NMR}$ (200 MHz, CD_3CN): δ 8.62 (d, 1H, H_A), 8.00 (d, 2H, H_E), 7.82 (d, 1H, H_D), 7.66 (m, 2H, H_B+H_C), 7.58 (t, 2H, H_F), 7.40 (t, 1H, H_G).

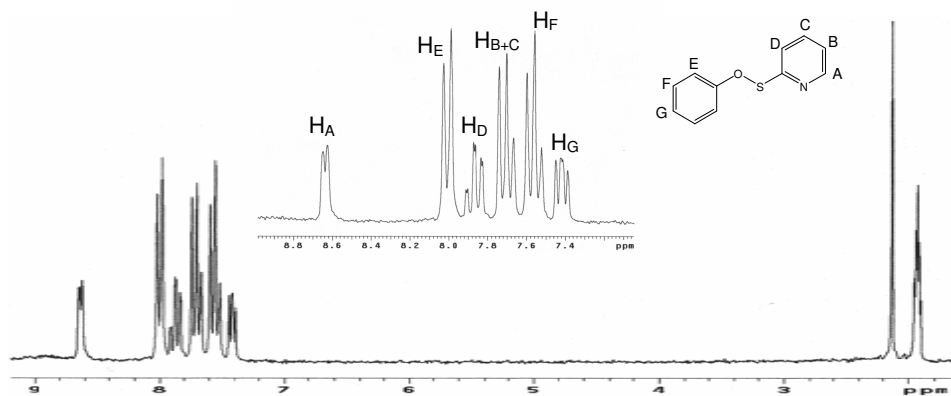


Figure 11: $^1\text{H-NMR}$ spectrum of S-2-pyridyl-4-benzothioate.

Step 2: Synthesis of 5-phenyldipyrromethane¹³¹

To a solution of 0.5 ml (5.0 mmol) benzaldehyde in 14 ml (200 mmol) pyrrole under nitrogen, a sample of TFA (8 μ l, 0.1 mmol) was added. The reaction was monitored by TLC (eluent hexane/ethyl acetate = 8/2), where the desired product had $R_F = 0.45$. After stirring for 40 min, the reaction was stopped by addition of 80 μ l triethylamine in 100 ml CH_2Cl_2 . The organic phase was washed first with 1 M NaOH and subsequently three times with water. After drying with Na_2SO_4 and evaporation of the solvent, the crude

product was purified by column chromatography (silica gel, eluent hexane/ethyl acetate/triethylamine = 80/20/1). The identity of the pure product was confirmed by $^1\text{H-NMR}$. The yield was 573 mg (2.6 mmol, 51%) of a white solid.

$^1\text{H-NMR}$ (200 MHz, CD_3CN): δ 8.89 (s, 2H, NH), 7.15-7.36 (m, 5H, Ar-H), 6.63 (t, 2H, H_A), 6.00 (t, 2H, H_B), 5.76 (d, 2H, H_C), 5.41 (s, 1H, H_{meso}).

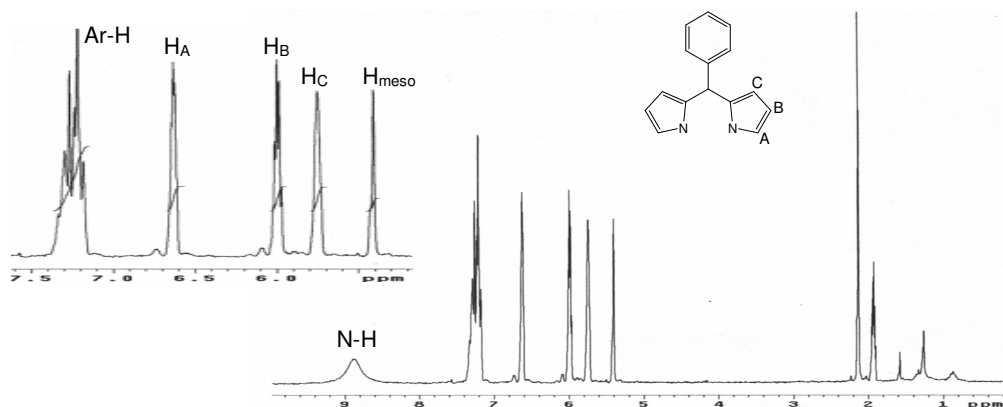


Figure 12: $^1\text{H-NMR}$ spectrum of 5-phenyldipyrromethane.

Step 3: Synthesis of 1-benzoyl-5-phenyldipyrromethane

A solution of EtMgBr (1 ml, 1.0 M in THF) was added carefully via syringe to a stirred solution of 111 mg (0.5 mmol) 5-phenyldipyrromethane in 0.5 ml THF. The reaction mixture was cooled to $-78\text{ }^\circ\text{C}$ and a solution of 107 mg (0.5 mmol) S-2-pyridyl-4-benzothioate in 0.5 ml THF was added. The reaction mixture was kept at $-78\text{ }^\circ\text{C}$ for 10 min, and was then allowed to slowly reach room temperature. The reaction was monitored by TLC (eluent $\text{CH}_2\text{Cl}_2/\text{ethyl acetate} = 25/1$), where the desired product had $R_F = 0.7$. After 45 min the reaction was quenched with a 1.0 M NH_4Cl solution till pH $\sim 5/6$. CH_2Cl_2 (10 ml) was added and the organic phase was washed several times with H_2O , and dried with Na_2SO_4 . Purification by flash column chromatography (silica, eluent from 100% CH_2Cl_2 to $\text{CH}_2\text{Cl}_2/\text{ethyl acetate} 100/6$) yielded a yellow oil (106 mg, 0.35 mmol, 70%). The identity of the product was confirmed by $^1\text{H-NMR}$.

$^1\text{H-NMR}$ (200 MHz, CD_3CN): δ 10.0 (s, 1H, N-H), 9.0 (s, 1H, N-H), 7.8 (m, 2H, Ar-H_I), 7.55 (m, 3H, Ar-H_J), 7.25 (m, 5H, Ar-H_E), 6.6 (d, 1H, H_A), 6.4 (d, 1H, H_G), 6.05 (m, 2H, H_{B+F}), 5.98 (t, 1H, H_C), 5.6 (s, 1H, H_D).

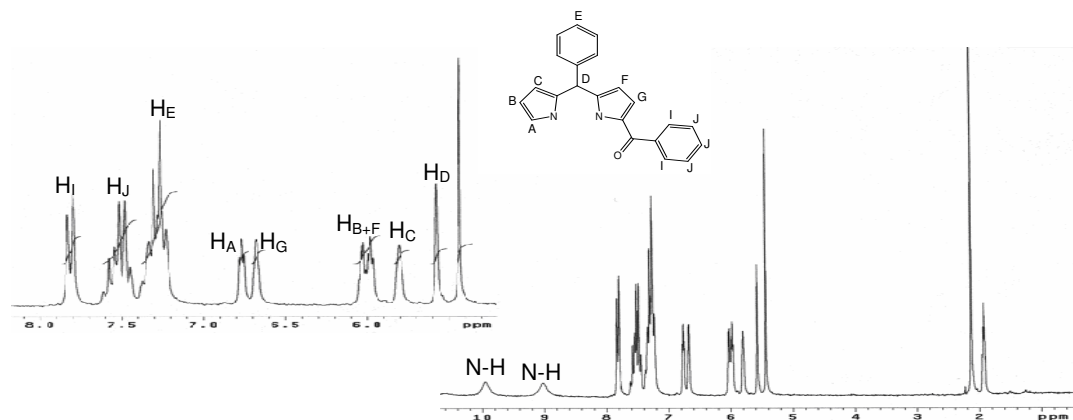


Figure 13: $^1\text{H-NMR}$ spectrum of 1-benzoyl-5-phenyldipyrromethane.

Step 4: Synthesis of 1-benzyl-5-phenyldipyrromethanecarbinol

To a solution of 1-benzoyl-5-phenyldipyrromethane (98 mg, 0.3 mmol) in 6 ml THF/MeOH = 3/1, 25 equivalents of NaBH_4 (7.5 mmol, 284 mg) were added. The reaction was monitored by TLC (eluent CH_2Cl_2 /ethyl acetate = 100/4). The reaction was complete after 1 h, the reaction mixture was quenched with water (12 ml) and poured in 15 ml CH_2Cl_2 . After extracting three times with H_2O , the organic layer was dried with K_2CO_3 and the solvent evaporated to yield an orange oil. Due to the high reactivity of this product, it was used immediately for step 5 of this synthesis, without ulterior purification steps. Therefore, no characterization of the product was performed.

Step 5: Synthesis of 5,10-diphenyl-15,20-bis(*p*-(phtalimidomethyl)phenyl)porphyrin

1-benzyl-5-phenyldipyrromethanecarbinol (98.5 mg, 0.3 mmol), 5-(4-phtalimidomethyl)phenyldipyrromethane (114 mg, 0.3 mmol) and 4-(formylbenzyl)phtalimide (79.6 mg, 0.3 mmol) were dissolved in 60 ml acetonitrile. To this solution, TFA (138 μl , 1.8 mmol) was added in aliquots of 10 μl . The reaction mixture instantly turned deep red. After stirring for 1 h, 2 equivalents of DDQ (136 mg, 0.6 mmol) were added and stirring was continued for 2 h. Triethylamine (251 μl , 1.8 mmol) was added and the entire reaction mixture was filtered through a pad of alumina (eluted with CH_2Cl_2) until the eluent was no longer dark. Removal of the solvent gave a dark solid, which was purified by column chromatography (silica, 100% CH_2Cl_2).

Three different porphyrins were eluted with the following R_F values (characterization by mass spectroscopy):

0,95 = tetraphenylporphyrin (9.34 mg, 15 μmol , 5.1%), mass spectrum 615.8 Da (calculated 614.7 Da);

0,80 = (*p*-(phtalimidomethyl)phenyl)triphenylporphyrin (14.8 mg, 19 μmol , 6.4%), mass spectrum 776.1 (calculated 774.5);

0,65 = 5,10-diphenyl-15,20-bis(*p*-(phtalimidomethyl)phenyl)porphyrin (22.5 mg, 24 μmol , 8.0%), mass spectrum 935.4 (calculated 933.0).

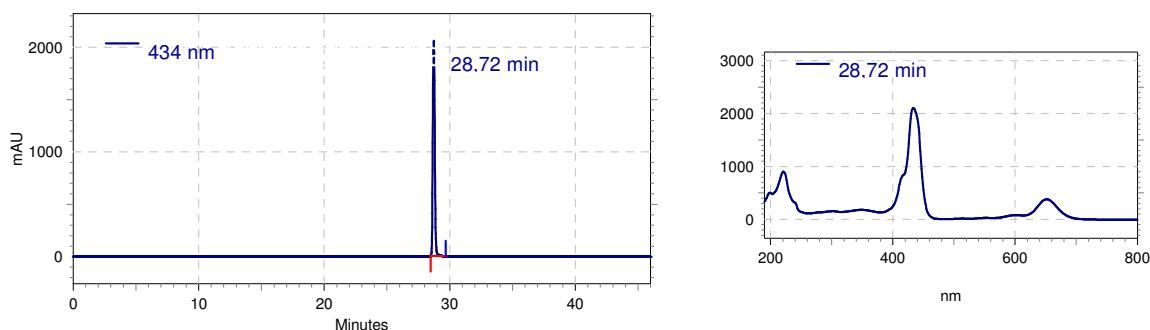


Figure 14: HPLC chromatogram and UV-VIS spectrum of 5,10-diphenyl-15,20-bis(*p*-(phtalimidomethyl)phenyl)porphyrin.

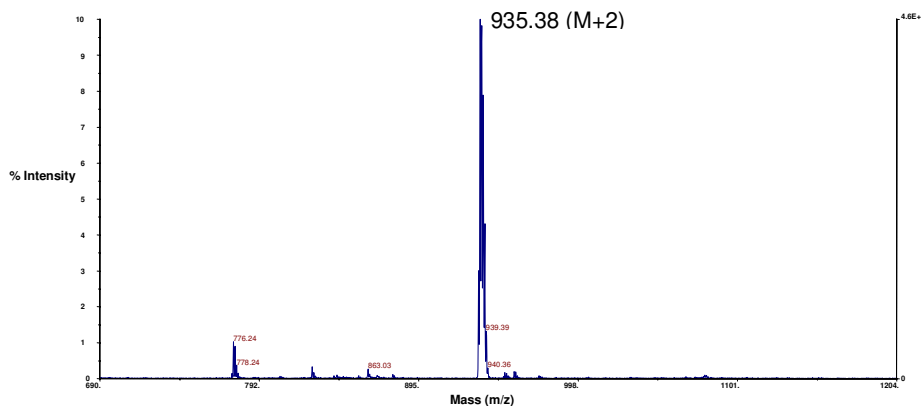


Figure 15: Mass spectrum of 5,10-diphenyl-15,20-bis(*p*-(phtalimidomethyl)phenyl)porphyrin.

Step 6: Synthesis of 5,10-diphenyl-15,20-bis(*p*-(aminomethyl)phenyl)porphyrin

22.5 mg (24 μmol) 10,20-diphenyl-5,15-bis(*p*-(phtalimidomethyl)phenyl)porphyrin was dissolved in 5 ml THF and 175 μl (0.0036 mmol) of hydrazine monohydrate was added. The reaction was monitored by HPLC, were slowly a new peak at 17.1 min started to form while the original porphyrin at 28.7 min slowly disappeared. When the reaction was complete, the solvent was evaporated, the residue was dissolved in acetonitrile and

the hydrazine salt was eliminated by centrifugation. The crude product was purified by HPLC. The mass spectrum confirmed the identity of the desired product (674.2 Da, calculated 672.8 Da). Yield: 14.2 mg (21 μ mol, 88%).

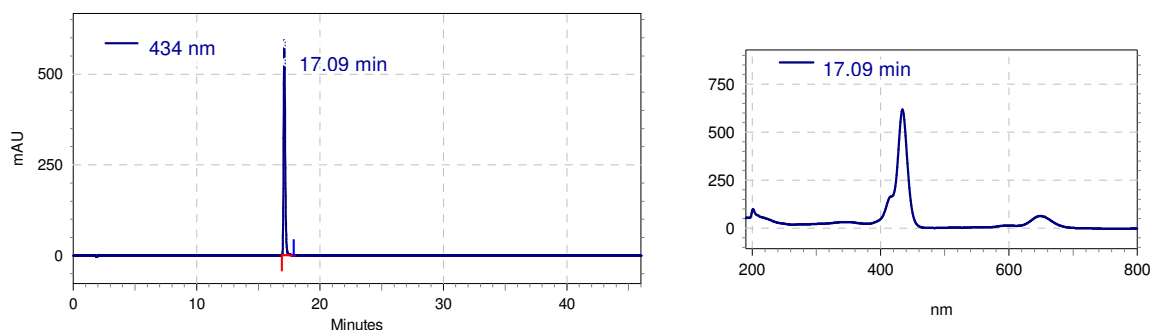


Figure 16: HPLC chromatogram and UV-VIS spectrum of 5,10-diphenyl-15,20-bis(*p*-(aminomethyl)-phenyl)porphyrin.

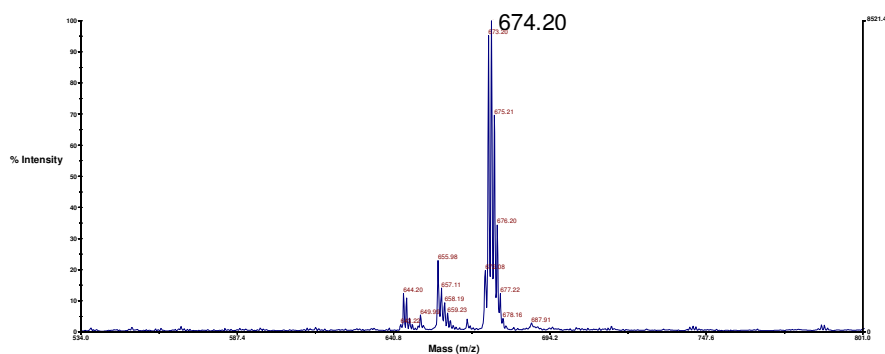


Figure 17: Mass spectrum of 5,10-diphenyl-15,20-bis(*p*-(aminomethyl)phenyl)porphyrin.

3.3.6 Synthesis of tetrakis(*p*-(aminomethyl)phenyl)porphyrin

1) Reaction between 4-(formylbenzyl)phthalimide and pyrrole

1.46 g (5.5 mmol) 4-(formylbenzyl)phthalimide and 0.36 ml (5.5 mmol) pyrrole were dissolved in 20 ml propionic acid and refluxed for 30 min. After cooling to room temperature, the reaction mixture was filtered and washed with MeOH and hot H₂O. The dark precipitate was purified by repeated column chromatography (silica, eluent: CH₂Cl₂/MeOH = 98/2). 1.06 g of crude product (still containing traces of propionic acid, as well as several polymeric compounds) yielded 371 mg (0.3 mmol, 22%) of the purified tetrakis(*p*-(phthalimidomethyl)phenyl)porphyrin.

2) Condensation of aldehyde and dipyrromethane

4-(formylbenzyl)phtalimide (80 mg, 0.3 mmol) and 4-(formylbenzyl)phtalimidyl dipyrromethane (115 mg, 0.3 mmol) were dissolved in CH₃CN under nitrogen. After addition of TFA (3 μ l) and stirring for 4 h, DDQ (102 mg, 0.45 mmol) was added to oxidize the formed porphyrinogen to porphyrin. The oxidation reaction was followed by HPLC, where the tetrakis(*p*-(phtalimidomethyl)phenyl)porphyrin had a retention time of 28.0 min. The identity of the product was confirmed by mass spectroscopy: 1251.8 Da (calculated: 1252.0 Da), and the product was purified by HPLC. The reaction yield was 31.2 mg (0.025 mmol, 16.6%).

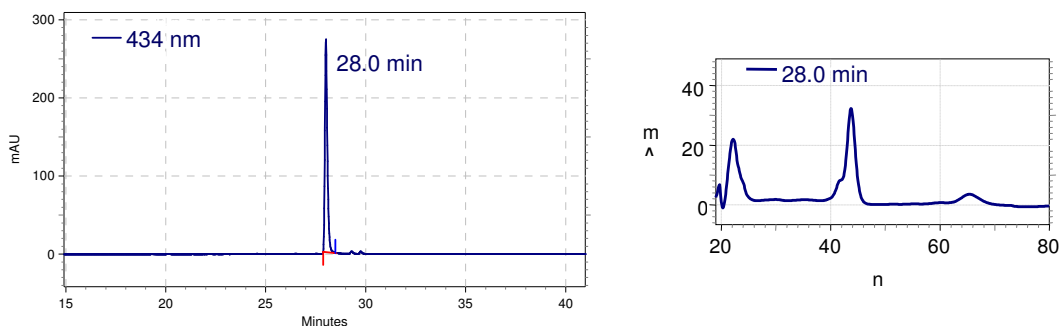


Figure 18: HPLC chromatogram and UV-VIS spectrum of tetrakis(*p*-(phtalimidomethyl)phenyl)porphyrin.

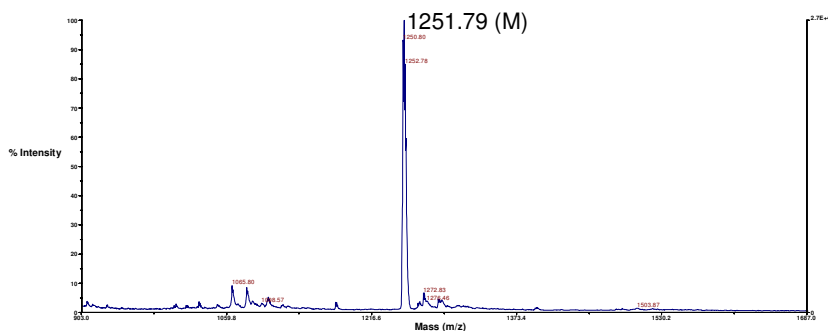


Figure 19: Mass spectrum of tetrakis(*p*-(phtalimidomethyl)phenyl)porphyrin.

Hydrolysis of the phtalimidyl groups took place by adding hydrazin (500 μ l 0.01 mmol) to 31.2 mg (0.025 mmol) tetrakis(*p*-(phtalimidomethyl)phenyl)porphyrin in 8 ml THF to yield 16.1 mg (0.022 mmol, 89%) of tetrakis(*p*-(aminomethyl)phenyl)porphyrin (TAMPP). The reaction was monitored by HPLC, where the completely hydrolyzed porphyrin had a retention time of 17.2 min. After purification by HPLC, the identity of the product was confirmed by mass spectroscopy: 732.6 Da (calculated: 731.7 Da).

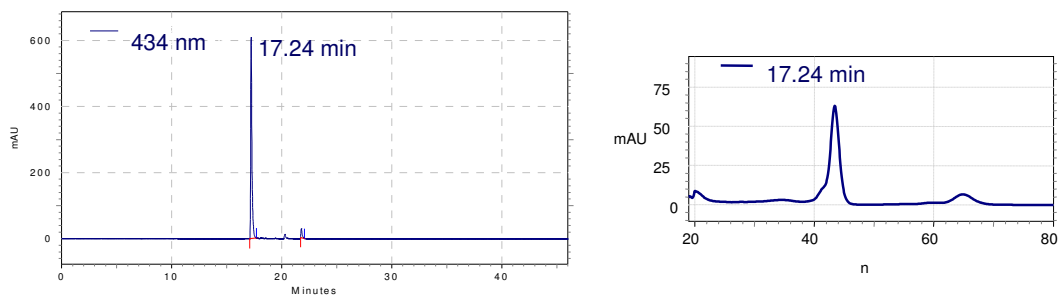


Figure 20: HPLC chromatogram and UV-VIS spectrum of tetrakis(*p*-(aminomethyl)phenyl)porphyrin.

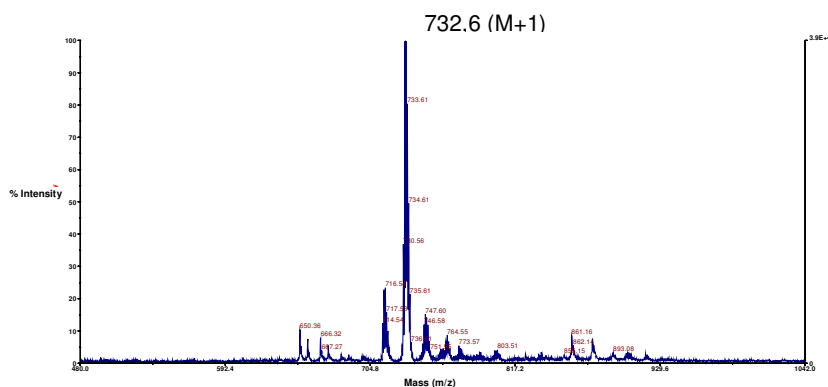


Figure 21: Mass spectrum of tetrakis(*p*-(aminomethyl)phenyl)porphyrin.

3.3.7 Partial protection with Boc

To obtain porphyrins which are partially protected with Boc, 14.1 mg (0.01 mmol) of tetrakis(*p*-(aminomethyl)phenyl)porphyrin was dissolved in 10 ml DMF and 2 equivalents of Boc-O-Su (4.3 mg, 0.02 mmol) were added. Subsequently, DIEA was added till pH ~ 9/10. The result was a mixture of partially protected porphyrins. The ratio between the various porphyrin compounds could be manipulated by changing the ratio porphyrin/Boc-O-Su.

The various porphyrins were purified by HPLC and the identity of the different products was determined by mass spectroscopy (shown in table 2). NMR spectra were registered to establish the identity of the *cis* and *trans* isomers. The *trans* porphyrin eluted 3 minutes before the *cis*, which rendered the purification relatively easy. The purified products were chemically stable and could be stored at $-20\text{ }^{\circ}\text{C}$ for an indefinite period of time.

Substitution	t (min) HPLC	% CH ₃ CN	Mass (Calcd)	Mass (Found)
0 Boc	17.3	31 %	730.9 Da	731.8 Da
1 Boc	22.1	42 %	831.0 Da	832.4 Da
2 Boc <i>trans</i>	25.6	50 %	931.1 Da	932.4 Da
2 Boc <i>cis</i>	28.5	50 %	931.1 Da	932.4 Da
3 Boc	33.3	66 %	1031.3 Da	1032.5 Da
4 Boc	38.9	90 %	1131.4 Da	1131.1 Da

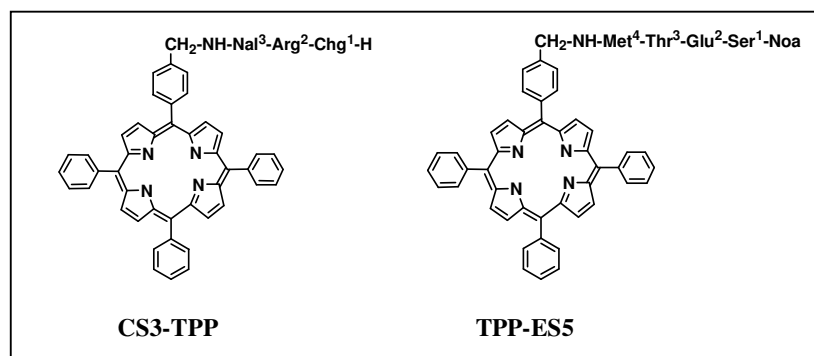
Table 2: Results of the reaction between TAMPP and Boc-O-Su, showing the retention time, elution percentage of acetonitrile and results of mass spectrum.

Chapter 4 Functionalization of the scaffolds

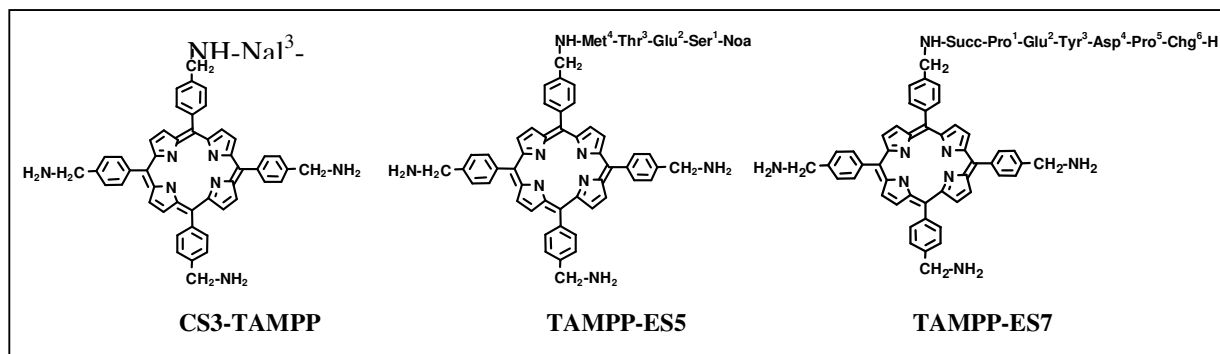
Introduction

The porphyrin scaffolds have been functionalized with three different peptides: Fmoc-Chg-Arg(Pbf)-2Nal-OH, 2Noa-Ser(tBu)-Glu(tBu)-Thr(tBu)-Met-OH and HO-Succ-Pro-Glu(tBu)-Tyr(tBu)-Asp(tBu)-Pro-Chg-OH. The functionalized scaffolds have been named according to the type of porphyrin: tetraphenylporphyrin (TPP) or tetrakis(*p*-aminomethylphenyl)porphyrin (TAMPP). The tripeptide H-Chg¹-Arg²-2Nal³-OH was designed to interact with the thrombin catalytic site (CS), whereas the pentapeptide 2Noa-Ser¹-Glu²-Thr³-Met⁴-OH and the heptapeptide HO-Succ-Pro¹-Glu²-Tyr³-Asp⁴-Pro⁵-Chg⁶-OH were designed interact with the thrombin exo site (ES). The peptides will therefore be indicated as follows: CS3 (tripeptide), ES5 (pentapeptide) e ES7 (heptapeptide). Insertion of manganese(II) yielded Mn^{III} complexes, as most Mn^{II}-porphyrin complexes are unstable in the presence of dioxygen^{132,133}. The following functionalized scaffolds were synthesized:

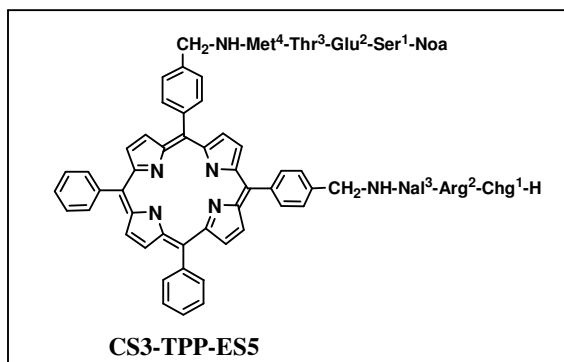
Mono-functionalized TPP compounds:



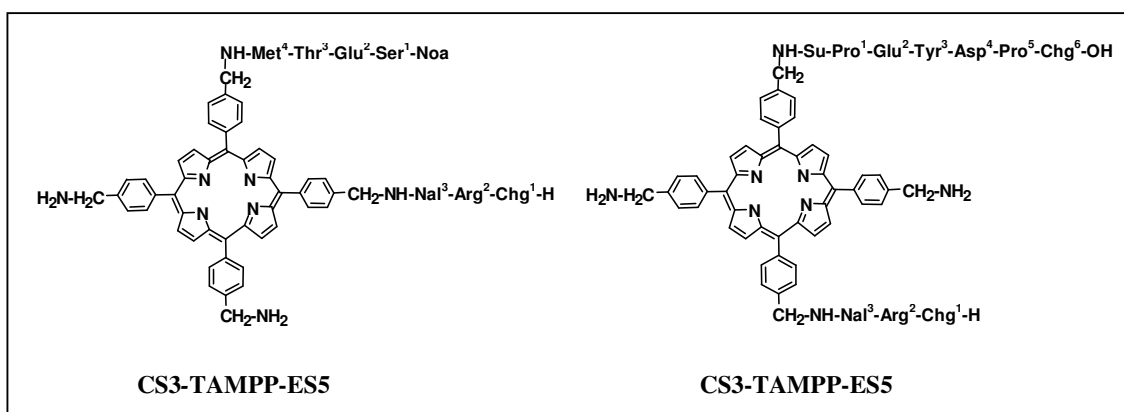
Mono-functionalized TAMPP compounds:



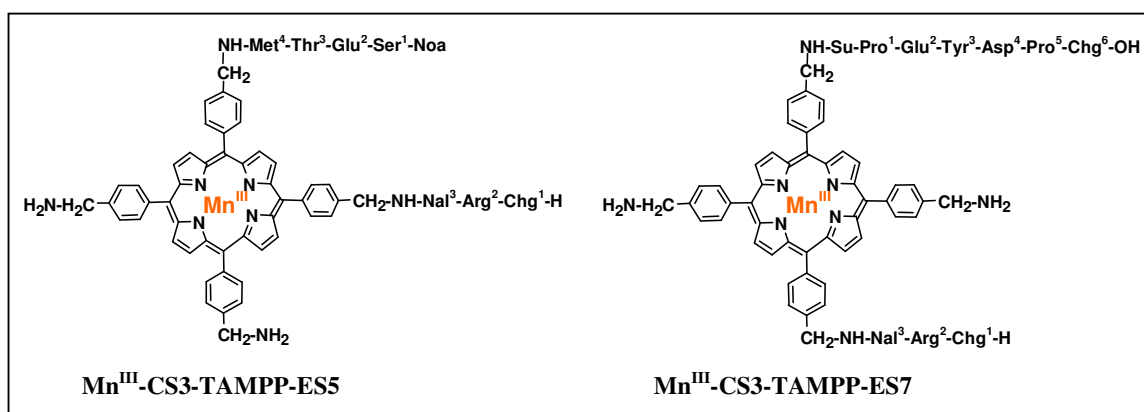
Bi-functionalized TPP compounds:



Bi-functionalized TAMPP compounds:



Mn^{III}-porphyrin complexes:



4.1 Results

4.1.1 Synthesis of the peptides

The following peptides were synthesized:

CS3 : H-Chg¹-Arg²-2Nal³-OH

ES5 : 2Noa-Ser¹-Glu²-Thr³-Met⁴-OH

ES7 : HO-Succ-Pro¹-Glu²-Tyr³-Asp⁴-Pro⁵-Chg⁶-OH

To avoid side reactions during the coupling of the peptides to the scaffold, fully protected peptides were synthesized using Fmoc solid phase peptide synthesis (SPPS)^{134,135}. This peptide synthesis protocol consists of anchoring of the first amino acid to the resin, followed by deprotection of the Fmoc protecting group in 20% piperidine in DMF, coupling of the next amino acid using 3 equivalents of the activators PyBop and HOBt in the presence of 6 equivalents of DIEA, and subsequent deprotection of the new Fmoc protecting group. The resin of choice for all four synthesized peptides was the 2-chloro-tritylchloride resin (shown in figure 1). This resin allows cleavage of the peptide from the resin while leaving all protecting groups on the side-chains, as well as on the N-terminal residue, intact^{136,137}.

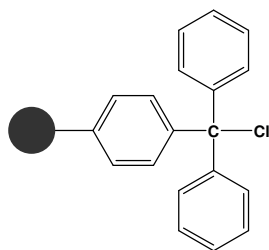


Figure 1: Resin 2-chloro-tritylchloride

Anchoring of the first amino acid on the 2-chloro-tritylchloride resin took place in DMF in the presence of 2,5 equivalents of DIEA. The 2-chloro-tritylchloride groups that did not react with the amino acid were blocked by MeOH. Final cleavage of the peptide from the resin took place in a CH₂Cl₂ solution containing 10% acetic acid and 10% trifluoroethanol (TFE).

The N-terminal amino acid of the peptides could be either Boc or Fmoc protected, as the porphyrin scaffolds were found to be stable in both deprotection reactions (50% TFA in CH₂Cl₂/DMF for deprotection of Boc, 20% piperidine in CH₂Cl₂/DMF for

deprotection of Fmoc). In fact, the tripeptide H-Chg-Arg(Pbf)-2Nal-OH was synthesized with Fmoc-Chg-OH as well as with Boc-Chg-OH as N-terminal amino acid, and the coupling to the porphyrin scaffold was performed with both peptides to prove the stability of the scaffold during the deprotection reaction. In the case of these particular peptides, having acid-labile side chain protecting groups, the presence of the Boc-protected peptide meant one less deprotection step, since the Boc protecting group could be removed together with the other protecting groups in a mixture of TFA and scavengers. However, it was important to determine the stability of the scaffolds in all possible conditions, to ascertain the possibility to use these extremely versatile scaffolds for other applications in which the peptide sequence might dictate a different use of protecting groups. For the synthesis of the three peptides the following amino acids were used:

CS3: Fmoc-Nal-OH, Fmoc-Arg(Pbf)-OH, Fmoc-Chg-OH / Boc-Chg-OH.

ES5: Fmoc-Met-OH, Fmoc-Ser(tBu)-OH, Fmoc-Glu(tBu)-OH, Fmoc-Thr(tBu)-OH, and 2-naphthoxyacetic acid (Noa, see figure 2).

ES7: Fmoc-Chg-OH, 2 Fmoc-Pro-OH, Fmoc-Asp(tBu)-OH, Fmoc-Tyr(tBu)-OH, Fmoc-Glu(tBu)-OH, and succinic anhydride (Succ).

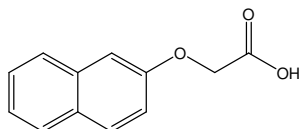


Figure 2: Structure of naphthoxyacetic acid

The peptides CS3 and ES5 were synthesized on a 0.25 mmol scale, using resin substitutions varying from 0.55 to 0.65 mmol/g. When the original resin substitution was significantly higher, the substitution was lowered to the desired amount by using a deficient amount of peptide for the anchoring of the first amino acid. After cleavage of the resin the products were pure and did not require further purification. The peptides were obtained as white solids with an average yield of 85%.

The hexapeptide H-Pro-Glu(tBu)-Tyr(tBu)-Asp(tBu)-Pro-Chg-OH was synthesized on a 0.1 mmol scale, with a resin substitution of 0.86 mmol/g. After completion of the synthesis, a small part of the resin (2.0 mg) was taken apart and cleavage was performed to confirm the identity and purity of the product. The peptide ES7 was designed to interact with the thrombin exo site by its C-terminal end, therefore it had to be linked to

the porphyrin scaffold by its N-terminal end. Succinic acid was chosen as an opportune spacer, and was introduced by bubbling the resin with a DMF solution containing 4% pyridine and 4.7% succinic anhydride. The peptide was not cleaved from the resin, since that would yield a peptide bearing two free carboxyl groups, while only the N-terminal end of the peptide had to be activated to react with the porphyrin scaffold. Therefore, activation of the peptide and coupling to the scaffold took place with the peptide still attached to the resin, and cleavage was performed only after the coupling reaction was complete.

4.1.2 Activation of the peptides

Peptide synthesis protocols usually employ activants such as PyBop, DCC, HOBt, HATU, or HBTU in the presence of DIEA, to activate the free carboxyl groups and perform the coupling reaction to the next amino acid¹³⁸. Essentially the coupling reaction between the amine groups of the porphyrin scaffolds and the carboxyl ends of the peptides should be the same as the coupling of two amino acids. However, difficulties were encountered when these activants were used for linking the synthesized peptides to the porphyrin scaffolds. It has been impossible to create reaction conditions for the functionalization reaction to take place using these activants, even when a single amino acid was used instead of the peptide. Therefore, the problem seemed to lie in the structure of the porphyrin scaffold, more specifically in the elevated hygroscopicity of the tetrakis(*p*-(aminomethyl)phenyl)porphyrin. It is known that the merest presence of water inactivates the herefore mentioned activants, which explains why the coupling reaction could not take place.

Since the porphyrin scaffold could not be easily obtained in complete absence of water, a different approach was used to link the peptides to the scaffold. The peptides were activated by N-hydroxysuccinimide¹³⁹, an activant that nowadays is not often employed. This activant allows the activation of the peptide carboxyl groups (in absence of water) and isolation of the activated product, while the second step, the coupling of the activated peptide to the free amine group, can take place in a variety of solvents, including water. Therefore, the presence of a small amount of water, due to the hygroscopicity of the porphyrin scaffold, does not interfere with the linking of the peptide to the scaffold.

The carboxyl groups of the peptides CS3 and ES5 were activated by N-hydroxysuccinimide in the presence of dicyclohexylcarbodiimide according to the following scheme:

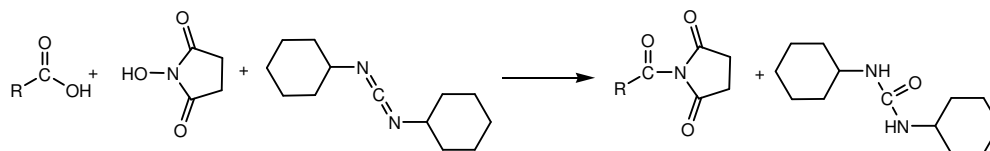


Figure 3: Activation of the carboxyl group of a peptide (R) with N-hydroxysuccinimide in the presence of dicyclohexylcarbodiimide.

The activation reaction took place at 4 °C. After stirring the peptide with the N-hydroxysuccinimide for 10 min, 1 equivalent of dicyclohexylcarbodiimide (DCC) was added. The reaction was complete after 24-36 h, the product was purified by HPLC and could be stored at -20 °C for an indefinite period of time. For the peptide ES7 the activation took place while the peptide was still attached to the resin, by adding excess (3 eq) of both N-hydroxysuccinimide and DCC to the resin and bubbling with nitrogen for 24 h. A small part of the resin was taken apart and the peptide was cleaved to confirm the completion of the activation reaction.

4.1.3 Functionalization of the scaffolds

The coupling reaction between the activated peptide and the porphyrin scaffold took place according to the following scheme:

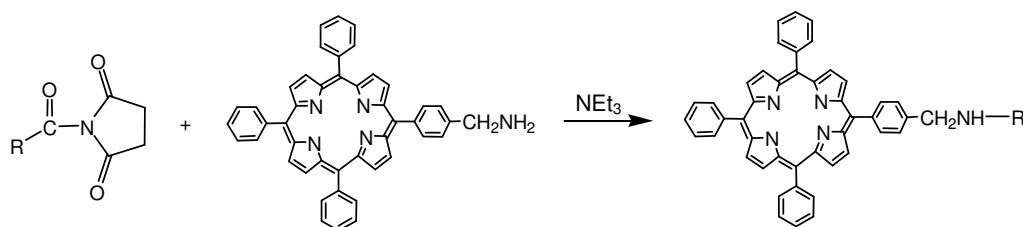


Figure 4: Reaction of the activated peptide (R) with the amine group of the porphyrin scaffold in the presence of triethylamine

The reaction took place in $\text{CH}_2\text{Cl}_2/\text{DMF}$ at room temperature. Triethylamine was added till pH ~ 9/10. The proceeding of the reaction was followed by TLC and RP-HPLC. After completion of the reaction, usually after 15-20 min, the product was purified either by chromatography on silica gel or by HPLC.

For the synthesis of bi-functionalized porphyrin compounds, two different approaches were possible. One possibility was to protect one of the free amine groups (for example with a Fmoc or Boc protecting group), so the first activated peptide could be added without formation of the dimer; the other possibility was to use no protecting groups, so a deficient amount of the activated peptide had to be added in order to avoid formation of the dimer. In this last case, it would not be possible to obtain a 100% yield of the mono-functionalized porphyrin. However, if one of the amine groups was protected, the protecting group would have to be removed after linking of the first peptide, without disturbing the protecting groups present on this peptide. Also, additional protection/deprotection/purification steps usually caused a small loss of the intermediates, resulting in lower yields. Therefore, it was decided to perform the synthesis of the bi-functionalized compounds without additional protecting groups, in order to avoid unnecessary loss of product. Even though the first functionalization step did not have a 100% yield, the starting compounds could be easily recovered and used in subsequent syntheses. Both CS3-TAMPP-ES5 and CS3-TAMPP-ES7 had the tripeptide Boc-Chg-Arg(Pbf)-2Nal-OH in common. For the CS3-TPP-ES7 the heptapeptide had to be linked to the scaffold while being still attached to the resin, so it was a logical choice to add first the tripeptide, and then the second (hepta)peptide. Even though there was no particular reason to favour one or other of the peptides in the case of CS3-TPP-ES5, the same procedure was followed, consisting of linking first the tripeptide and afterwards the second (penta)peptide.

The mono-functionalized porphyrins CS3-TPP, TPP-ES5, CS3-TAMPP, TAMPP-ES5 and TAMPP-ES7 were synthesized with an average yield of 80%. For the bi-functionalized porphyrins, the linking of the first peptide had an average yield of 45%, whereas the coupling of the second peptide usually had yields of 70-80%, resulting in overall yields of 30-35%.

The deprotection of the protecting groups took place at 0 °C in the following mixture:

9 eq trifluoroacetic acid (TFA)
1 eq thioanisole
0.6 eq ethanedithiol (EDT)
0.3 eq β-mercapto-ethanol
0.2 eq anisole

The thiol-based scavengers were added to avoid any side reactions that might occur when the protecting groups were removed from the peptide side chains. For the

compounds containing only the peptide ES5 or ES7, the deprotection was usually complete after 1 h, when the peptide CS3 was present reaction times of 2-3 h were necessary, due to the presence of the Pbf protecting group which required a prolonged reaction time. After completion of the reaction the solvent was evaporated, the major part of the scavengers was removed by extraction with diethyl ether, and the product was further purified by HPLC. Average yields were 60-70%.

4.1.4 Insertion of manganese in the peptide-porphyrin compounds

For the insertion of manganese, the previously mentioned acetate method was used (see paragraph 1.2.2). The reaction took place in a 50% solution of acetic acid in methanol, using manganese(II) acetate as metal provider¹⁴⁰. Upon insertion of the metal in the porphyrin ring, the Mn^{II} ion was oxidized to Mn^{III} . During the reaction the colour of the reaction mixture changed from green to brown/green, indicating the formation of the manganese(III) porphyrin complex. The reaction was monitored by HPLC and UV-VIS, where slowly the characteristic Mn^{III} -porphyrin spectrum became dominant¹⁴¹ (see figure 5). After circa 20 h the reaction was complete and the product was purified by HPLC.

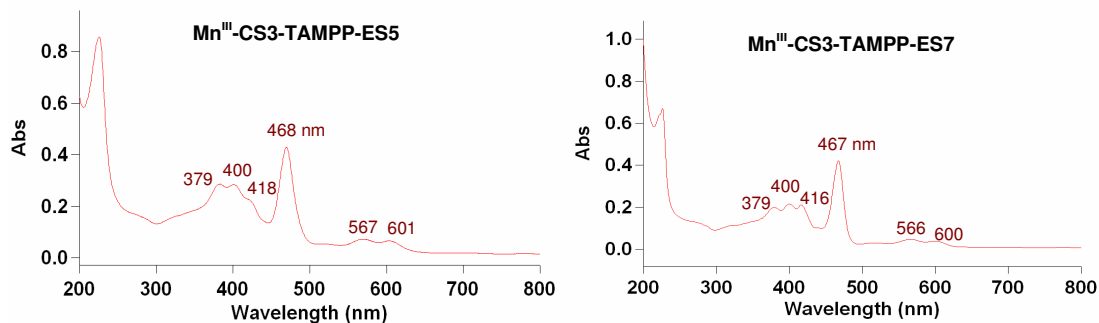


Figure 5: UV-VIS spectrum of the Mn^{III} -complexes of CS3-TAMPP-ES5 and CS3-TAMPP-ES7 in EtOH.

4.2 Discussion

The functionalization of the previously synthesized porphyrin scaffolds was successful in all cases. It was found that peptides had to be activated by N-hydroxysuccinimide, since other activants, such as PyBop, HOBt, HATU did not produce the desired results. It was shown that the functionalization reaction could take place either in solution, or with the activated peptide still attached to the resin. Both Fmoc and Boc protected peptides could be used for functionalization of the scaffolds, as the versatile porphyrin scaffolds proved to be stable in both deprotection protocols. The functionalization reaction could take place either in solution or with the activated peptide still attached to the resin. The straightforward synthesis and work-up using HPLC or column chromatography lead to stable, chemically pure compounds. Removal of the protecting groups took place using a mixture of scavengers in TFA, to avoid undesired alteration of the peptide-porphyrin compound. When stored at $-20\text{ }^{\circ}\text{C}$, the peptide-functionalized porphyrin compounds could be kept for an indefinite period of time. Average yields were 80-90% for the mono-functionalized compounds and 30-35% for the bi-functionalized compounds. However, in the case of the bi-functionalized scaffolds, part of the starting compound used in the first functionalization step could be recovered and used to repeat the reaction, so the actual yields were much higher.

Insertion with manganese took place using $\text{Mn}^{\text{II}}\text{Ac}_2$ in a 50% acetic acid/MeOH solution, upon which Mn^{III} -porphyrin complexes were formed. Since the peptide-porphyrin compounds had the tendency to aggregate in aqueous solutions, all extinction coefficients were determined in ethanol.

4.3 Experimental section

4.3.1 Materials and methods

Unless otherwise stated, solvents of anhydroscale grade were used for all reactions. Reagents were obtained from commercial suppliers and used as received. All manipulations and reactions were carried out using standard Schlenk techniques. Solid phase peptide synthesis was performed manually in a 20 ml reactor. Analysis of reaction mixtures and products was performed by TLC on silica, or by using a RP-HPLC Shimadzu system LC-10AD VP with a spectrophotometric detector Diode Array SPD-M10A VP. Linear gradients were used of H₂O 0.1% TFA and CH₃CN 0.1% TFA. UV-VIS spectra were recorded with a Varian Cary 5000 spectrophotometer. Mass spectrometry was carried out on a Voyager DEPRO MALDI-TOF spectrometer (Applied Biosystems) in the linear mode, using bovine insulin as internal calibration standard. The matrix α -cyano-4-hydroxycinnamic acid was recrystallized from EtOH / H₂O prior to use.

4.3.2 Synthesis of the peptides

Synthesis of the tripeptide Fmoc-Chg-Arg(Pbf)-2Nal-OH

The substitution of the resin was 0.64 mmol/g, the reaction scale 0.25 mmol. The following amino acids were used: Fmoc-Nal-OH, Fmoc-Arg(Pbf)-OH and Fmoc-Chg-OH. As shown by the HPLC chromatogram, after cleavage from the resin, the product, with a retention time of 25.98 min, was pure and did not require further purification. The identity of the product was determined by mass spectroscopy: 985.62 Da (calculated 984.0 Da). After evaporation of the solvent the peptide was dissolved in H₂O 0.1% TFA and CH₃CN 0.1% TFA, and freeze-dried to obtain 206.6 mg of a white solid (0.21 mmol, 84 %).

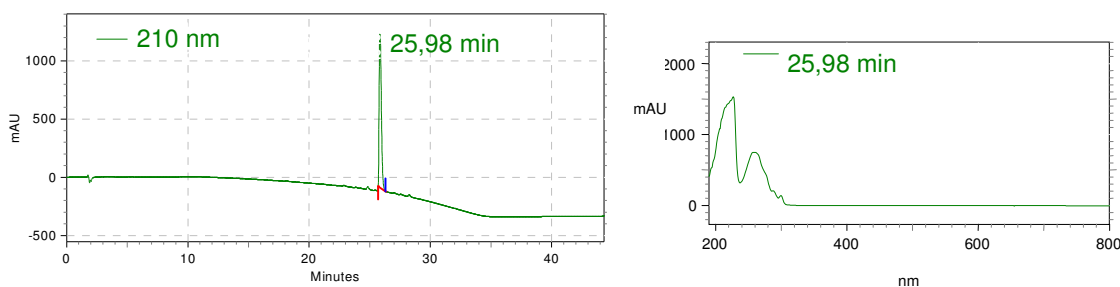


Figure 6: HPLC chromatogram and UV-VIS spectrum of Fmoc-Chg-Arg(Pbf)-2Nal-OH.

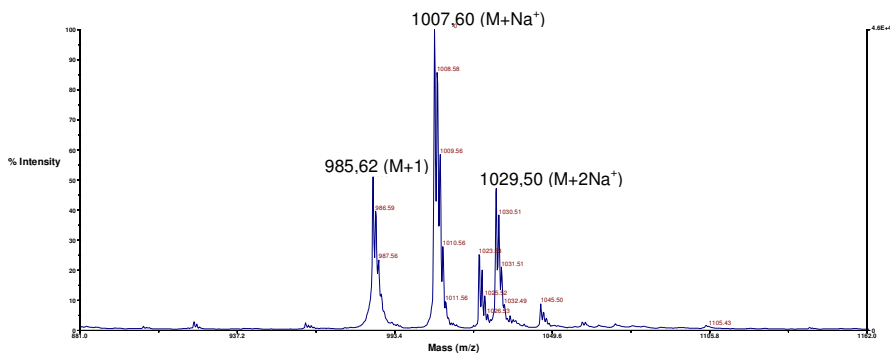


Figure 7: Mass spectrum of Fmoc-Chg-Arg(Pbf)-2Nal-OH.

Synthesis of the tripeptide Boc-Chg-Arg(Pbf)-2Nal-OH

The original substitution of the resin was 1.69 mmol/g. By adding a deficient amount of the first amino acid followed by capping with MeOH, the substitution was lowered to 0.65 mmol/g. The reaction scale was 0.25 mmol. The following amino acids were used: Fmoc-Nal-OH, Fmoc-Arg(Pbf)-OH and Boc-Chg-OH. As shown by the HPLC chromatogram of the product after cleavage from the resin, the product was pure and did not require further purification. The identity of the product was determined by mass spectroscopy: 884.2 Da (calculated: 861.8 Da, 884.2 Da = $M+Na^+$). After evaporation of the solvent, the peptide was dissolved in H₂O 0,1% TFA and CH₃CN 0,1% TFA, and freeze-dried to obtain 203 mg of a white solid (0.236 mmol, 94.4%).

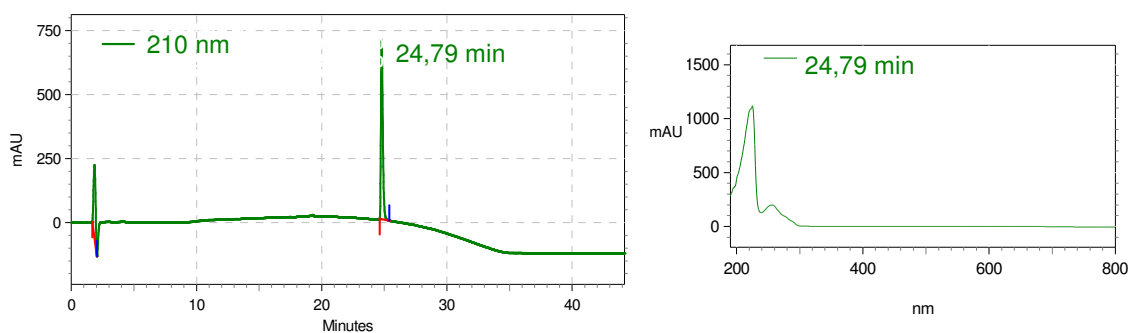


Figure 8: HPLC chromatogram and UV-VIS spectrum of Boc-Chg-Arg(Pbf)-2Nal-OH.

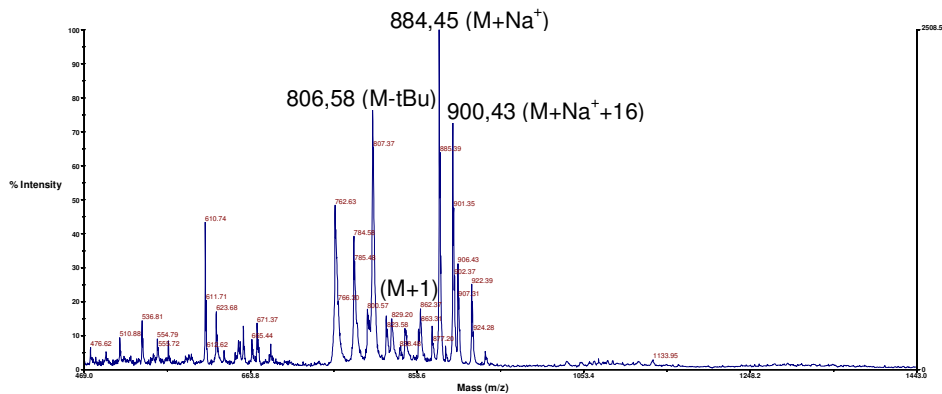


Figure 9: Mass spectrum of Boc-Chg-Arg(Pbf)-2NaI-OH.

Synthesis of the pentapeptide 2Noa-Thr(tBu)-Glu(tBu)-Ser(tBu)-Met-OH

The substitution of the resin was 0.55 mmol/g, the reaction scale 0.25 mmol. The following amino acids were used: Fmoc-Met-OH, Fmoc-Ser(tBu)-OH, Fmoc-Glu(tBu)-OH, Fmoc-Thr(tBu)-OH and 2-naphtyloxyacetic acid. As shown by the HPLC chromatogram of the product after cleavage from the resin, the product was pure and did not require further purification. The identity of the product was determined by mass spectroscopy: 842.1 Da (calculated: 819.0 Da, 842.1 Da = M+Na⁺). After evaporation of the solvent, the peptide was dissolved in H₂O 0.1% TFA and CH₃CN 0.1% TFA, and freeze-dried to obtain 160 mg of a white solid (0.20 mmol, 78%).

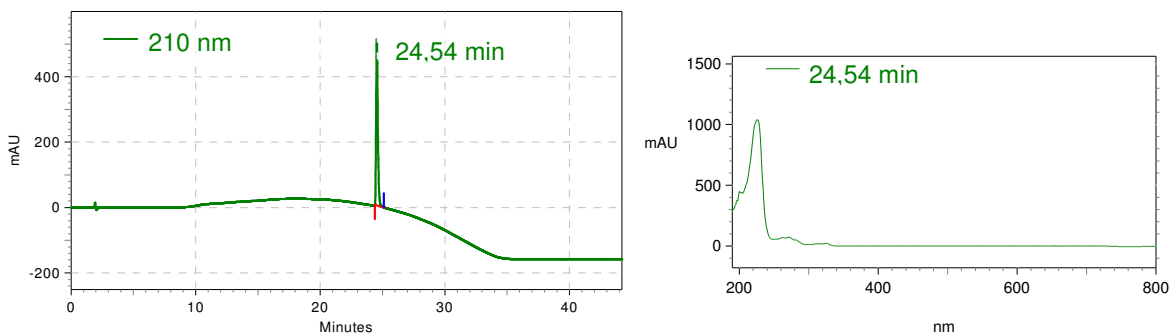


Figure 10: HPLC chromatogram and UV-VIS spectrum of 2Noa-Thr(tBu)-Glu(tBu)-Ser(tBu)-Met-OH.

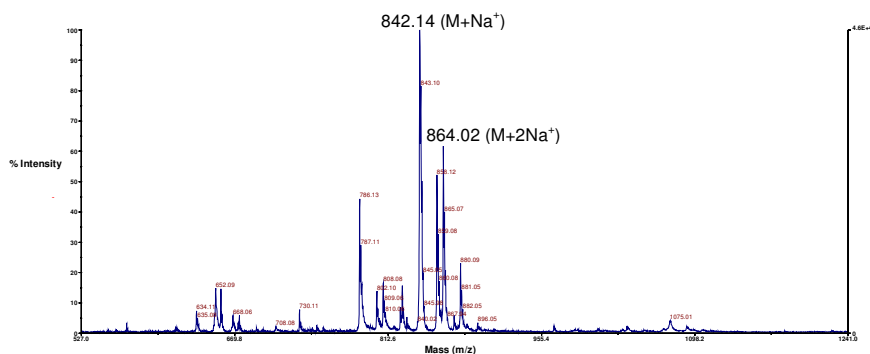


Figure 11: Mass spectrum of 2Noa-Thr(tBu)-Glu(tBu)-Ser(tBu)-Met-OH

Synthesis of HO-Succ-Pro-Glu(tBu)-Tyr(tBu)-Asp(tBu)-Pro-Chg-OH

The substitution of the resin was 0.86 mmol/g, the reaction scale 0.1 mmol. The following amino acids were used: Fmoc-Chg-OH, Fmoc-Pro-OH, Fmoc-Asp(tBu)-OH, Fmoc-Tyr(tBu)-OH and Fmoc-Glu(tBu)-OH. To confirm the identity of the hexapeptide H-Pro-Glu(tBu)-Tyr(tBu)-Asp(tBu)-Pro-Chg-OH, a small part of the resin (2.0 mg) was taken apart and cleavage of the peptide from the resin was performed using 10 ml $\text{CH}_2\text{Cl}_2/\text{TFE}/\text{HAc} = 8/1/1$ for 30 min. The HPLC chromatogram showed the presence of one major product, of which the identity was determined by mass spectroscopy: 949.5 Da (calculated 927.15 Da, 949.5 Da = $M+\text{Na}^+$).

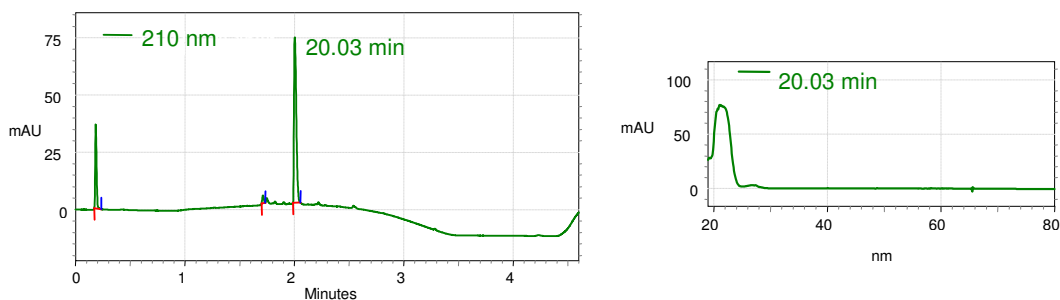


Figure 12: HPLC chromatogram and UV-VIS spectrum of the hexapeptide H-Pro-Glu(tBu)-Tyr(tBu)-Asp(tBu)-Pro-Chg-OH.

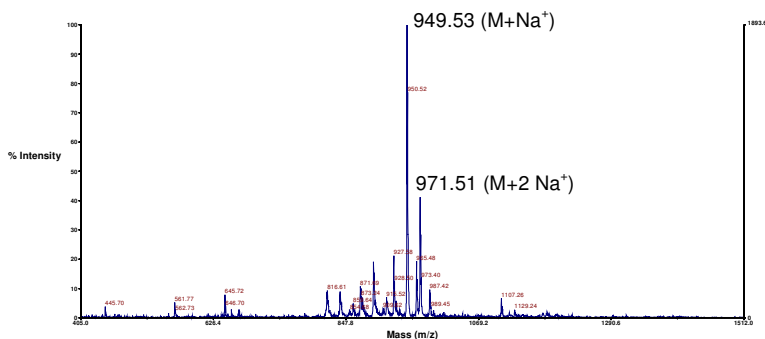


Figure 13: Mass spectrum of the hexapeptide H-Pro-Glu(tBu)-Tyr(tBu)-Asp(tBu)-Pro-Chg-OH.

Since this peptide was designed to bind the amine group of the porphyrin scaffold with its N-terminal end, succinic acid was introduced at the N-terminus of the peptide by bubbling the resin with a 4% pyridine 4.7% succinic anhydride DMF solution, for 15 min, repeated two times. Again, a small part of the resin (2.0 mg) was taken apart to confirm the formation of the desired product. Cleavage of the peptide from the resin was performed using 10 ml $\text{CH}_2\text{Cl}_2/\text{TFE}/\text{HAc} = 8/1/1$ for 30 min. The HPLC chromatogram showed the presence of one major product, of which the identity was determined by mass spectroscopy: 1049.2 Da (calculated 1026.2 Da, 1049.2 Da = $\text{M}+\text{Na}^+$). The peptide remained attached to the resin.

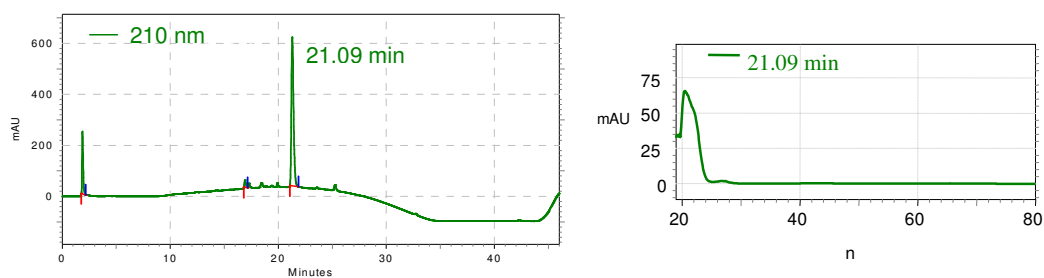


Figure 14: HPLC chromatogram and UV-VIS spectrum of HO-Succ-Pro-Glu(tBu)-Tyr(tBu)-Asp(tBu)-Pro-Chg-OH.

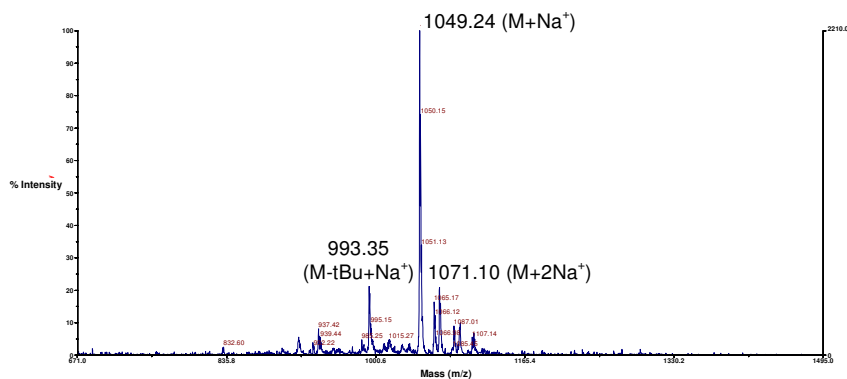


Figure 15: Mass spectrum of HO-Succ-Pro-Glu(tBu)-Tyr(tBu)-Asp(tBu)-Pro-Chg-OH.

4.3.3 Activation of the peptides

Activation of the tripeptide Fmoc-Chg-Arg(Pbf)-2Nal-OH

10.2 mg (0.01 mmol) of the Fmoc-tripeptide was dissolved in 6 ml CH_2Cl_2 , after which 1.2 mg (1 eq) of N-hydroxysuccinimide was added. After stirring for 10 min at 4 °C, 21 μl 0.5 M (1 eq) of DCC in CH_2Cl_2 was added slowly to the reaction mixture. After 24 h at 4 °C, a white precipitate (N,N'-dicyclohexylurea) had formed. The HPLC chromatogram showed the presence of a new peak with a retention time of ~1,1 min more than the original peptide. The identity of the product was determined by mass spectroscopy: 1104.5 Da (calculated 1081.1 Da, 1104.49 Da = M+Na⁺). The activated peptide was purified by HPLC and freeze-dried to obtain 7.8 mg of a white solid (0.007 mmol, 72%).

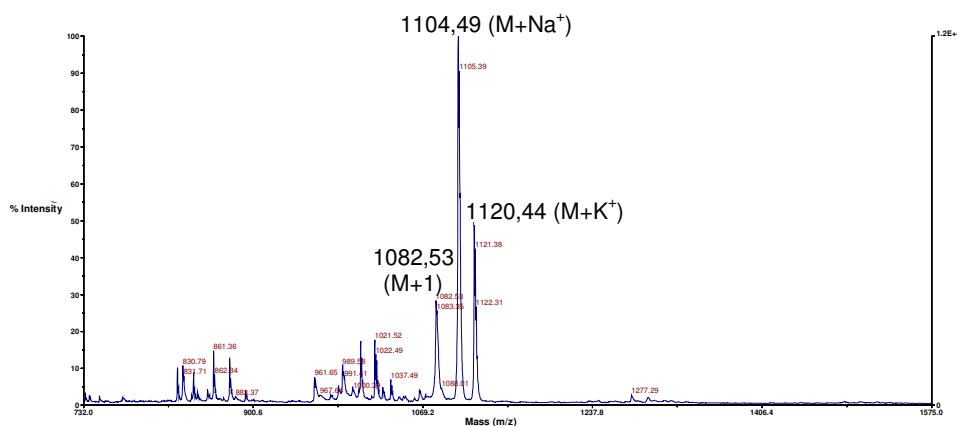


Figure 16: Mass spectrum of the activated Fmoc-Chg-Arg(Pbf)-2Nal-N-Su.

Activation of the tripeptide Boc-Chg-Arg(Pbf)-2Nal-OH

21.5 mg (0.025 mmol) of the Boc-tripeptide was dissolved in 10 ml CH_2Cl_2 , after which 2.88 mg (1 eq) of N-hydroxysuccinimide was added. After stirring for 10 min at 4 °C, 50 μl 0.5 M (1 eq) of DCC in CH_2Cl_2 was added slowly to the reaction mixture. After 24 h at 4 °C a white precipitate had formed. The HPLC chromatogram showed the presence of a new peak with a retention time of ~1,4 min more than the original peptide. The identity of the product was determined by mass spectroscopy: 982.8 Da (calculated 959.0 Da, 982.8 Da = M+Na⁺). The activated peptide was purified by HPLC and freeze-dried to obtain 18.2 mg of a white solid (0.019 mmol, 76%).

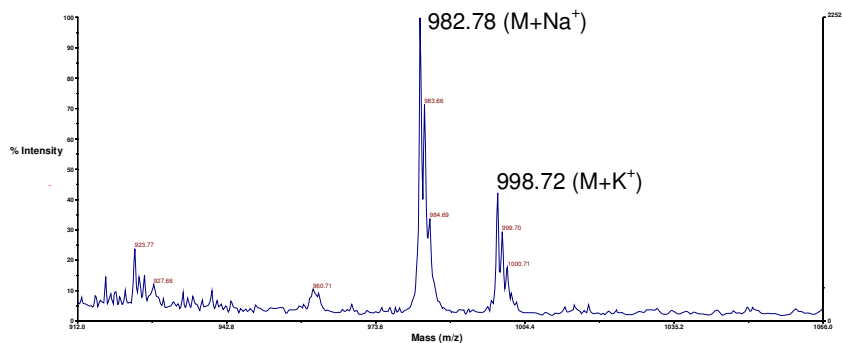


Figure 17: Mass spectrum of the activated Boc-Chg-Arg(Pbf)-2Nal-N-Su.

Activation of the pentapeptide 2Noa-Thr(tBu)-Glu(tBu)-Ser(tBu)-Met-OH

12.3 mg (0.015 mmol) of the pentapeptide was dissolved in 10 ml CH_2Cl_2 , after which 1.73 mg (1 eq) of N-hydroxysuccinimide was added. After stirring for 10 min at 4°C , $30 \mu\text{l}$ 0.5 M (1 eq) of DCC in CH_2Cl_2 was slowly added to the reaction mixture. After 24 h at 4°C a white precipitate was formed. The HPLC chromatogram showed the presence of a new peak with a retention time of ~ 1.4 min more than the original peptide. The identity of the product was determined by mass spectroscopy: 955.2 Da (calculated 916.0 Da, $955.2 \text{ Da} = \text{M}+\text{K}^+$). The activated peptide was purified by HPLC and freeze-dried to obtain 9.34 mg of a white solid (0.010 mmol, 68%).

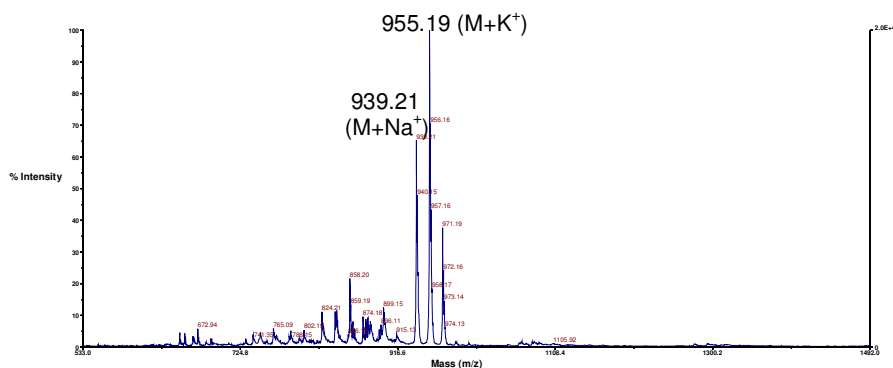


Figure 18: Mass spectrum of the activated 2Noa-Thr(tBu)-Glu(tBu)-Ser(tBu)-Met-N-Su.

Activation of HO-Succ-Pro-Glu(tBu)-Tyr(tBu)-Asp(tBu)-Pro-Chg-OH

While bubbling with N_2 , a solution of 10 mg (0.087 mmol, 10 eq) N-hydroxysuccinimide in 10 ml of $\text{CH}_2\text{Cl}_2/\text{DMF} = 1/1$ was added at room temperature to 22.8 mg di resin ($8.7 \mu\text{mol}$ peptide, substitution = 0.38 mmol/g). After 10 min, $200 \mu\text{l}$ 0.5 M DCC in CH_2Cl_2 (1.1 eq) was added, after which the solution was kept for 24 h.

The resin was washed 5 times with $\text{CH}_2\text{Cl}_2/\text{DMF}$ and dried with N_2 . The activated peptide remained attached to the resin.

4.3.4 Coupling of the peptides to the porphyrin scaffolds

Mono-functionalized scaffolds

Synthesis of CS3-TPP

1.6 mg (2.5 μmol) tetrakis(*p*-aminomethylphenyl)porphyrin and 1 eq (2.7 mg) activated Fmoc-Chg-Arg(Pbf)-Nal-N-Su were dissolved in a mixture of $\text{CH}_2\text{Cl}_2/\text{DMF}$ (50/50). Triethylamine was added till pH \sim 9/10 (approximately 1.5 μl). After 15 min, the HPLC chromatogram showed that the starting porphyrin at 20.4 min had almost completely disappeared, and a new porphyrin had appeared with retention time 31.0 min. The identity of this product was confirmed by mass spectroscopy to be the desired CS3-TPP (protecting groups included): 1633.8 Da (calculated 1609.8 Da; 1633.8 Da corresponds to the sodium salt of CS3-TPP). The product was purified by HPLC and freeze-dried to obtain 3.0 mg (2.0 μmol , 79%) of a green solid.

The first deprotection reaction involved the removal of the Fmoc group in 20% piperidine in DMF. The reaction was followed by TLC (silica, eluent $\text{CH}_2\text{Cl}_2/\text{MeOH} = 9/1$), where the protected CS3-TPP had $R_F = 0.58$. After 30 min the reaction was complete: the starting compound had disappeared and a new compound had formed with $R_F = 0.3$. The solvent was removed in vacuo, after which the remaining Pbf protecting group was removed by dissolving the product in 4 ml of the earlier described cleavage mixture (see paragraph 4.1.3) and stirring for 2 h. The reaction was followed by HPLC, where slowly a new porphyrin appeared at retention time 22.9 min. When the reaction was complete, the solvent was evaporated, the product washed several times with diethyl ether to remove the major part of the scavengers, purified by HPLC and freeze-dried to obtain 2.5 mg (1,6 μmol , 80%) of a green solid. The mass spectrum confirmed the identity of the completely deprotected CS3-TPP: 1137.7 Da (calculated 1137.5 Da).

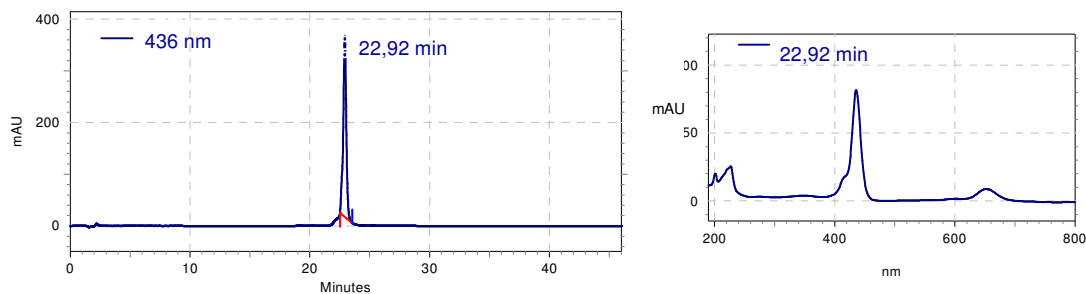


Figure 19: HPLC chromatogram and UV-VIS spectrum of CS3-TPP.

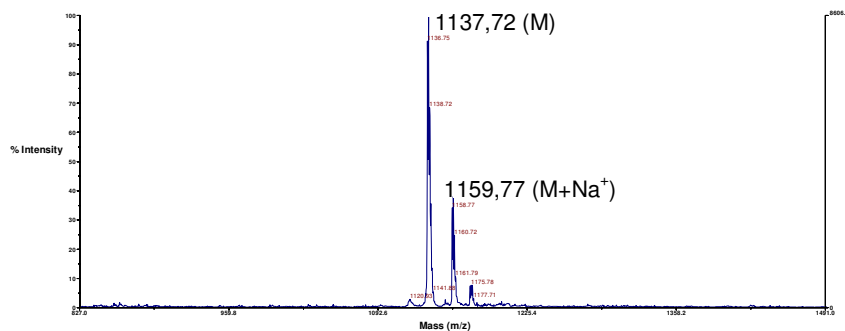


Figure 20: Mass spectrum of CS3-TPP.

Synthesis of TPP-ES5

0.64 mg (1.0 μmol) *p*-aminomethyltetraphenylporphyrin and 1 eq (0.92 mg) activated ES5 were dissolved in a mixture of $\text{CH}_2\text{Cl}_2/\text{DMF}$ (50/50). Triethylamine was added till pH \sim 9/10 (approximately 0.7 μl). After 15 min, the TLC (eluent: $\text{CH}_2\text{Cl}_2/\text{MeOH} = 9/1$) showed that the starting porphyrin ($R_F = 0.2$) had disappeared, whereas a new porphyrin had appeared with $R_F = 0.5$). The same tendency was observed in the HPLC chromatogram, where the starting porphyrin at 20.4 min had almost completely disappeared, and a new porphyrin had appeared at retention time 31.1 min. The product was purified by HPLC and freeze-dried to obtain 1.2 mg (0.7 μmol , 70%) of a green solid.

The protecting groups were removed by dissolving the product in 4 ml of the earlier described cleavage mixture (see paragraph 4.1.3) and stirring for 1 h. The reaction was followed by HPLC, where slowly a new porphyrin appeared at retention time 21.8 min. When the reaction was complete, the solvent was evaporated, the product washed several times with diethyl ether to remove the major part of the scavengers, purified by HPLC and freeze-dried to obtain 0.8 mg (0.53 μmol , 75%) of a green solid. The mass spectrum confirmed the identity of the completely deprotected TPP-ES5: 1293.7 Da

(calculated 1276.8 Da, 1293.7 Da corresponds to TPP-ES5 with the methionine residue oxidized to Met(O)).

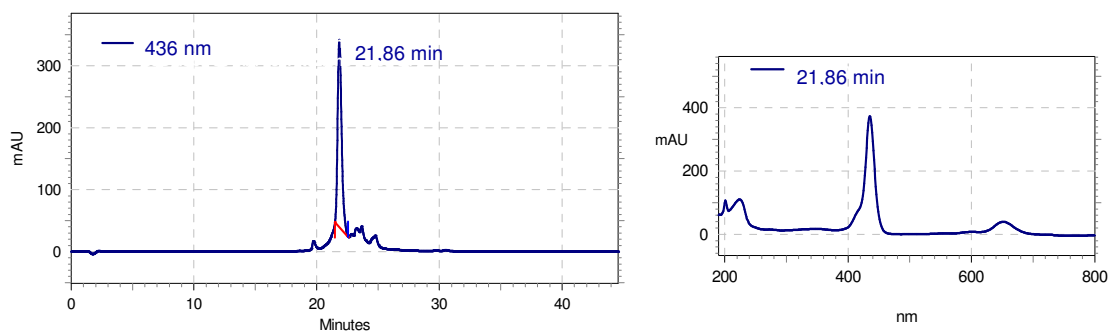


Figure 21: HPLC chromatogram and UV-VIS spectrum of TPP-ES5.

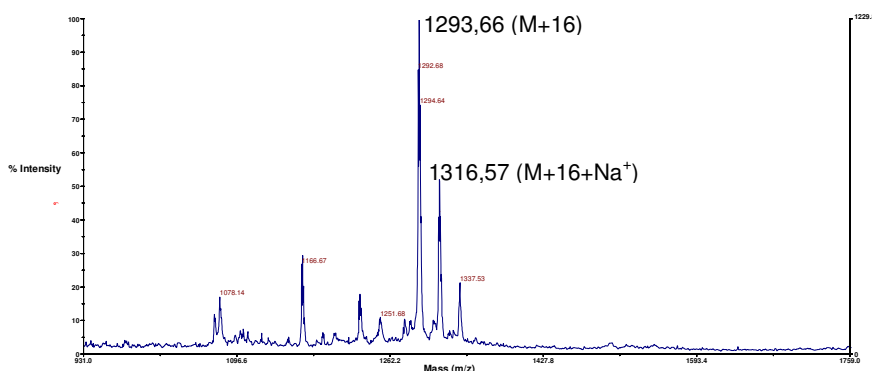


Figure 22: Mass spectrum of TPP-ES5.

Synthesis of CS3-TAMPP

4.6 mg (3.4 μmol) 3Boc-TAMPP and 1 eq (3.2 mg) activated Boc-tripeptide were dissolved in a mixture of $\text{CH}_2\text{Cl}_2/\text{DMF}$ (50/50). Triethylamine was added till pH \sim 9/10 (approximately 1,4 μl). After 15 min, the TLC (eluent: $\text{CH}_2\text{Cl}_2/\text{MeOH}$ = 9/1) showed that the starting porphyrin (R_F = 0,2) had disappeared, whereas a new porphyrin had appeared with R_F = 0.5). The same tendency was observed in the HPLC chromatogram, where the starting porphyrin had almost completely disappeared, and a new porphyrin had appeared at retention time 28.6 min. The product was purified by column chromatography (silica gel, eluent $\text{CH}_2\text{Cl}_2/\text{MeOH}$ = 9/1). After evaporation of the solvent, 5.61 mg (3.0 μmol , 90%) of a dark red solid was obtained.

The protecting groups were removed by dissolving the product in 4 ml of the earlier described cleavage mixture (see paragraph 4.1.3) and stirring for 2 h. The reaction was followed by HPLC, where slowly a new porphyrin appeared at retention time 22.0 min. When the reaction was complete, the solvent was evaporated, the product washed

several times with diethyl ether to remove the major part of the scavengers, purified by HPLC and freeze-dried to obtain 4.89 mg (1.6 μmol , 80%) of a green solid. The mass spectrum confirmed the identity of the completely deprotected CS3-TAMPP: 1223.9 Da (calculated 1223.0 Da).

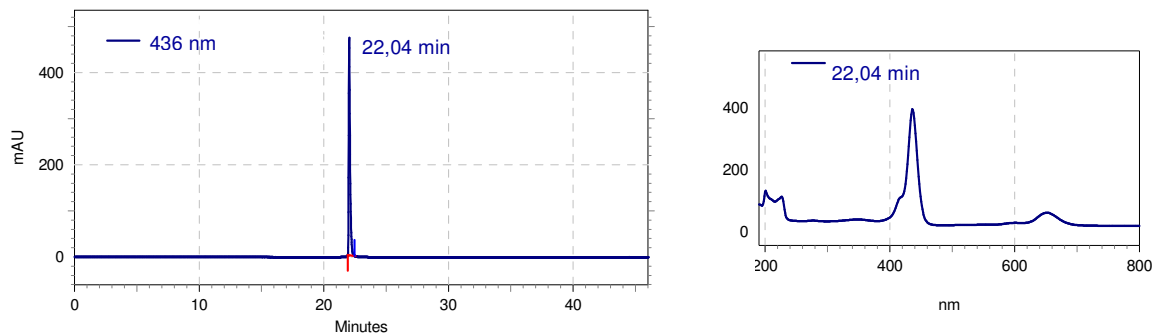


Figure 23: HPLC chromatogram and UV-VIS spectrum of CS3-TAMPP.

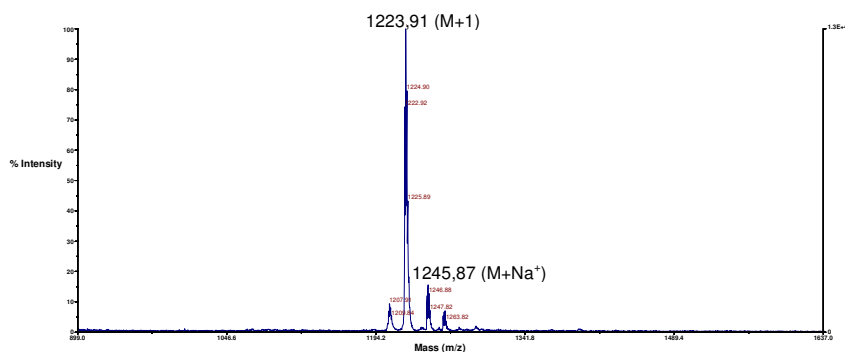


Figure 24: Mass spectrum of CS3-TAMPP.

The extinction coefficient of the pure CS3-TAMPP was determined by measuring the absorbance at 416 nm of different concentrations of CS3-TAMPP in ethanol. The resulting graph of absorbance versus concentration is shown in figure 26. The extinction coefficient $\epsilon_{416 \text{ nm}}$ is calculated to be $3.4 \cdot 10^5 \text{ L} \cdot \text{M}^{-1} \cdot \text{cm}^{-1}$.

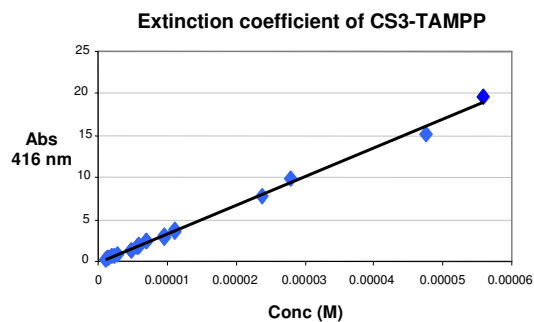


Figure 25: The extinction coefficient of CS3-TAMPP.

Synthesis of TAMPP-ES5

4.6 mg (3.4 μmol) 3Boc-TAMPP and 1 eq (3.1 mg) activated pentapeptide were dissolved in a mixture of $\text{CH}_2\text{Cl}_2/\text{DMF}$ (50/50). Triethylamine was added till pH $\sim 9/10$ (approximately 1.4 μl). After 15 min, the TLC (eluent: $\text{CH}_2\text{Cl}_2/\text{MeOH} = 9/1$) showed that the starting porphyrin ($R_F = 0.2$) had disappeared, whereas a new porphyrin had appeared with $R_F = 0.5$). The same tendency was observed in the HPLC chromatogram, where the starting porphyrin had almost completely disappeared, and a new porphyrin had appeared at retention time 28.2 min. The product was purified by column chromatography (silica gel, eluent $\text{CH}_2\text{Cl}_2/\text{MeOH} = 9/1$). After evaporation of the solvent, 4.8 mg (2.3 μmol , 69%) of a dark red solid is obtained. The protecting groups were removed by dissolving the product in 3 ml of the earlier described cleavage mixture (see paragraph 4.1.3) and stirring for 1 h. The reaction was followed by HPLC, where slowly a new porphyrin appeared at retention time 21.9 min. When the reaction was complete, the solvent was evaporated, the product washed several times with diethyl ether to remove the major part of the scavengers, purified by HPLC and freeze-dried to obtain 3.2 mg (2.0 μmol , 87%) of a green solid. The mass spectrum confirmed the identity of the completely deprotected TAMPP-ES5: 1379.6 Da (calculated 1364.0 Da, 1379.6 Da = Met(O)).

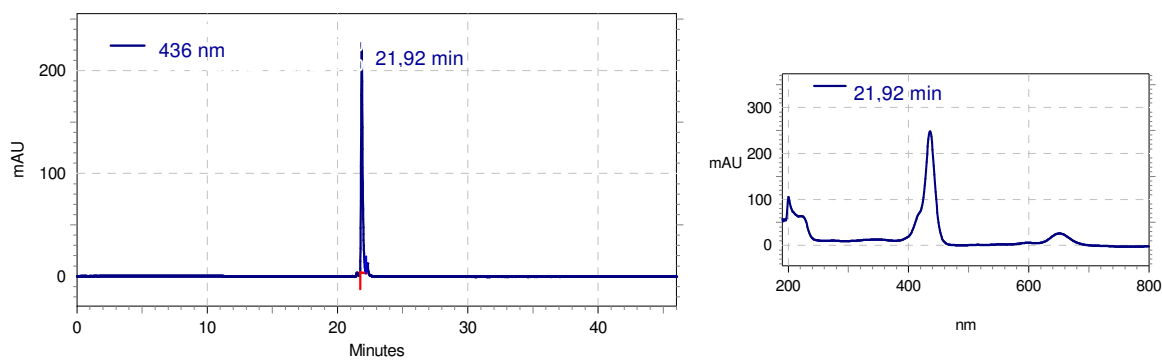


Figure 26: HPLC chromatogram and UV-VIS spectrum of TAMPP-ES5.

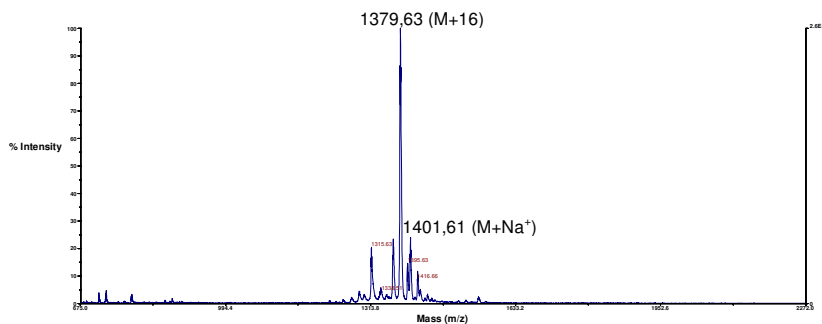


Figure 27: Mass spectrum of TAMPP-ES5.

Synthesis of TAMPP-ES7

2.5 mg (1.8 μmol) 3Boc-TAMPP dissolved in 10 ml $\text{CH}_2\text{Cl}_2/\text{DMF}$ were added to 10 mg of resin containing 3.7 μmol of activated peptide ES7. Triethylamine was added till pH $\sim 9/10$ (approximately 6.0 μl). After 60 min the resin was washed several times with DMF and CH_2Cl_2 . The colour of the resin had changed from yellow to red, indicating the presence of the porphyrin scaffold on the resin. Cleavage of the peptide-porphyrin compound took place by bubbling a solution of $\text{CH}_2\text{Cl}_2/\text{TFE}/\text{acetic acid} = 8/1/1$ for 30 min, repeated two times. After washing the resin several times with CH_2Cl_2 , the fractions were reunited and the solvent was evaporated under vacuo. The TLC (eluent: $\text{CH}_2\text{Cl}_2/\text{MeOH} = 9/1$) showed that the starting porphyrin ($R_F = 0.2$) had disappeared, whereas a new porphyrin had appeared with $R_F = 0.35$). The same tendency was observed in the HPLC chromatogram, where the starting porphyrin had almost completely disappeared, and a new porphyrin had appeared at retention time 27.1 min. The product was purified by column chromatography (silica gel, eluent $\text{CH}_2\text{Cl}_2/\text{MeOH} = 9/1$). After evaporation of the solvent, 2.26 mg (1.3 μmol , 72 %) of a dark red solid is obtained. The protecting groups were removed by dissolving the product in 3 ml of the earlier described cleavage mixture (see paragraph 4.1.3) and stirring for 1 h. The reaction was followed by HPLC, where slowly a new porphyrin appeared at retention time 19.85 min. When the reaction was complete, the solvent was evaporated, the product washed several times with diethyl ether to remove the major part of the scavengers, purified by HPLC and freeze-dried to obtain 1.88 mg (1.2 μmol , 92 %) of a green solid. The mass spectrum confirmed the identity of the completely deprotected TAMPP-ES7: 1569,1 Da (calculated 1568.2 Da).

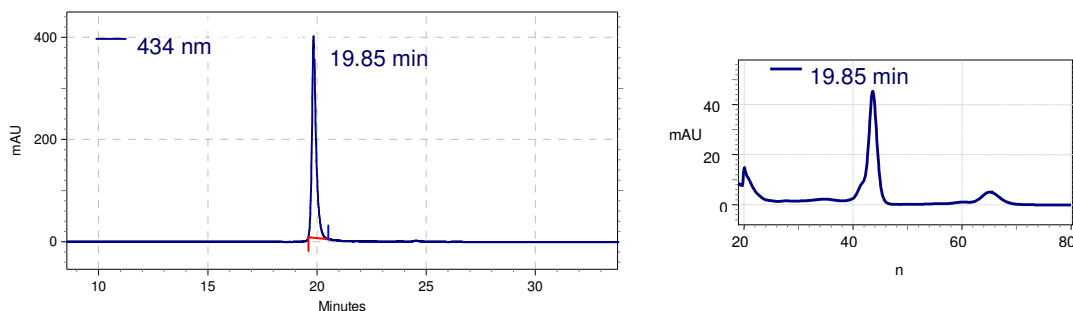


Figure 28: HPLC chromatogram and UV-VIS spectrum of TAMPP-ES7.

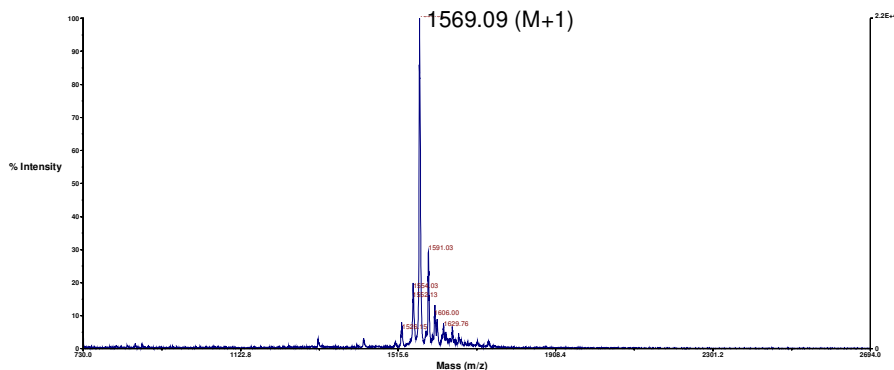


Figure 29: Mass spectrum of TAMPP-ES7.

Bi-functionalized TPP compounds

Synthesis of *cis*-CS3-TPP-ES5

10 mg (8.8 μmol) of 5,10-diphenyl-15,20-bis(*p*-(aminomethyl)phenyl)porphyrin and 5 eq (5.2 μl) TEA were dissolved in 10 ml $\text{CH}_2\text{Cl}_2/\text{DMF}$. A solution of 7.7 mg (7.1 μmol , 0.8 eq) Fmoc-Chg-Arg(Pbf)-2Nal-N-Su in 1,0 ml $\text{CH}_2\text{Cl}_2/\text{DMF}$ was slowly added to the reaction mixture, while at regular intervals the proceeding of the reaction was checked by TLC (silica, eluent $\text{CH}_2\text{Cl}_2/\text{MeOH} = 9/1$). The starting porphyrin had $R_F = 0.0$, the mono-functionalized porphyrin had $R_F = 0.2$. After addition of ~ 0.6 eq of the peptide, a small amount of the dimer ($R_F = 0.5$) started to form, and the reaction was stopped. In the HPLC chromatogram the mono-functionalized porphyrin *cis*-CS3-TPP-NH₂ had a retention time of 27.7 min, the bi-functionalized porphyrin *cis*-2CS3-TPP had a retention time of 34.6 min. The mass spectrum confirmed the identity of the protected *cis*-CS3-TPP-NH₂: 1641.7 Da (calculated 1640.0 Da). The solvent was evaporated in vacuo, the product was purified by HPLC and freeze-dried to obtain 2.16 mg of a green solid (1.1 μmol , 13%).

The second peptide was added by dissolving 2.2 mg (1.1 μmol) of CS3-TPP-NH₂ and 1.21 mg (1 eq) of activated pentapeptide in 4 ml $\text{CH}_2\text{Cl}_2/\text{DMF}$. Subsequently 0.9 μl (5 eq) of TEA was added and the reaction was monitored by TLC (silica, eluent $\text{CH}_2\text{Cl}_2/\text{MeOH} = 9/1$). Only one product was formed, with $R_F = 0.6$, which was purified by column chromatography (silica gel, eluent $\text{CH}_2\text{Cl}_2/\text{MeOH} = 9/1$). After evaporation of the solvent 2.1 mg (0.87 μmol , 79%) of a dark red solid was obtained.

In the first deprotection reaction the Fmoc group was removed in a solution of 20% piperidine in DMF. After 30 min, the HPLC chromatogram showed the disappearance of the starting compound and the formation of a new compound with a retention time of

29.0 min. The solvent was evaporated, after which the remaining protecting groups were removed by dissolving the product in 3 ml of the earlier described cleavage mixture (see paragraph 4.1.3) and stirring for 2 h. The reaction was followed by HPLC, where slowly a new porphyrin appeared at retention time 21,6 min. When the reaction was complete, the solvent was evaporated, the product washed several times with diethyl ether to remove the major part of the scavengers, purified by HPLC and freeze-dried to obtain 1.2 mg (0.52 μmol , 60%) of a green solid. The mass spectrum confirmed the identity of the completely deprotected CS3-TPP-ES5: 1814.0 Da (calculated 1797.2 Da; 1814.0 Da corresponds to CS3-TPP-ES5 containing oxidized methionine Met(O)).

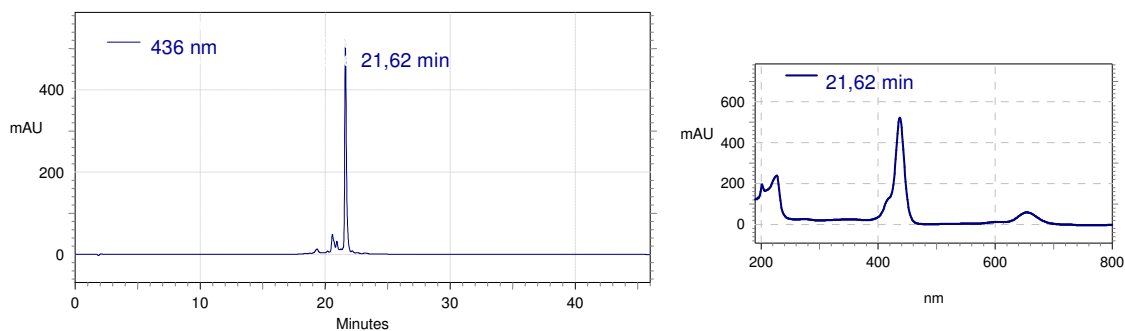


Figure 30: HPLC chromatogram and UV-VIS spectrum of CS3-TPP-ES5.

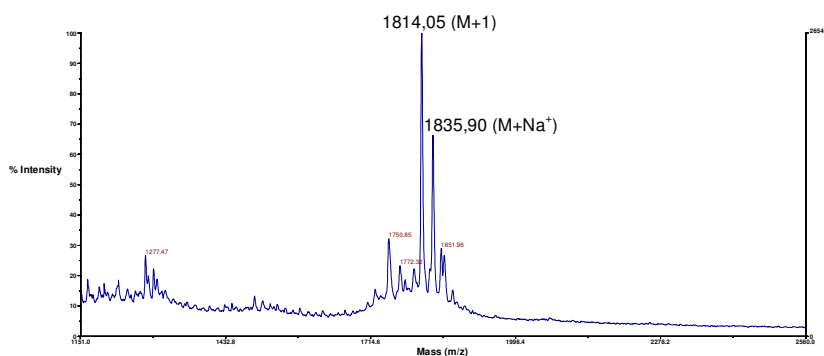


Figure 31: Mass spectrum of CS3-TPP-ES5.

Synthesis of *cis* CS3-TAMPP-ES5

11.5 mg (8.3 μmol) of *cis*-2Boc-TAMPP and 5 eq (5.8 μl) TEA were dissolved in 4 ml $\text{CH}_2\text{Cl}_2/\text{DMF}$. A solution of 7.95 mg (1 eq) activated Boc-tripeptide in 1.0 ml CH_2Cl_2 was slowly added to the reaction mixture, while at regular intervals the proceeding of the reaction was checked by TLC (silica, eluent $\text{CH}_2\text{Cl}_2/\text{MeOH} = 85/15$). The starting porphyrin had $R_F = 0$, whereas the mono-functionalized porphyrin had $R_F = 0.45$. After addition of ~ 0.6 eq of the peptide, a small amount of the dimer ($R_F = 0.8$) started to form, and the reaction was stopped. In the HPLC chromatogram the mono-

functionalized porphyrin *cis*-CS3-TAMPP-2Boc had a retention time of 25.5 min, the di-functionalized porphyrin *cis*-2CS3-TAMPP-2Boc had a retention time of 30.9 min. The mass spectrum confirmed the identity of the protected *cis*-CS3-TAMPP-2Boc: 1776.5 Da (calculated 1775.0 Da). The solvent was evaporated in vacuo, the product was purified by HPLC and freeze-dried to obtain 8.2 mg of a green solid (3.9 μ mol, 47%).

The *cis*-CS3-TAMPP-2Boc (8.2 mg, 3.9 μ mol) was dissolved in 4 ml $\text{CH}_2\text{Cl}_2/\text{DMF}$ and 3.6 mg (1 eq) of activated pentapeptide was added, together with 2.2 μ l (5 eq) of TEA. The reaction was followed by TLC (silica, eluent $\text{CH}_2\text{Cl}_2/\text{MeOH} = 85/15$). Only one product with $R_F = 0.9$ was formed, which was purified by column chromatography (silica gel, eluent $\text{CH}_2\text{Cl}_2/\text{MeOH} = 85/15$). After evaporation of the solvent 8.2 mg (3.2 μ mol, 82%) of a dark red solid was obtained. The HPLC chromatogram confirmed the presence of one product, with a retention time of 30.8 min.

The protecting groups were removed by dissolving the product in 4ml of the earlier described cleavage mixture (see paragraph 4.1.3) and stirring for 2 h. The reaction was followed by HPLC, where slowly a new porphyrin appeared at retention time 24.7 min. When the reaction was complete the solvent was evaporated, and the product was washed several times with diethyl ether to remove the major part of the scavengers, purified by HPLC and freeze-dried to obtain 4.3 mg (1.7 μ mol, 53%) of a green solid. The mass spectrum confirmed the identity of the completely deprotected CS3-TAMPP-ES5: 1870.3 Da (calculated 1855.0 Da; 1870.3 Da corresponds to CS3-TAMPP-ES5 containing oxidized methionine Met(O)).

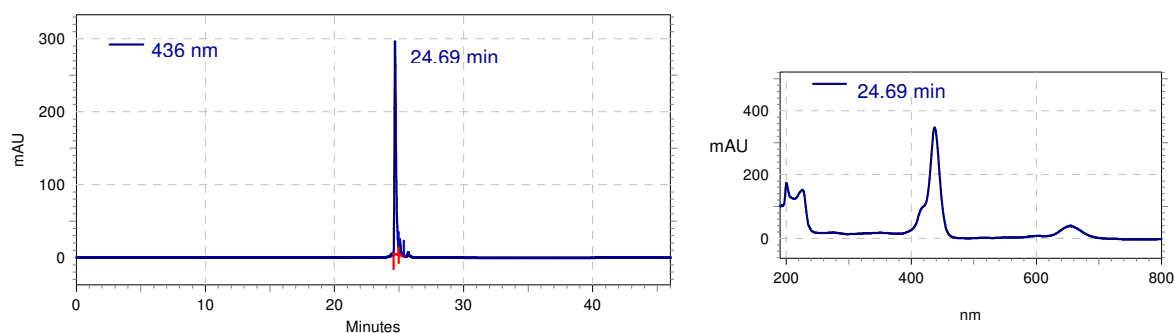


Figure 32: HPLC chromatogram and UV-VIS spectrum of CS3-TAMPP-ES5.

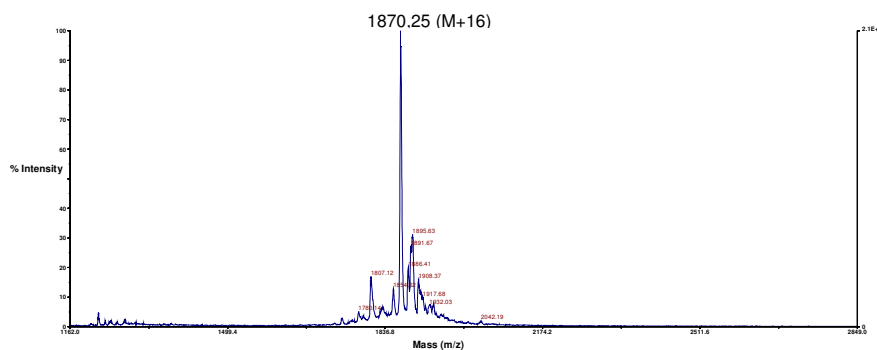


Figure 33: Mass spectrum of CS3-TAMPP-ES5.

The extinction coefficient of the pure CS3-TAMPP-ES5 compound was determined by measuring the absorbance at 416 nm of different concentrations of CS3-TAMPP-ES5 in ethanol. The resulting graph of absorbance versus concentration is shown in figure 34. The extinction coefficient $\epsilon_{416 \text{ nm}}$ is calculated to be $3.9 \cdot 10^5 \text{ L} \cdot \text{M}^{-1} \cdot \text{cm}^{-1}$.

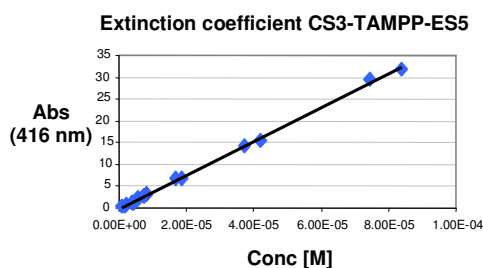


Figure 34: The extinction coefficient of CS3-TAMP-ES5.

Synthesis of *trans* CS3-TAMPP-ES7

9.3 mg (6.7 μmol) of *trans*-2Boc-TAMPP and 5 eq (4.7 μl) TEA were dissolved in 10 ml $\text{CH}_2\text{Cl}_2/\text{DMF}$. A solution of 7.0 mg (1 eq) activated Boc-tripeptide in 1.0 ml $\text{CH}_2\text{Cl}_2/\text{DMF}$ was slowly added to the reaction mixture, while at regular intervals the proceeding of the reaction was checked by TLC (silica, eluent $\text{CH}_2\text{Cl}_2/\text{MeOH} = 85/15$). The starting porphyrin had $R_F = 0$, the mono-functionalized porphyrin had $R_F = 0.55$. After addition of ~ 0.6 eq of the peptide, a small amount of the dimer ($R_F = 0.9$) started to form, and the reaction was stopped. In the HPLC chromatogram the mono-functionalized porphyrin *trans*-CS3-TAMPP-2Boc had a retention time of 24.9 min, the bi-functionalized porphyrin *trans*-2CS3-TAMPP had a retention time of 30.3 min. The mass spectrum confirmed the identity of the protected *trans*-CS3-TAMPP-2Boc: 1776.3 Da (calculated 1775.1 Da). The solvent was evaporated in vacuo, the product was purified by HPLC and freeze-dried to obtain 5.9 mg of a green solid (2.8 μmol , 42%).

The second (hepta)peptide was linked to the porphyrin scaffold while still attached to the resin. The *trans*-CS3-TAMPP-2Boc (5.9 mg, 3.4 μmol) was dissolved in 10 ml $\text{CH}_2\text{Cl}_2/\text{DMF}$ and added to 13.4 mg of resin (substitution 0.38 mmol) containing 5.1 μmol (2 eq) of activated heptapeptide. Triethylamine was added till pH $\sim 9/10$ (approximately 2.0 μl). After 1 h of bubbling with N_2 , the resin was washed several times with $\text{CH}_2\text{Cl}_2/\text{DMF}$. The colour of the resin had changed from yellow to pink, indicating the presence of the porphyrin scaffold on the resin. Cleavage of the peptide-porphyrin compound took place by bubbling a solution of $\text{CH}_2\text{Cl}_2/\text{TFE}/\text{acetic acid} = 8/1/1$ for 30 min, repeated two times. After washing the resin several times with CH_2Cl_2 , the fractions were reunited and the solvent was evaporated under vacuo. In the HPLC chromatogram, the starting porphyrin compound had disappeared and a new porphyrin had appeared at retention time 29.5 min. The product was slightly contaminated by excess of peptide (retention time 22.3 min), the major part of which was removed by column chromatography (silica gel, eluent: first CH_2Cl_2 100%, subsequently $\text{CH}_2\text{Cl}_2/\text{MeOH} = 9/1$). Even though the product was not completely pure, no problems were encountered during the deprotection reaction, after which total purification took place.

The protecting groups were removed by dissolving the product in 4 ml of the earlier described cleavage mixture (see paragraph 4.1.3) and stirring for 2 h. The reaction was followed by HPLC, where slowly a new porphyrin appeared at retention time 22.8 min. When the reaction was complete, the solvent was evaporated, the product was washed several times with diethyl ether to remove the major part of the scavengers, purified by HPLC and freeze-dried to obtain 2.47 mg (0.94 μmol , 34%) of a green solid. The mass spectrum confirmed the identity of the completely deprotected CS3-TAMPP-ES7: 2065.8 Da (calculated 2064.3 Da).

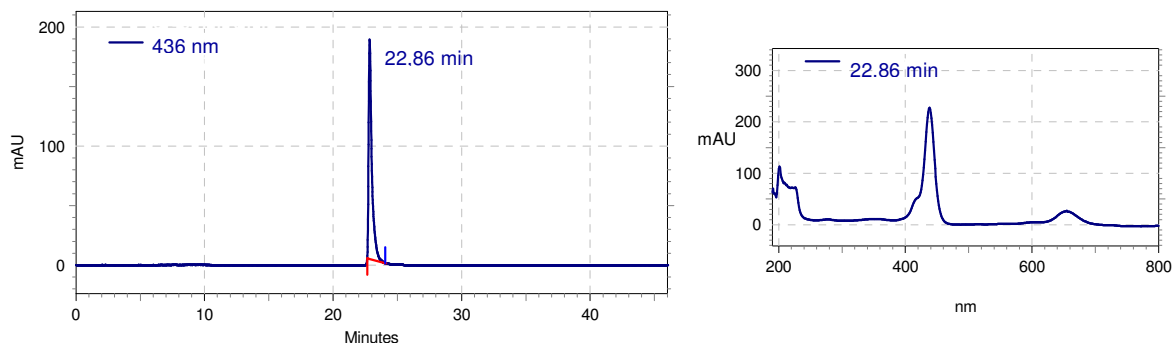


Figure 35: HPLC chromatogram and UV-VIS spectrum of CS3-TAMPP-ES7.

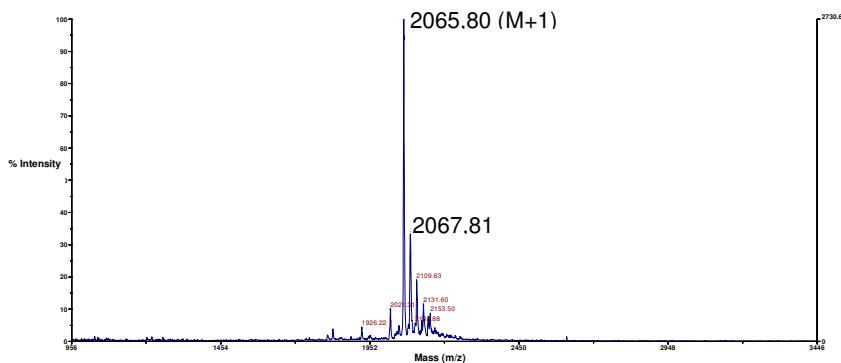


Figure 36: Mass spectrum of CS3-TAMPP-ES7.

4.3.5 Insertion of manganese

Synthesis of *cis* Mn^{III}-CS3-TAMPP-ES5

5.5 mg (2.2 μmol) of CS3-TAMPP-ES5 was dissolved in 4 ml 50% acetic acid in MeOH. MnAc₂·4H₂O was added (10 eq, 5.3 mg) and stirring was continued overnight. The reaction mixture turned slowly brown-green, and the HPLC chromatogram showed the presence of a new peak at 22.9 min with the characteristic UV spectrum of a Mn^{III}-porphyrin complex. The product was purified by HPLC, after which 2.93 mg (1.23 μmol , 57%) of a dark green solid was obtained. The mass spectrum confirmed the identity of the desired product: 1924.8 Da (calculated 1925.0 Da).

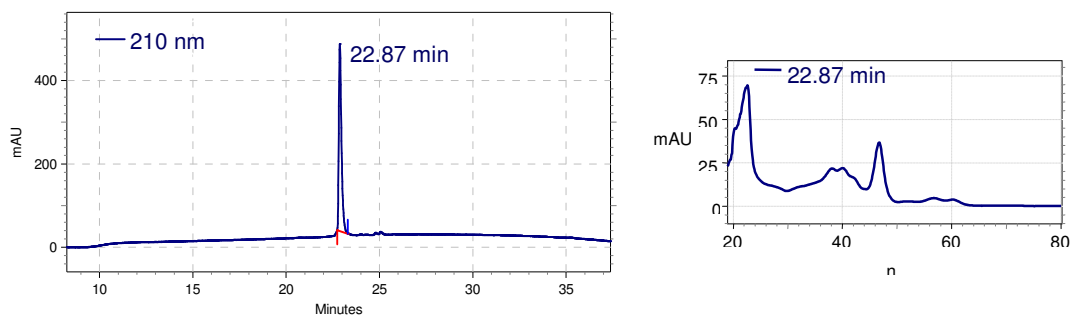


Figure 37: HPLC chromatogram and UV-VIS spectrum of Mn^{III}-CS3-TAMPP-ES5.

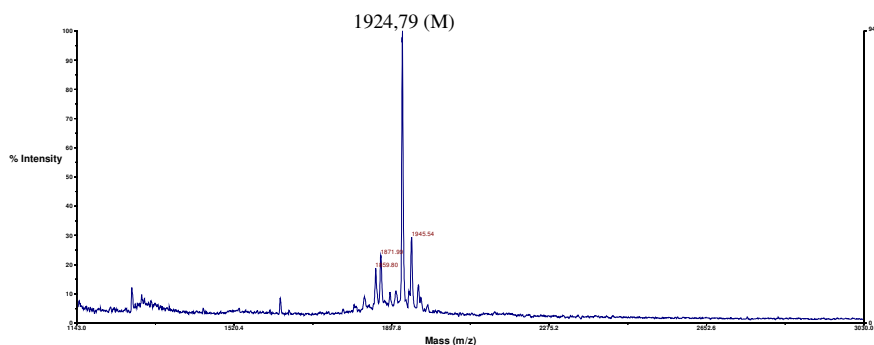


Figure 38: Mass spectrum of Mn-CS3-TAMPP-ES5.

The extinction coefficient of the pure Mn^{III}-CS3-TAMPP-ES5 complex was determined by measuring the absorbance at 467 nm of different concentrations of Mn^{III}-CS3-TAMPP-ES5 in ethanol. The resulting graph of absorbance versus concentration is shown in figure 39. The extinction coefficient ϵ at 467 nm is calculated to be $8.9 \cdot 10^4 \text{ L} \cdot \text{M}^{-1} \cdot \text{cm}^{-1}$.

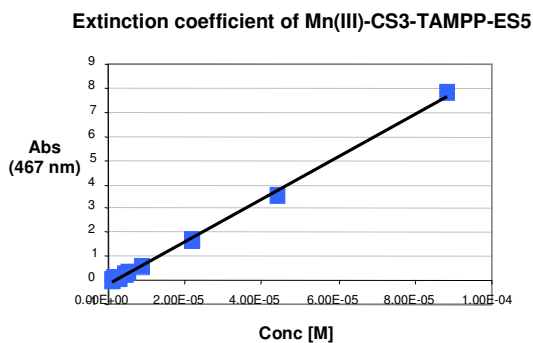


Figure 39: The extinction coefficient of Mn^{III}-CS3-TAMPP-ES5

The value of $\epsilon_{467 \text{ nm}}$ was confirmed by atomic adsorption and corresponds with values found in literature of Mn^{III}-porphyrin complexes¹⁴².

Synthesis of *cis* Mn^{III}-CS3-TAMPP-ES7

2.0 mg (1.0 μmol) of CS3-TAMPP-ES7 was dissolved in 3 ml 50% acetic acid in MeOH. MnAc₂·4H₂O was added (10 eq, 2.4 mg) and stirring was continued overnight. The reaction mixture turned slowly brown-green, and the HPLC chromatogram showed the presence of a new peak at 22.1 min with the characteristic UV spectrum of a Mn^{III}-porphyrin complex. The product was purified by HPLC, after which 1.01 mg (0.51 μmol , 51%) of a dark green solid was obtained. The mass spectrum confirmed the identity of the desired product: 2117.3 Da (calculated 2117.3 Da).

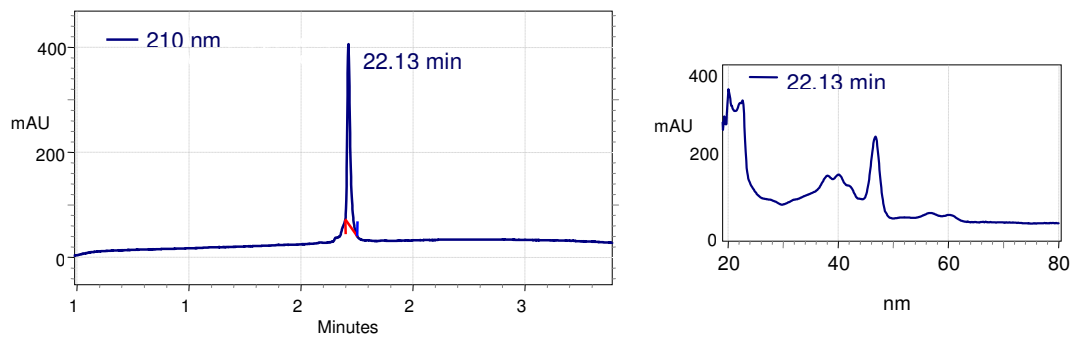


Figure 40: HPLC chromatogram and UV-VIS spectrum of Mn^{III} -CS3-TAMPP-ES7.

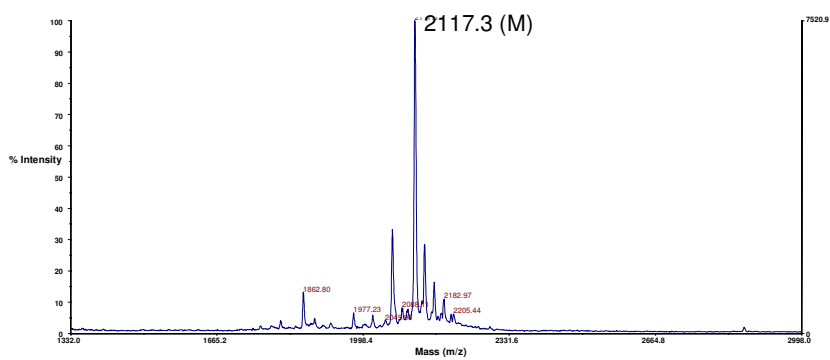


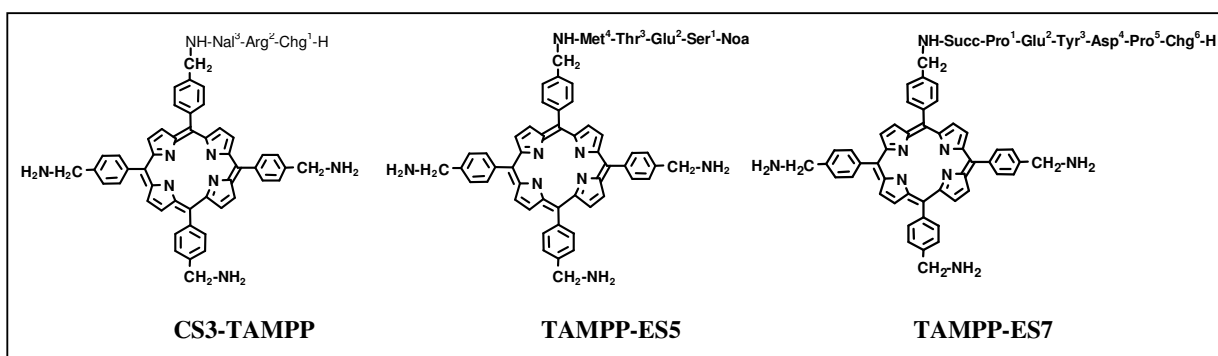
Figure 41: Mass spectrum of Mn-CS3-TAMPP-ES7.

Chapter 5 Tests of inhibition of human α -thrombin

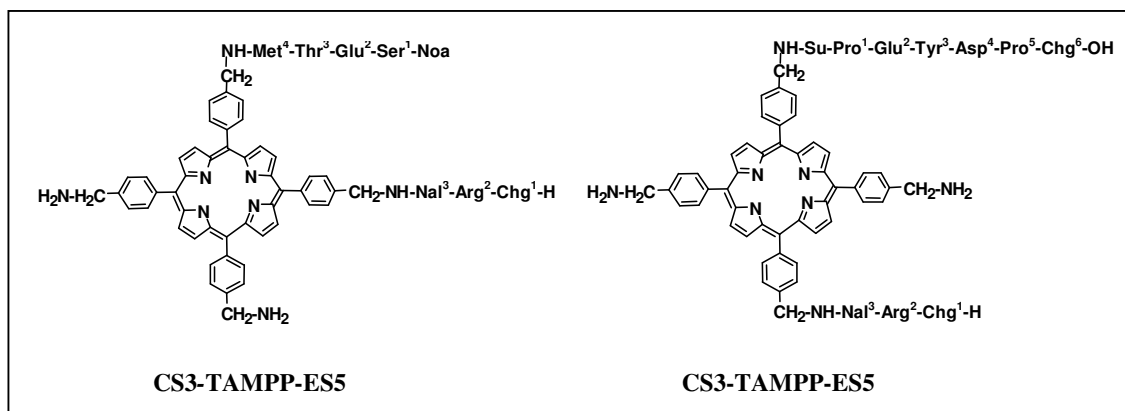
Introduction

The TAMPP-based functionalized scaffolds resulted to be more soluble in H₂O than their TPP counterparts. The functionalized TAMPP scaffolds were therefore more suitable as potential inhibitors, since all inhibition tests of thrombin took place in aqueous solutions, usually in Tris buffer of pH = 7.8. Highly concentrated stock solutions were prepared in either ethanol or DMSO. The following functionalized scaffolds were studied for their specificity of binding to human α -thrombin:

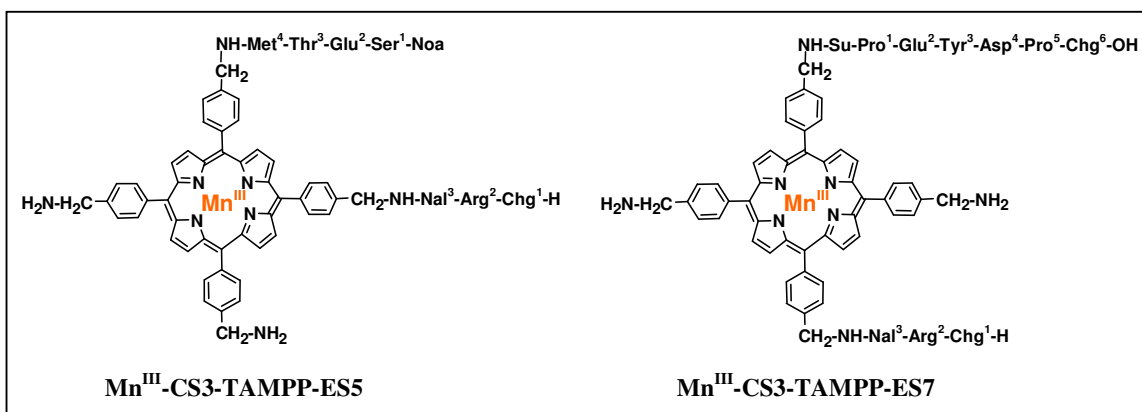
Mono-functionalized TAMPP compounds:



Bi-functionalized TAMPP compounds:



Mn^{III}-porphyrin complexes:



The mono-functionalized compounds were used to establish the interaction of the individual peptides with thrombin, and to measure their contribution to the inhibition of thrombin proteolytic activity. The following tests were performed:

- Inhibition of the catalytic activity
- Stability of the inhibitors to enzymatic degradation
- Selectivity of the inhibitors for different proteolytic enzymes
- Interaction with the exo site
- Inhibition of clot-bound thrombin

Specific low molecular weight substrates have been developed for thrombin, consisting of peptides mimicking the amino acid sequence adjacent to the substrate's cleavage site (the α -chain of fibrinopeptide A). Usually, these peptide-based synthetic substrates present chromogenic or fluorogenic groups to facilitate monitoring of the cleavage reaction¹⁴³. The first synthetic substrates that have been developed for the enzymes thrombin, trypsin and plasmin were *para*-nitro-anilide containing peptides. A *p*-nitro-aniline (*p*NA) group is added to these peptides, in order to produce a chromogenic product after cleavage. Examples of highly specific substrates for α -thrombin are Bz-Phe-Val-Arg-*p*NA.HCl (also known as S-2160), H-D-Phe-Pip-Arg-*p*NA.2HCl (S-2238), Z-Gly-Pro-Arg-*p*NA.HCl (Cbz-Chromozym TH) and Tos-Gly-Pro-Arg-*p*NA.HCl (Tos-Chromozym TH or Chromozym TH).

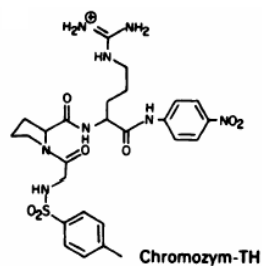


Figure 1: Structure of Tosyl-glycyl-L-prolyl-L-arginine *p*-nitroanilide (Chromozym TH).

Tos-Chromozym TH is less specific than the Cbz-derivative, but has a higher sensibility towards thrombin and is therefore mainly used in hydrolytic assays. Another advantage of these small synthetic substrates is that they also react with the hydrolysed β and γ forms of thrombin, with only a small loss of catalytic activity. In fact, mixtures of α , β and γ thrombin still retain up to 94% of the initial catalytic activity towards Chromozym TH^{144,145}.

5.1 Results

5.1.1 Calculation of K_m

The substrate Tos-Gly-Pro-Arg-*p*-nitro-anilide (Chromozym TH) was used for the inhibition test of the catalytic site. Cleavage of the Arg-nitroanilide bond yielded *p*-nitroaniline, which had a strong absorption at 405 nm. The affinity constant K_m was calculated by measuring the velocity of substrate hydrolysis at different substrate concentrations (from 10 to 100 μM).

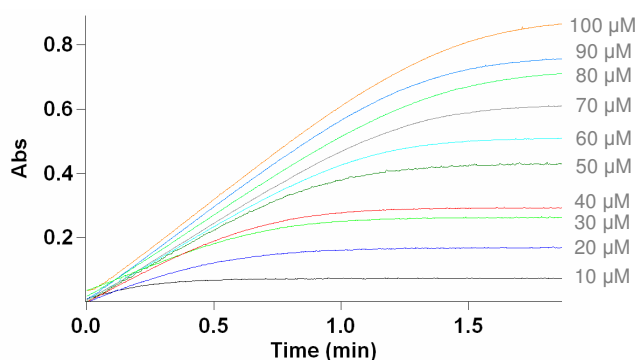


Figure 2: Graph of absorbance at 405 nm vs time, showing the hydrolysis of the substrate Chromozym TH by human α -thrombin at different substrate concentrations.

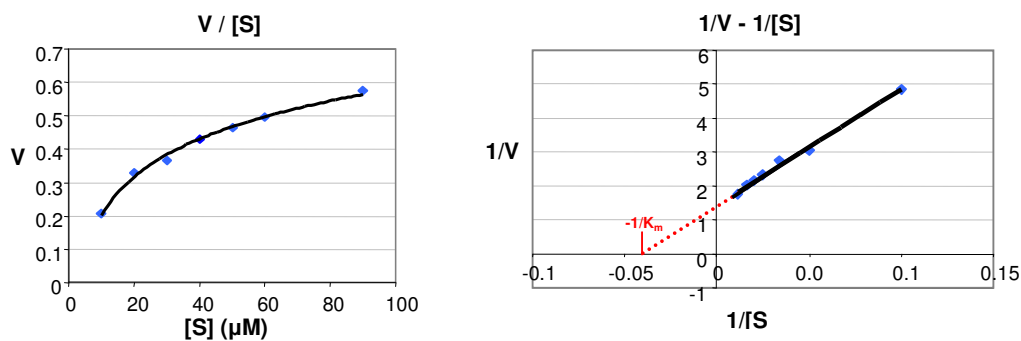


Figure 3: Graphs of V vs $[S]$ and $1/V$ vs $1/[S]$ (Lineweaver-Burk plot). Calculation of K_m .

Hydrolysis of the chromogenic substrate catalyzed by human α -thrombin showed a K_m value of 20.0 μM under our experimental conditions, which agrees well with values reported in literature¹⁴⁶.

5.1.2 Inhibition of the catalytic site

To be able to compare the experimental data of the new inhibitors with known inhibitors, the exact same procedure of the inhibition test has been performed using the inhibitor Hirunorm II. Hirunorm II has a known inhibition constant K_i of 8.45 nM⁴. In our experiments, using substrate concentrations of 40 and 125 μ M at inhibitor concentrations ranging from 0 to 80 nM, an inhibition constant K_i of 16.3 nM has been found (as shown in figure 4).

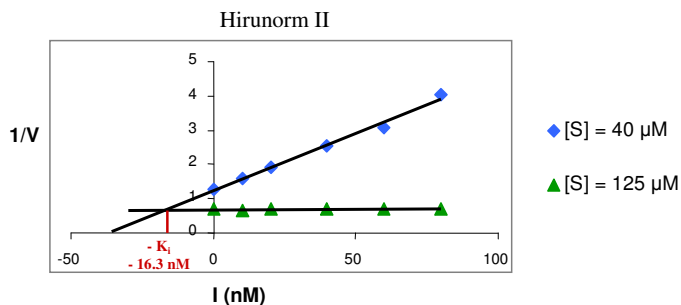


Figure 4: Dixon plot of human α thrombin inhibition by Hirunorm II at substrate concentrations of 40 and 125 μ M.

The inhibition constants K_i for the hydrolysis of Chromozym TH by the new porphyrin-based inhibitors are reported in table 1. The inhibition tests were not performed with inhibitors TAMPP-ES5 and TAMPP-ES7, as these were designed to interact with the thrombin fibrinogen recognition site, and not with the catalytic site. Initial rate velocities were recorded and used to construct Dixon plots (shown in figure 5).

Compound	K_i (μ M)
CS3-TAMPP	1.04
CS3-TAMPP-ES5	1.01
CS3-TAMPP-ES7	1.04
Mn ^{III} -CS3-TAMPP-ES5	1.63

Table 1: Inhibition constants of the new inhibitors

The inhibitors all showed inhibition constants in the micromolar range, with a slightly higher value for the Mn^{III}-inhibitor complex Mn^{III}-CS3-TAMPP-ES5. The K_i values are significantly higher than for the Hirunorm compounds, which exhibit inhibition constants in the nanomolar and even picomolar range. However, the fact that these inhibitors were capable to inhibit the hydrolysis of the substrate Chromozym TH, indicated that the tripeptide CS3 was capable to interact with the thrombin catalytic site

as was intended. Surprisingly, the presence or not of the second peptide, ES5 or ES7, designed to interact with the thrombin exo-site, does not seem to have any major effect on the activity of the catalytic site.

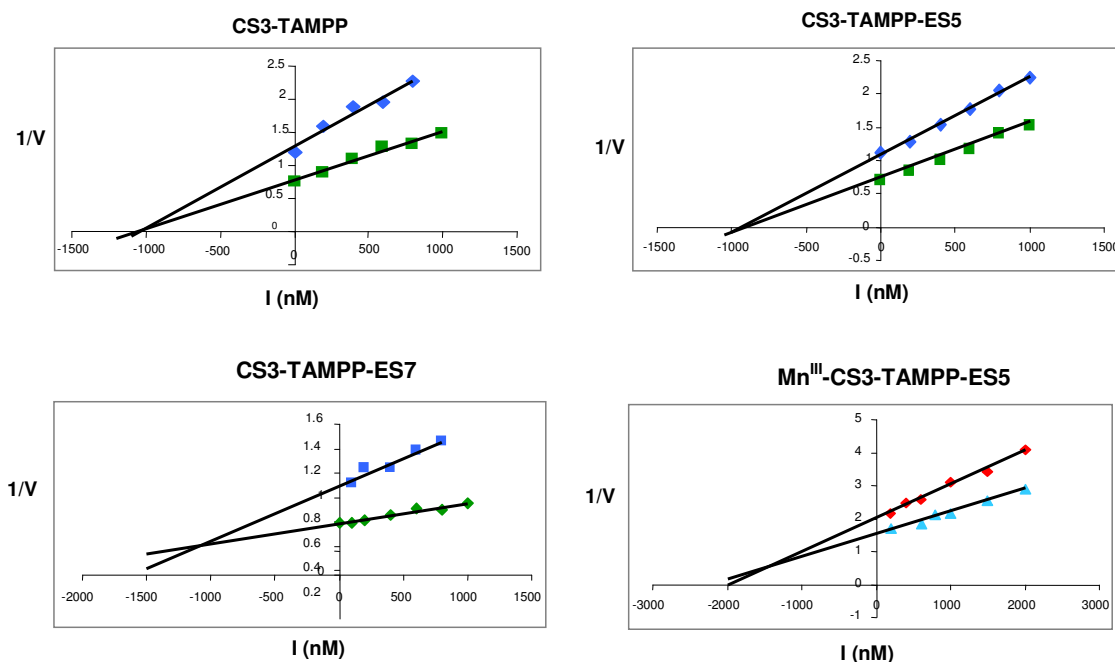


Figure 5: Dixon plots of human α -thrombin inhibition by the new inhibitors. Each point represents the average of triplicate determinations. Substrate concentrations are: \blacklozenge = 40 μ M, \blacksquare = 100 μ M, \blacklozenge = 60 μ M, \blacktriangle = 150 μ M.

The slightly higher K_i value of the manganese(III) complex of CS3-TAMPP-ES5 is probably due to the presence of the positively charged metal ion in the hydrophobic pocket that accommodates the porphyrin macrocycle. Apparently, the metal ion partly disrupts the hydrophobic interactions between the porphyrin ring and the thrombin surface.

5.1.3 Stability of the inhibitors

The stability of the inhibitors CS3-TAMPP-ES5 and CS3-TAMPP-ES7 against enzymatic degradation by thrombin was tested by incubation of the inhibitors with thrombin at 37 °C. The HPLC chromatograms, registered after 24 h of incubation, showed that more than 85% of the original compound was still present in the incubation mixture. Therefore, the new inhibitors resulted to be very stable in the presence of thrombin, compared to hirulog-1 that is known to be rapidly degraded (100% after 30 min with 1.6 NIH/ml thrombin)¹⁴⁷.

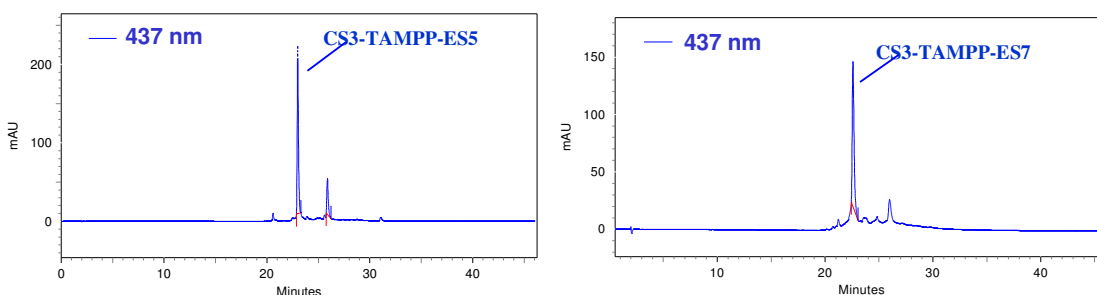
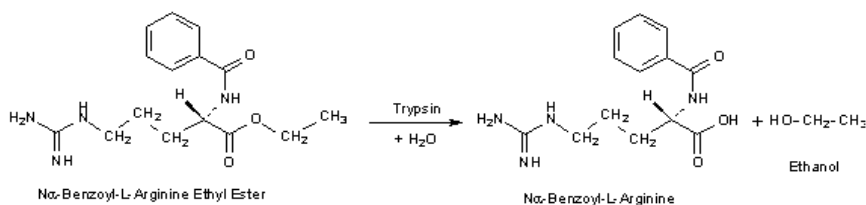


Figure 6: HPLC chromatograms of the incubation mixtures of CS3-TAMPP-ES5 and CS3-TAMPP-ES7 after 24 h.

5.1.4 Selectivity of the inhibitors

Apart from its inhibition constant, another important feature of an inhibitor is its selectivity. In order to be useful as a specific thrombin inhibitor, it should not have a major inhibition effect on other proteases of the same family, not even at elevated concentrations. To test the selectivity of the newly synthesized inhibitors, bovine trypsin inhibition was assayed using benzoylarginine ethyl ester (BAEE) as substrate¹⁴⁸:



The reactions were initiated by addition of trypsin to the incubation mixture, containing the substrate in phosphate buffer and the inhibitor at concentrations up to 10 μM . The change in absorbance was recorded continuously at 253 nm. As is shown in figure 5, the new inhibitors did not affect the hydrolysis of the substrate by trypsin, not even at high concentrations. The inhibitors could therefore be considered highly specific for thrombin.

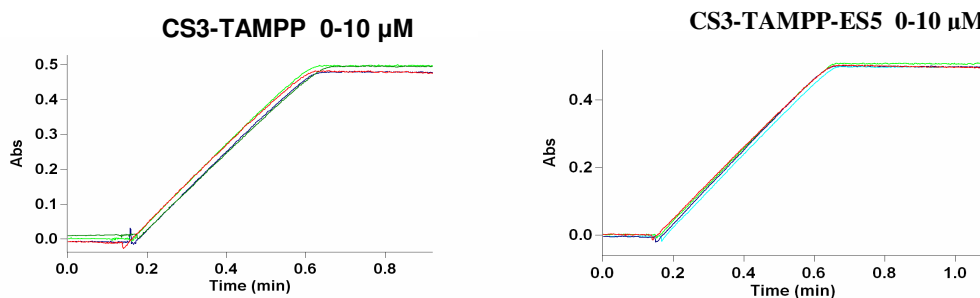


Figure 7: Hydrolysis of BAEE by trypsin in the presence of inhibitors CS3-TAMPP and CS3-TAMPP-ES5 at concentrations of 0, 1, 5 and 10 μM . The presence of the inhibitors does not affect the hydrolysis rate.

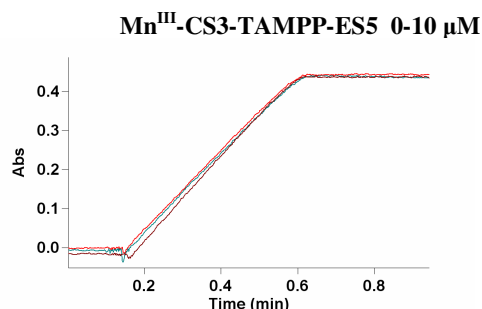


Figure 8: Hydrolysis of BAEE by trypsin in the presence of inhibitor Mn^{III}-CS3-TAMPP-ES5 at concentrations of 0, 1, 5 and 10 μM. The presence of the inhibitor does not affect the hydrolysis rate.

5.1.5 Interaction with the exo site

The interaction of the peptides ES5 and ES7 with the thrombin exo site was assayed by measuring the fluorescence intensity of thrombin at an excitation wavelength of 290 nm, when only the tryptophan residues of the protein contribute to the fluorescence. Residue Trp¹⁴⁸ is positioned in close proximity of the exo site, therefore upon inhibitor binding, the Trp side chain is supposed to be involved in hydrophobic interactions with the porphyrin macrocycle (see paragraph 2.5.2). The fluorescence of this Trp residue should be quenched by the presence of the inhibitor, and the total fluorescence of thrombin should diminish. To ascertain that the change of fluorescence is due to this particular Trp residue, the thrombin-inhibitor complex was treated with N-acetyl-hirudin^{54'-65'} (IRU-1), a potent inhibitor of thrombin with a high affinity for the exo site, that should be able to replace the porphyrin-based inhibitor at the exo site. The change in the fluorescence intensity of thrombin in the presence of the compounds TAMPP-ES5 and TAMPP-ES7 is shown in figure 9. Upon addition of TAMPP-ES5 or TAMPP-ES7, the fluorescence intensity diminished, whereas upon subsequent addition of IRU-1 the fluorescence was almost completely recovered. These results indicated that IRU-1 displaced at least part of the porphyrin compounds from the exo site, and therefore that both peptides ES5 and ES7 are capable of interacting with the exo site. As expected, for the compound TAMPP-ES7 the change in fluorescence intensity is larger than for TAMPP-ES5. When the peptide ES7 interacts with the exosite, the porphyrin macrocycle is positioned directly above the residue Trp¹⁴⁸. In the case of peptide ES5 the distance between the porphyrin macrocycle and Trp¹⁴⁸ is greater, resulting in a smaller quenching effect.

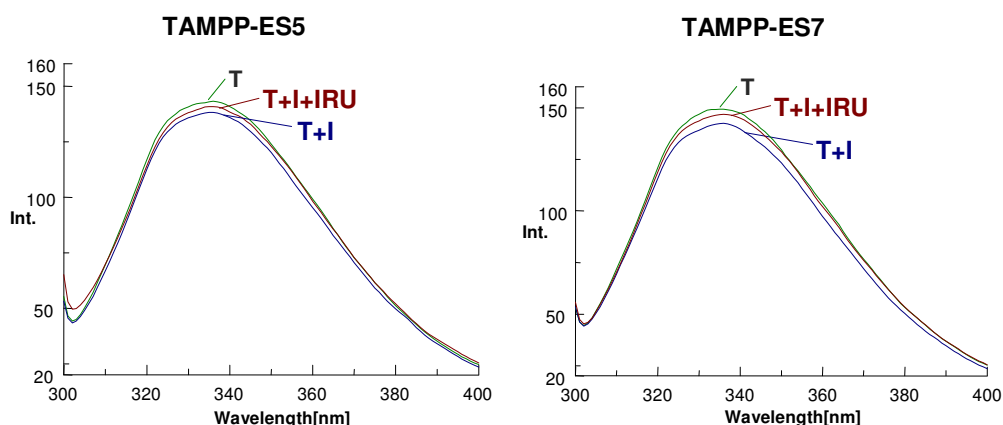


Figure 9: Fluorescence assays of TAMPP-ES5 and TAMPP-ES7. Excitation wavelength 290 nm. T = thrombin, I = inhibitor, IRU = N-acetyl-hirudin^{54'-65'}.

5.1.6 Inhibition of clot-bound thrombin

Fibrin clots were obtained by mixing thrombin and fibrinogen at 37 °C, after which the clots were washed repeatedly to remove the free thrombin as well as any unreacted fibrinogen. The clots were then pre-incubated for 1 h at 37 °C at inhibitor concentrations ranging from 0 to 10 μM. After repeated washing with buffer solution, the presence of the inhibitor on the fibrin clot was proved by the change in colour from white to yellow, as is shown in figure 10.

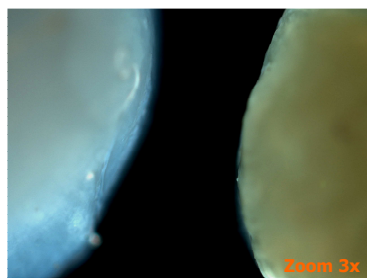


Figure 10: Macroscopic view of fibrin clots before (left) and after (right) pre-incubation with 10 μM inhibitor.

The ability of clot-bound thrombin to promote clot growth after pre-incubation with inhibitor was tested by incubating the washed clots at 37 °C with a fresh fibrinogen solution. The increase in clot size was inhibited concentration-dependently by pre-incubation with inhibitor Mn^{III}-CS3-TAMPP-ES5, as shown in figure 11. After pre-incubation with a 10 μM inhibitor solution, clot growth was only 60% of the growth of the uninhibited clots.

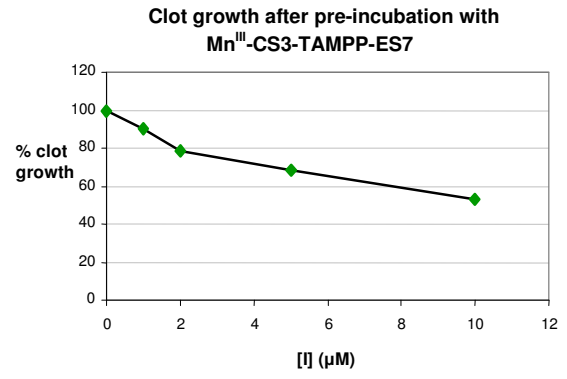
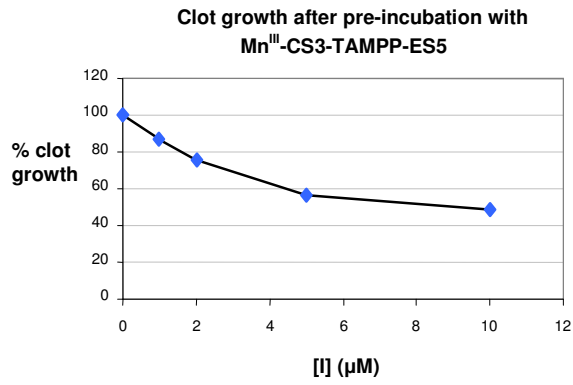


Figure 11: Percentage clot growth after pre-incubation with inhibitors Mn^{III}-CS3-TAMPP-ES5 and Mn^{III}-CS3-TAMPP-ES7. Each point is the result of six separate measurements.

5.2 Discussion

The various biological tests so far described demonstrated that the newly synthesized inhibitors CS3-TAMPP-ES5 and CS3-TAMPP-ES7, as well as their Mn^{III}-complexes, were able to interact with both the catalytic site and the exo site of thrombin. The mono-functionalized porphyrin scaffolds were used to establish the interaction of the individual peptides with thrombin. The tests of inhibition of the catalytic site using the substrate Chromozym TH allowed the calculation of the inhibition constants K_i for all inhibitors. CS3-TAMPP, CS3-TAMPP-ES5, CS3-TAMPP-ES7 all had a K_i value of 1.0 μM , whereas Mn^{III}-CS3-TAMPP-ES5 had a slightly higher K_i of 1.6 μM . Surprisingly, the presence of the peptides ES5 and ES7 had no effect on the value of the inhibition constant.

The inhibitors CS3-TAMPP-ES5 and CS3-TAMPP-ES7 resulted to be very resistant against enzymatic degradation by thrombin, as after 24 h 85% of the original compound was still intact.

Assays of inhibition of trypsin with the substrate BAEE proved the selectivity of the new inhibitors, since even at elevated concentrations (up to 10 μM) the inhibitors did not affect the hydrolysis rate of the reaction.

The ability of the new inhibitors to interact with the thrombin exo site by the peptides ES5 and ES7 was proved by fluorescence spectroscopy. The fluorescence of Trp¹⁴⁸, in close proximity of the exo site, was quenched when the compounds TAMPP-ES5 and TAMPP-ES7 were added. Addition of IRU-1, replacing the inhibitor at the exo site, allowed the fluorescence intensity to return to almost the original level. For the compound TAMPP-ES7 this effect is more pronounced than for TAMPP-ES5, probably because the distance between the porphyrin macrocycle and the residue Trp¹⁴⁸ is smaller in the case of TAMPP-ES7.

The manganese(III) complexes of the inhibitors CS3-TAMPP-ES5 and CS3-TAMPP-ES7 were capable of interacting with clot-bound thrombin, and partially inhibited clot-growth in the presence of fresh fibrinogen. After 1h pre-incubation with a 10 μM inhibitor solution, clot growth was decreased to 60% compared to the uninhibited clots.

5.3 Experimental section

5.3.1 Materials and methods

Buffer solutions were prepared in spectroscopic grade H₂O supplied by Romil. The Tris buffer contained 0.05 M Tris-HCl, 0.1 M NaCl, 0.1% PEG 6000, and NaOH was added till pH = 7.8. Reagents were obtained from commercial suppliers and used as received. Human α -thrombin, with a specific activity of 3032 NIH units/mg protein, was supplied by Calbiochem, as well as fibrinogen which was dissolved in aqueous solution by continued stirring at 37 °C. Chromozym TH was supplied by Roche Diagnostics. N-acetyl-hirudin^{54'-65'} (IRU-1) was previously synthesized using standard Fmoc SPPS protocols, and purified by RP-HPLC. Analysis of reaction mixtures was performed using a RP-HPLC Shimadzu system LC-10AD VP with a spectrophotometric detector Diode Array SPD-M10A VP. Linear gradients were used of H₂O 0.1% TFA and CH₃CN 0.1% TFA. UV-VIS spectra were recorded on a Varian Cary 5000 spectrophotometer. Fluorescence spectra were recorded on a Jasco FP-750 spectrofluorometer. Fibrin clots were analysed using a Zeiss Axioskop 40 optical microscope with an Axiocam MRc5 colour camera.

5.3.2 Inhibition tests

Inhibition of the catalytic site

The human α -thrombin catalyzed hydrolysis of Tos-Gly-Pro-Arg-*p*-nitro-anilide (Chromozym TH) was monitored at 405 nm on a Cary 5000 spectrophotometer and recorded continuously as a function of time. The hydrolytic reactions were performed at 37 °C in 0.05 M Tris-HCl buffer, pH 7.8, containing 0.1 M NaCl and 0.1% polyethylene glycol 6000. The concentration of α -thrombin was determined spectrophotometrically using an extinction coefficient at 280 nm of 1.83 ml·mg⁻¹·cm⁻¹. The incubation mixtures contained 895 μ l buffer, 5 μ l 5.0·10⁻⁶ M α -thrombin (final concentration 2.5·10⁻⁸ M) and 50 μ l inhibitor in ethanol (final concentrations ranging from 0 to 1000 nM). The reactions were initiated by addition of 50 μ l of substrate solution (final concentration 20-150 μ M). Initial rate velocities were recorded and used to construct Dixon plots.

Stability of the inhibitors

Resistance of the new inhibitors to the enzymatic degradation by thrombin was evaluated by HPLC. Thrombin (50 NIH/ml) was incubated up to 24 h at 37 °C with 500 nM inhibitors in Tris buffer (pH = 7.8). At regular intervals, samples were withdrawn and acidified with H₂O 0.1% TFA before injection into the HPLC system. The HPLC chromatograms showed that the peptide-porphyrin compounds CS3-TAMPP-ES5 and CS3-TAMPP-ES7 were stable against degradation by thrombin, and that even after 24 h more than 85% of the compound was still intact.

Selectivity of the inhibitors

Bovine trypsin inhibition was assayed using benzoylarginine ethyl ester (BAEE) as substrate¹⁴⁹. The assays were performed at 25 °C in a 0.067 M sodium phosphate buffer at pH = 7.6. The concentration of trypsin was determined spectrophotometrically using an extinction coefficient at 280 nm of 1.44 ml·mg⁻¹·cm⁻¹.

The incubation mixtures contained 880 µl buffer, 20 µl 6.3·10⁻⁵ M trypsin in 1.0 mM HCl (final concentration 1.9·10⁻⁶ M), 50 µl 1.0·10⁻² M BAEE in phosphate buffer (final concentration 5.0·10⁻⁴ M) and 50 µl inhibitor in ethanol (final concentrations ranging from 0 to 10 µM). The reactions were initiated by addition of trypsin to the incubation mixture. The change in absorbance was recorded continuously at 253 nm.

Inhibition of the exosite

The fluorescence was measured at 25 °C between 300 and 400 nm, after excitation at 290 nm. The concentration of thrombin was 5.0·10⁻⁷ M in Tris buffer. The initial fluorescence was registered, an equimolar amount of inhibitor was added and the sample was mixed thoroughly. After measuring the fluorescence of the thrombin-inhibitor complex, an equimolar amount of IRU-1 was added, and the fluorescence measurement was repeated. All assays were repeated three times.

Inhibition of clot-bound thrombin

Fibrin clots were prepared by adding 50 µl human α-thrombin (25 NIH units/ml) to mixture of 200 µl of a 5 mg/ml solution of human fibrinogen in 0.18% NaCl solution containing 0.01% Tween 80 (NT solution), and 25 µl of a 200 mg/ml solution of human

albumin in water. After 15 min incubation at 37 °C, the liquid phase was removed and the remaining fibrin clot was washed five times with 3 ml of NT solution to remove free thrombin and unreacted fibrinogen.

The washed clots were incubated for 1 h at 37 °C in 700 µl Tris buffer containing from 0 to 10 µM inhibitor (Mn^{III}-CS3-TAMPP-ES5 or Mn^{III}-CS3-TAMPP-ES7), after which the liquid was removed and the clots washed three times with buffer solution in order to remove the free inhibitor. Fibrinogen solution (500 µl) was added and the incubation was repeated for another 2h.

At the end of the incubation time, the clots were washed five times with NT solution and three times with acetone. Clot size was determined by weight after drying for 24 h in vacuo.

Chapter 6 General discussions and future prospects

Introduction

The aim of the research described in this thesis has been the design and synthesis of new molecular scaffolds based on tetraphenylporphyrin, and to test the versatility of these scaffolds by functionalization with various peptides. An application of the functionalized scaffolds has been found in the design and synthesis of new inhibitors of thrombin, an enzyme of fundamental importance in the blood coagulation process. The inhibitors CS3-TAMPP-ES5, CS3-TAMPP-ES7 and their Mn^{III}-complexes have been successfully synthesized, and their capacity to interact with both the catalytic site and the fibrinogen recognition site of thrombin has been studied. These compounds, by interacting specifically with clot-bound thrombin, will allow detection of fibrin clots by non-invasive techniques such as MRI.

6.3 Functionalized tetraphenylporphyrins as versatile scaffold

Tetraphenylporphyrins carrying from one to four aminomethyl groups have been synthesized as scaffolds. The mixed aldehyde condensation of benzaldehyde and 4-(formylbenzyl)phtalimide in pyrrole yielded mono, di-*trans*, di-*cis*, and tri-substituted porphyrins, with average yields of 4-6%. To enhance the yields of the *cis* and *trans* di-substituted porphyrins, two alternative strategies have been developed. The *trans* porphyrin was synthesized by a 2+2 condensation of 5-(4-phtalimidomethyl)phenyl-dipyrromethane, with a yield of 7%. For the *cis* porphyrin a modified version of the ABCD-porphyrin synthesis, consisting of six steps, was applied. Although the final condensation reaction had an 8% yield of *cis* porphyrin, the entire six-step synthesis required several laborious purifications as well as elevated costs. Therefore, for the synthesis of this particular scaffold the mixed aldehyde condensation might be a better choice. For the synthesis of tetrakis(*p*-(aminomethyl)phenyl)porphyrin, two different methods were applied: 1) the reaction of 4-(formylbenzyl)phtalimide and pyrrole in propionic acid, and 2) the TFA catalyzed condensation of 4-(formylbenzyl)phtalimide and 5-(4-phtalimidomethyl)phenyldipyrromethane.

Although this latter method had a lower yield (16.6% versus 22%), the reaction was relatively clean with almost no polymeric byproducts. The final product could therefore be purified by HPLC, as opposed to the repeated column chromatography that was required in the first strategy. Therefore, for the synthesis of tetrakis-

(*p*-(aminomethyl)phenyl)porphyrin, the condensation of 4-(formylbenzyl)phtalimide and 5-(4-phtalimidomethyl)phenyldipyrromethane is recommended.

The aminomethyl groups of the scaffolds were protected with the Boc protecting group to allow a selective functionalization of the scaffold. The protected porphyrin scaffolds were stable and were easily purified by HPLC. The Boc protecting groups could be removed with a 50% solution of TFA in CH₂Cl₂ to yield the original scaffold without loss of product.

All scaffolds were stable in a wide range of solvents and at different values of pH. Storage at -20 °C for prolonged periods of time did not cause any alteration in the scaffolds.

The functionalization of the synthesized porphyrin scaffolds with peptides was successful in all cases. Activation of the peptides required the use of N-hydroxy-succinimide, since other activants, such as PyBop, HOBt, HATU did not produce the desired results. The functionalization reaction could take place either in solution, or with the activated peptide still attached to the resin. Both Fmoc and Boc protected peptides could be used for functionalization of the scaffolds, as the porphyrin scaffolds proved to be stable in both deprotection protocols. No alteration of the peptide-porphyrin compound was observed during the synthesis. When stored at -20 °C, the peptide-functionalized porphyrin compounds could be kept for a prolonged period of time. Average yields of the functionalization reactions were 80-90% for the mono-functionalized compounds and 30-35% for the bi-functionalized compounds. Stable Mn^{III}-porphyrin complexes were obtained by insertion of manganese using Mn^{II}Ac₂ in a 50% acetic acid/MeOH solution.

6.4 New inhibitors of thrombin

The inhibitors CS3-TAMPP-ES5 and CS3-TAMPP-ES7, as well as their Mn^{III}-complexes, were able to interact with both the catalytic site and the exo site of thrombin. CS3-TAMPP, CS3-TAMPP-ES5, CS3-TAMPP-ES7 all had a K_i value of 1.0 μM, whereas Mn^{III}-CS3-TAMPP-ES5 had a slightly higher K_i of 1.6 μM. The presence of the peptides ES5 and ES7 did not affect the value of the inhibition constant.

The inhibitors resulted to be very resistant against enzymatic degradation by thrombin, as after 24 h 85% of the original compound was still intact. Assays of inhibition of trypsin with the substrate BAEE proved the high selectivity of the new inhibitors. Even at elevated concentrations (up to 10 μM) the inhibitors did not affect the hydrolysis rate

of the reaction. The ability of the new inhibitors to interact with the thrombin exo site by the peptides ES5 and ES7 was proved by fluorescence spectroscopy. The fluorescence of Trp¹⁴⁸, in close proximity of the exo site, was quenched when the porphyrin-based inhibitors were added. Addition of IRU-1, replacing the inhibitor at the exo site, allowed the fluorescence intensity to return to almost its original level.

The manganese complexes of the new inhibitors were capable of interacting with clot-bound thrombin, and did partly inhibit clot growth in the presence of fresh fibrinogen. After 1h pre-incubation with a 10 μ M inhibitor solution, clot growth was decreased to 60% compared to the uninhibited clots. The change of colour of the fibrin clot from white to yellow, after pre-incubation with the inhibitors, proved the presence of the inhibitors on the fibrin clot.

To the best of our knowledge, the compounds Mn^{III}-CS3-TAMPP-ES5 and Mn^{III}-CS3-TAMPP-ES7 are the first specific inhibitors of thrombin that might be employed for diagnostic purposes, due to the presence of a paramagnetic metal ion inside the porphyrin structure. The high stability against degradation by thrombin, and the high selectivity of these compounds make them extremely interesting for various (medical) applications.

6.5 Suggestions for further research

Since the results of the inhibition tests *in vitro* are very promising, the next step will be to test the new compounds *in vivo*, and to measure the MRI response of inhibitor-containing fibrin clots. X-ray structures of the thrombin-inhibitor complexes are required to fully understand the specific binding mode of the new inhibitors to thrombin. Once these structures will be solved, new peptide chains can be designed to enhance the binding affinity of these compounds for thrombin.

References

- ¹ Reedy, C.J., Gibney, B.R. *Chem. Rev.* **2004**, 104, 617649.
- ² Lombardi, A., Nastri, F., Pavone, V. *Chem. Rev.* **2001**, 101, 31653189.
- ³ Loew, G.H., Harris, D.L. *Chem. Rev.* **2000**, 100, 407419.
- ⁴ Biesaga, M., Pyrzyńska, K., Trojanowicz, M. *Talanta*, **2000**, 51, 209-224.
- ⁵ Lomova, T.N., Berezin, B.D. *Russian J. of Coord. Chem.*, **2001**, 27, 85–104.
- ⁶ Dolphin, D. *The Porphyrins, Volume I, Structure and Synthesis Part A*, **1978**, Academic Press Inc., London.
- ⁷ Dolphin, D. *The Porphyrins, Volume II, Structure and Synthesis Part B*, **1978**, Academic Press Inc., London.
- ⁸ Camenzind, M. J., Hollander, F.J., Hill, C.L. *Inorg. Chem.* **1982**, 21, 4301-4308.
- ⁹ Smith, K. *J. Porphyrins Phthalocyanines* **2000**, 4, 319–324.
- ¹⁰ Shanmugathasan, S., Edwards, C., Boyle, R.W. *Tetrahedron*, **2000**, 56, 1025–1046.
- ¹¹ Burrell, A.K., Officer, D.L., Plieger, P.G., Reid, D.C.W. *Chem. Rev.*, **2001**, 101, 2751-2796.
- ¹² Rothmund, P., Menotti, A. R. *J. Am. Chem. Soc.* **1941**, 63, 267.
- ¹³ Adler, A. D., Longo, F. R., Finarelli, J. D., Goldmacher, J., Assour, J., Korsakoff, L. *J. Org. Chem.* **1967**, 32, 476.
- ¹⁴ Lindsey, J. S., Hsu, H. C., Schreiman, I. C. *Tetrahedron Lett.* **1986**, 27, 4969.
- ¹⁵ Lindsey, J. S., Schreiman, I. C., Hsu, H. C., Kearney, P. C., Marguerettaz, A. M. *J. Org. Chem.* **1987**, 52, 827.
- ¹⁶ Lindsey, J. S., MacCrum, K. A., Tyhonas, J. S., Chuang, Y.Y. *J. Org. Chem.* **1994**, 59, 579.
- ¹⁷ Arsenault, G. P., Bullock, E., MacDonald, S. F. *J. Am. Chem. Soc.* **1960**, 82, 4384.
- ¹⁸ Boudif, A., Momenteau, M. *J. Chem. Soc., Chem. Commun.*, **1994**, 2069-2070.
- ¹⁹ Boudif, A., Momenteau, M. *J. Chem. Soc., Perkin Trans. 1*, **1996**, 1235.
- ²⁰ Broadhurst, M.J., Grigg, R., Johnson, A.W. *J. Chem. Soc. (C)*, **1971**, 3681-3690.
- ²¹ Bauer, V.J., Clive, D.R., Dolphin, D., Paine III, J.B., Harris, F.L., King, M.M., Loder, J., Wang, S-W.C., Woodward, R.B. *J. Am. Chem. Soc.* **1983**, 105, 6429.
- ²² Lash, T.D. *Journal of Porphyrins and Phthalocyanines*, **1997**, 1, 29–44.
- ²³ Lin, Y., Lash, T. D. *Tetrahedron Lett.* **1995**, 36, 9441-9444.
- ²⁴ Chandrasekar, P., Lash, T. D. *Tetrahedron Lett.* **1996**, 37, 4873-4876.

-
- ²⁵ Lindsey, J. S. *Tetrahedron* **1995**, 51, 11645.
- ²⁶ Dharma Rao, P., Dhanalekshmi, S., Littler, B.J., Lindsey, J.S. *J. Org. Chem.* **2000**, 65, 7323-7344.
- ²⁷ Wijsekera, T. P., Dolphin, D. *Synlett*, **1990**, 235.
- ²⁸ Schneider, J.P., Kelly, J.W. *Chem. Rev.*, **1995**, 95, 2169-2187.
- ²⁹ Ogoshi, H., Mizutani, T. *Acc. Chem. Res.*, **1998**, 31, 81-89.
- ³⁰ Lawson, M.A., Blackwell, G.G., Pohost, G.M. *Acc. Current Journal Review*, **1995**, Jan/Feb.
- ³¹ Okuhata, Y. *Advanced Drug Delivery Reviews*, **1999**, 37, 121-137.
- ³² Chen, C., Cohen, J.S., Myers, C.E., Sohn, M. *FEBS*, **1984**, 168, 70-74.
- ³³ Murugesan, S., Shetty, S.J., Srivastava, T.S., Noronha, O.P.D., Samuel, A.M. *Applied Radiation and Isotopes*, **2001**, 55, 641-646.
- ³⁴ Policard, A., Leuller, A. *Compt. Rend. Soc. Wood*, **1924**, 91, 1423-1424.
- ³⁵ Megnin, F., Faustino, P.J., Lyon, R.C., Lelkes, P.I., Cohen, J.S. *Biochimica et Biophysica Acta*, **1987**, 929, 173- 181.
- ³⁶ Nakajima, S., Takemura, T., Sakata, I. *Cancer Letters*, **1995**, 92, 113-118.
- ³⁷ Ali, H., Lier, J.E. van; *Chem. Rev.*, **1999**, 99, 2379-2450.
- ³⁸ Chatterjee, S.R., Kamat, J.P., Shetty, S.J., Banerjee, S., Srivastava, T.S., Devasagayam, T.P.A. *Radiat. Phys. Chem.*, **1997**, 49, 135-140.
- ³⁹ MacDonald, I.J., Dougherty, T.J. *J. Porphyrins Phthalocyanines*, **2001**, 5, 105-129.
- ⁴⁰ Pandey, R.K. *J. Porphyrins Phthalocyanines*, **2000**, 4, 368-373.
- ⁴¹ Mettath, S., Munson, B.R., Pandey, R.K. *Bioconjugate Chem.*, **1999**, 10, 94-102.
- ⁴² Meunier, B. *Chem. Rev.* **1992**, 92, 1411-1456.
- ⁴³ Fiel, R. J., Datta-Gupta, N., Mark, E. H., and Howard, J.C. *Cancer Res.*, **1981**, 41, 3543-3545.
- ⁴⁴ Mehta, G., Muthusamy, S., Maiya, B.G., Arounagiri, S. *Tetrahedron Letters*, **1997**, 38, 7125-7128.
- ⁴⁵ Maiya, B.G. *J. Porphyrins Phthalocyanines*, **2000**, 4, 393-397.
- ⁴⁶ Purrello, R., Gurrieri, S., Lauceri, R. *Coord. Chem. Rev.*, **1999**, 190-192, 683-706.
- ⁴⁷ Sirish, M., Schneider, H-J. *Chem. Commun.*, **1999**, 907-908.
- ⁴⁸ Mizutani, T., Wada, K., Kitagawa, S. *J.Am.Chem. Soc.*, **1999**, 121, 11425-11431.
- ⁴⁹ Toma, H.E., Araki, K. *Coord. Chem. Rev.*, **2000**, 196, 307-329.

-
- ⁵⁰ Suslick, K.S., Rakow, N.A., Kosal, M.E., Chou, J-H. *J. Porphyrins Phthalocyanines*, **2000**, 4, 407-413.
- ⁵¹ Iengo, E., Zangrando, E., Minatel, R., Alessio, E. *J. Am. Chem. Soc.*, 2002, 124, 1003-1013.
- ⁵² Ashok Kumar, A., Giribabu, L., Raghunath Reddy, D., Maiya, B.G. *Inorg. Chem.*, **2001**, 40, 6757-6766.
- ⁵³ Khoury, R.G., Jaquinod, L., Smith, K.M. *Chem. Commun.*, **1997**, 1057-1058.
- ⁵⁴ Higuchi, H., Shimizu, K.; Ojima, J., Sugiura, K., Sakata, Y. *Tetrahedron Lett.* **1995**, 36, 5359-5362.
- ⁵⁵ Seth, J., Palaniappan, V., Johnson, T.E., Prathapan, S., Lindsey, J.S., Bocian, D.F. *J. Am. Chem. Soc.*, **1994**, 116, 10578-10592.
- ⁵⁶ Nagata, T., Osuka, A., Maruyama, K. *J. Am. Chem. Soc.*, **1990**, 112, 3054-3059.
- ⁵⁷ Okumura, A., Funatsu, K., Sasaki, Y., Imamura, T. *Chem. Lett.* **1999**, 779.
- ⁵⁸ Blake Hill, R., Raleigh, D.P., Lombardi, A., DeGrado, W.F. *Acc. Chem. Res.*, **2000**, 33, 745-754.
- ⁵⁹ Tuchscherer, G., Mutter, M. *Journal of Biotechnology*, **1995**, 41, 197-210.
- ⁶⁰ Causton, A.S., Sherman, J.C. *Bioorganic & Medicinal Chemistry*, **1999**, 7, 23-27.
- ⁶¹ Lombardi, A., Natri, F., Pavone, V. *Chem. Rev.*, **2001**, 101, 3165-3189.
- ⁶² Huffman, D. L., Rosenblatt, M. M., Suslick, K. S. *J. Am. Chem. Soc.* **1998**, 120, 6183.
- ⁶³ Huffman, D. L., Suslick, K. S. *Inorg. Chem.* **2000**, 39, 5418-5419.
- ⁶⁴ Sasaki, T.; Kaiser, E. T. *J. Am. Chem. Soc.* **1989**, 111, 380.
- ⁶⁵ Anderson, G.W., Zimmerman, J.E., Callahan, F.M. *J. Am. Chem. Soc.*, **1963**, 85, 3039.
- ⁶⁶ Anderson, G.W., Zimmerman, J.E., Callahan, F.M. *J. Am. Chem. Soc.*, **1964**, 86, 1839-1842.
- ⁶⁷ Carpino, L.A., *J. Am. Chem. Soc.*, **1957**, 79, 4427-4430.
- ⁶⁸ Carpino, L.A., Han, G.Y., *J. Am. Chem. Soc.*, **1970**, 92, 5748-5749.
- ⁶⁹ Davie, E.W., Fujikawa, K., Kisiels, W. *Biochemistry*, **1991**, 30, 10364-10370.
- ⁷⁰ Markwardt, F. *Ann. N.Y. Acad. Sci.*, **1986**, 485, 204-214.
- ⁷¹ Fenton, J.W., Fasco, M.J., Stackrow, A.B. *J. Biol. Chem.* **1977**, 252, 3587-3598.
- ⁷² Doolittle, R.F., *Ann. Rev. Biochem.* **1984**, 53, 195-229.

-
- ⁷³ Fenton, J.W., et al., in *Chemistry and Biology of Thrombin*, ed. R.L. Lundblad, J.W. Fenton, K.G. Mann, 43-70, Ann Arbor, MI: Ann Arbor Science Publishers, Inc., **1977**.
- ⁷⁴ Boissel, J.P., et al., *J. Biol. Chem.*, **1984**, 259, 5691-5697.
- ⁷⁵ Chang, J-Y. *Biochem. J.*, **1986**, 240, 797-802.
- ⁷⁶ Fazal Mohammed, S., Whitworth, C., Chuang, H.Y.K., Lundblad, R.L., Mason, R.G. *Proc. Natl. Acad. Sci. USA* **1976**, 73, No. 5, 1660-1663.
- ⁷⁷ Blombäck, B., Hessel, B., Iwanaga, S. *Nature* **1967**, 215, 1445-1448.
- ⁷⁸ Hogg, D.H., Blombäck, B. *Thromb. Res.* **1978**, 12, 953-964.
- ⁷⁹ Bode, W. et al., *EMBO J.*, **1989**, 8, 3467-3475.
- ⁸⁰ Bode, W., Turk, D., Karshikov, A., *Protein Science*, **1992**, 1, 426-471.
- ⁸¹ Jhoti, H., Cleasby, A., Reid, S., Thomas, P.J., Weir, M., Wonacott, A. *Biochemistry*, **1999**, 38, 7969-7977.
- ⁸² Schechter, I., Berger, A., *Biochem. Biophys. Res. Commun.*, **1967**, 27, 1576-162.
- ⁸³ Lebonniec, B.F., Guinto, G.R., Esmon, C.T., *J. Biol. Chem.*, **1992**, 267, 19341-19348.
- ⁸⁴ Stubbs, M.T., Oschkinat, H., Mayr, I., Huber, R., Angliker, H., Stone, S.R., Bode, W., *Eur. J. Biochem.*, **1992**, 206, 187-195.
- ⁸⁵ Liu, C.Y., Nossel, H.L., Kaplan, K.L. *J. Biol. Chem.*, 1979, 254, 10421-10425.
- ⁸⁶ Liu, C.Y., Nossel, H.L., Kaplan, K.L. *Thromb, Haemostasis.*, **1979**, 42, 79.
- ⁸⁷ Fredenburgh, J.C., Stafford, A.R., Pospisil, C.H., Weitz, J.I. *Biophysical Chemistry*, **2004**, 112, 277-284.
- ⁸⁸ Bode, W., Huber, R., *Eur. J. Biochem.*, **1992**, 204, 433-451.
- ⁸⁹ Olson, S.T., Shore, J.D., *J. Biol. Chem.*, **1982**, 257, 14891.
- ⁹⁰ Rosenberg, R.D., Damus, P.S., *J. Biol. Chem.*, **1973**, 248, 6490-6505.
- ⁹¹ Tollefsen, D.M., Majerus, D.W., Blank, M.K., *J. Biol. Chem.*, **1982**, 257, 2162-2169.
- ⁹² Derechin, V.M., Blinder, M.A., Tollefsen, D.M., *J. Biol. Chem.* **1990**, 265, 5623-5628.
- ⁹³ Scott, R.W. et al., *J. Biol. Chem.*, **1985**, 260, 7029-7034.
- ⁹⁴ Farrell, D.H., Cunningham, D.D., *Biochem. J.*, **1987**, 245, 543-550.
- ⁹⁵ Wen, D., Dittman, W.A., Ye, R.D., Deaven, L.L., Majerus, P.W., Sadler, J.E., *Biochemistry*, **1987**, 26, 4350-4357.
- ⁹⁶ Sadler, J.E., *Thromb Haemost*, **1997**, 78, 392-395.

-
- ⁹⁷ Machovich, R., Borsodi, A., Blaskó, G., Orakzai, S.A., *Biochem. J.*, **1977**, 167, 393-398.
- ⁹⁸ Hamipel, P.C., Mosesson, M.W., *J. Clin. Invest.*, **1973**, 52, 2175-2184.
- ⁹⁹ Folkers, P. J. M., Clore, G. M., Driscoll, P. C., Dodt, J., Kohler, S., Gronenborn, A. *M. Biochemistry*, **1989**, 28, 2601-2617.
- ¹⁰⁰ Nicastro, G., Baumer, L., Bolis, G., Tatò, M., *Biopolymers*, **1997**, 41, 731-749.
- ¹⁰¹ Betz, A., Hofsteenge, J., Stone, S.R., *Biochemistry* **1992**, 31, 4557-4562.
- ¹⁰² Lazar, J.B., Winant, R.C., Johnson, P.H., *J. Biol. Chem.*, **1991**, 266, 685-688.
- ¹⁰³ De Filippis, V., Colombo, G., Russo, I., Spadari, B., Fontana, A., *Biochemistry*, 2002, 41, 13556-13569.
- ¹⁰⁴ Lombardi, A., De Simone, G., Galdiero, S., Staiano, N., Natri, F., *Biopolymers*, **1999**, 51, 19-39.
- ¹⁰⁵ Strube, K.H., Kröger, B., Bialojan, S., Otte, M., Dodt, J. *J. Biol. Chem.*, 1993, 268, 8590-8595.
- ¹⁰⁶ Richardson, J.L., Fuentes-Prior, P., Sadler, J.E., Huber, R., Bode, W. *Biochemistry*, **2002**, 41, 2535-2542.
- ¹⁰⁷ Richardson, J. L., Kröger, B., Hoeffken, W., Sadler, J. E., Pereira, P., Huber, R., Bode, W., Fuentes-Prior, P. *EMBO J.*, **2000**, 19, 5650-5660.
- ¹⁰⁸ Turpie, A.G.G., Weitz, J.I., Hirsh, J. *Thrombosis and Haemostasis*, **1995**, 74, 565-571.
- ¹⁰⁹ Weitz, J.I., Crowther, M. *Thrombosis Research*, **2002**, 106, 275-284.
- ¹¹⁰ Malley, M.F., Taberner, L., Chang, C.Y., Ohringer, S.L., Roberts, D.G.M., Das, J., Sack, J.S *Protein Sci.*, **1996**, 5, 221-228.
- ¹¹¹ Stuerzebecher, J., et al. *Thrombosis Research*, **1983**, 29, 635-642.
- ¹¹² Brandstetter, H., Turk, D., Hoemen, H.W., Grosse, D., Stürzebecher, J., Martin, P.D., Edwards, B.F.P., Bode, W. *J. Mol. Biol.*, **1992**, 226, 1085-1099.
- ¹¹³ Kikumoto, R., Okamoto, S. et al, *Biochemistry*, **1984**, 23, 85-90.
- ¹¹⁴ Krstenansky, J.L., Mao, S.J.T. *FEBS Letters*. **1987**, 211, 10-16.
- ¹¹⁵ Vijkayalakshmi, J., Padmanabhan, K.P., Tulinsky, A. *Protein Science*, **1994**, 3, 2254-2271.
- ¹¹⁶ Skrzypczak-Jankun, E., Carperos, V.E., Ravichandran, K.G., Tulinsky, G. *J. Mol. Biol.*, **1991**, 221, 1379-1393.

-
- ¹¹⁷ Krstenansky, J.L., Owen, T.J., Yates, M.T., Mao, S.J.T. *FEBS Letters*, **1990**, 269, 425-429.
- ¹¹⁸ Maraganore, J.M., Bourdon, P., Jablonski, J., Ramachandran, K.L., Fenton, J.W. II *Biochemistry*, **1990**, 29, 7095-7101.
- ¹¹⁹ Qiu, X., Padmanabhan, K.P., Carperos, V.E., Tulinsky, A., Kline, T., Maraganore, J.M., Fenton, J.W. *Biochemistry*, **1992**, 31, 11689-11697.
- ¹²⁰ DiMaio, J., Ni, F., Gibbs, B., Konishi, Y. *FEBS Letters*, **1991**, 282, 47-52.
- ¹²¹ Lombardi, A., Natri, F., Della Morte, R., Rossi, A., De Rosa, A., Staiano, N., Pedone, C., Pavone, V. *J. Med. Chem.*, **1996**, 39, 2008-2017.
- ¹²² De Simone, G., Lombardi, A., Galdiero, S., Natri, F., Della Morte, R., Staiano, N., Pedone, C., Bolognesi, M., Pavone, V. *Protein Sci.*, **1998**, 7, 243-253.
- ¹²³ Paquet, A. *Can. J. Chem.*, **1982**, 60, 976.
- ¹²⁴ Lavalley, D.K., Xu, Z., Rina, R. *J. Org. Chem.*, **1993**, 58, 6000-6008.
- ¹²⁵ Wallace, D.M., Leung, S.H., Senge, M.O., Smith, K. M. *J. Org. Chem.*, **1993**, 58, 7245-7257.
- ¹²⁶ Littler, B.J., Ciringh, Y., Lindsey, J.S. *J. Org. Chem.*, **1999**, 64, 2864-2872.
- ¹²⁷ Manka, J.S., Lawrence, D.S. *Tetrahedron Letters*, **1989**, 30, 6989-6992.
- ¹²⁸ Lindsey, J.S., Schreimann, I.C., Hsu, H.C., Kearney, P.C., Marguerettaz, A.M. *J. Org. Chem.*, **1987**, 52, 827-836.
- ¹²⁹ Dharma Rao, P., Littler, B.J., Geier, G.R., Lindsey, J.S. *J. Org. Chem.*, **2000**, 65, 1084-1092.
- ¹³⁰ Dharma Rao, Dhanalekshmi, S.P., Littler, G.R., Lindsey, J.S. *J. Org. Chem.*, **2000**, 65, 7323-7344.
- ¹³¹ Lee, C.H., Lindsey, J.S. *Tetrahedron*, **1994**, 50, 11427-11440.
- ¹³² Gonzalez, B., Kouba, J., Yee, S., Reed, C.A. *J. Am. Chem. Soc.*, **1975**, 97, 3247-3249.
- ¹³³ Loach, P.A., Calvin, M. *Biochemistry*, **1963**, 2, 361-371.
- ¹³⁴ Merrifield, R.B. *J. Am. Chem. Soc.*, **1963**, 85, 2149-2154.
- ¹³⁵ Carpino, L.A. Han, G.Y. *J. Org. Chem.*, **1972**, 37, 3404-3409.
- ¹³⁶ Barlos, K., Gatos, D., Kallitsis, J., Papaphotiou, G., Wenquing, Y., Schäfer, W. *Tetrahedron Letters*, **1989**, 30, 3943-3946.
- ¹³⁷ Barlos, K., Chatzi, O., Gatos, D., Stavropoulos, G. *Int. J. Peptide Protein Res.*, **1991**, 37, 513-520.

-
- ¹³⁸ Coste, J., Le-Nguyen, D., Castro, B. *Tetrahedron Letters*, **1990**, 31, 205-208.
- ¹³⁹ Anderson, G.W., Zimmerman, J.E., Callahan, F.M. *J. Am. Chem. Soc.*, **1963**, 85, 3039.
- ¹⁴⁰ Boucher, L.J. *J. Am. Chem. Soc.*, **1968**, 90, 6640-6645.
- ¹⁴¹ Boucher, L.J. *Coord Chem. Rev.*, **1972**, 7, 289-329.
- ¹⁴² Camenzind, M. J., Hollander, F.J., Hill, C.L. *Inorg. Chem.* **1982**, 21, 4301-4308.
- ¹⁴³ Sonder, S.A., Fenton, J.W. *Clin. Chem.*, **1986**, 32, 934-937.
- ¹⁴⁴ Lottenberg, R., Hall, J.A., Fenton, J.W., Jackson, C.M. *Thromb Res.*, **1982**, 28, 313-332.
- ¹⁴⁵ Witting, J.I., Miller, T.M., Fenton, J.W. *Thromb Res.* **1987**, 46, 567-574.
- ¹⁴⁶ Lombardi, A., Natri, F., Della Morte, R., Rossi, A., De Rosa, A. Staiano, N., Pedone, C., Pavone, V. *J. Med. Chem.*, **1996**, 39, 2008-2017.
- ¹⁴⁷ Cirillo, R., Lippi, A., Subissi, A., Agnelli, G., Criscuoli, M. *Thromb. Haemost.*, **1996**, 76, 384-392.
- ¹⁴⁸ Schwert, G.W., Takenaka, Y. *Biochim. Biophys. Acta*, **1955**, 16, 570-575.
- ¹⁴⁹ Zhou, J.M., Liu, C., Tsou, C.L. *Biochemistry* **1989**, 28, 1070-1076.